DUDLEY KNOX LIBRARY
NAVAL POSTGRADUATE SCHOOL
MONTEREY, CALIFORNIA 93943-5002

NAVAL POSTGRADUATE SCHOOL
Monterey, California

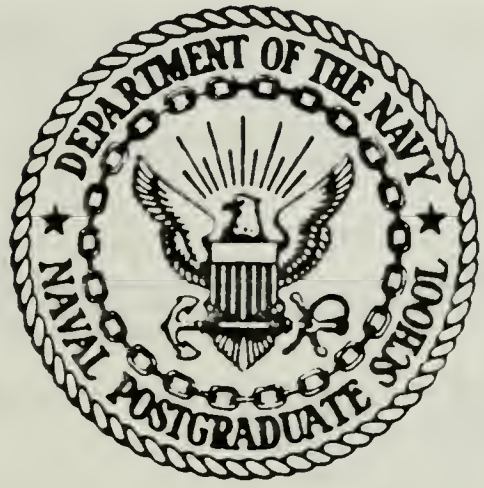

THESIS

A DYNAMIC SIMULATION AND FEEDBACK CONTROL SCHEME FOR THE U. S. MARINE CORPS' AIRBORNE REMOTELY OPERATED DEVICE (AROD)

by

William Glen Bassett

September 1987

Thesis Advisor: H. A. TITUS

Approved for public release; distribution is unlimited

T234130

SECURITY CLASSIFICATION OF THIS PAGE

REPORT DOCUMENTATION PAGE

1a REPORT SECURITY CLASSIFICATION UNCLASSIFIED	1b RESTRICTIVE MARKINGS NONE
2a SECURITY CLASSIFICATION AUTHORITY	3 DISTRIBUTION / AVAILABILITY OF REPORT Approved for public release; distribution is unlimited
2b DECLASSIFICATION / DOWNGRADING SCHEDULE	
4 PERFORMING ORGANIZATION REPORT NUMBER(S)	5 MONITORING ORGANIZATION REPORT NUMBER(S)
6a NAME OF PERFORMING ORGANIZATION Naval Postgraduate School	6b OFFICE SYMBOL (If applicable) 62
7a NAME OF MONITORING ORGANIZATION Naval Postgraduate School	
6c ADDRESS (City, State, and ZIP Code) Monterey, California 93943-5000	7b ADDRESS (City, State, and ZIP Code) Monterey, California 93943-5000
8a NAME OF FUNDING / SPONSORING ORGANIZATION	8b OFFICE SYMBOL (If applicable)
9 PROCUREMENT INSTRUMENT IDENTIFICATION NUMBER	
8c ADDRESS (City, State, and ZIP Code)	10 SOURCE OF FUNDING NUMBERS PROGRAM ELEMENT NO / PROJECT NO / TASK NO / WORK UNIT ACCESSION NO

11 TITLE (Include Security Classification)
A DYNAMIC SIMULATION AND FEEDBACK CONTROL SCHEME FOR THE U.S. MARINE CORPS' AIRBORNE REMOTELY OPERATED DEVICE (AROD)

12 PERSONAL AUTHOR(S)
BASSETT, William G.

13a TYPE OF REPORT	13b TIME COVERED	14 DATE OF REPORT (Year Month Day)	15 PAGE COUNT
Master's Thesis	FROM _____ TO _____	1987 September	166

16 SUPPLEMENTARY NOTATION

17 COSATI CODES			18 SUBJECT TERMS (Continue on reverse if necessary and identify by block number)
FIELD	GROUP	SUB-GROUP	Remotely Piloted Vehicle(RPV); AROD; Multiple-Input,Multiple-Output(MIMO); Optimal Control; UHF Antenna; Dynamic Simulation; Modelling

19 ABSTRACT (Continue on reverse if necessary and identify by block number)

The equations of motion for a ducted fan hovering device are developed and programmed in a computer simulation. Experimental aerodynamic data is integrated with the computer model. A feedback control scheme for the multiple-input, multiple-output system is determined using optimal control techniques. Time response results are obtained and analyzed.

As a separate issue, the body of the device is modelled for electromagnetic analysis and a basic antenna design is determined for UHF transmission.

20 DISTRIBUTION / AVAILABILITY OF ABSTRACT	21 ABSTRACT SECURITY CLASSIFICATION
☐ UNCLASSIFIED/UNLIMITED ☐ SAME AS RPT ☐ DTIC USERS	UNCLASSIFIED
22a NAME OF RESPONSIBLE INDIVIDUAL H. A. TITUS	22b TELEPHONE (Include Area Code) (408) 646-2454 / 22c OFFICE SYMBOL 62

FORM 1473, 84 MAR 83 APR edition may be used until exhausted
All other editions are obsolete

SECURITY CLASSIFICATION OF THIS PAGE

Approved for public release; distribution is unlimited.

A Dynamic Simulation and Feedback Control Scheme for the U. S. Marine Corps' Airborne Remotely Operated Device (AROD)

by

William Glen Bassett
Captain, United States Marine Corps
B.S., Cornell University, 1980

Submitted in partial fulfillment of the
requirements for the degree of

MASTER OF SCIENCE IN ELECTRICAL ENGINEERING

from the

NAVAL POSTGRADUATE SCHOOL
September 1987

ABSTRACT

The equations of motion for a ducted fan hovering device are developed and programmed in a computer simulation. Experimental aerodynamic data is integrated with the computer model. A feedback control scheme for the multiple-input, multiple-output system is determined using optimal control techniques. Time response results are obtained and analyzed.

As a separate issue, the body of the device is modelled for electromagnetic analysis and a basic antenna design is determined for UHF transmission.

Thesis
8242555
c.1

TABLE OF CONTENTS

TABLE OF SYMBOLS

Symbol	Description	Units
Coordinate Definitions		
X,Y,Z	Body-Fixed Coordinate Axes	
i,j,k	Unit vectors in X,Y,Z, respectively	
X',Y',Z'	Earth-Fixed Coordinate Axes	
Dynamic States		
U,V,W	Body-Fixed Velocities along X,Y,Z	ft/sec
U',V',W'	Earth-Fixed Velocities	ft/sec
P,Q,R	Body-Fixed Roll, Pitch, and Yaw	rad/sec
φ,Θ,ψ	Earth-Fixed Euler Angles	radians
ω	Total Body Angular Velocity	rad/sec
ω_r	Rotor Angular Velocity	rad/sec
Constants		
I_x,I_y,I_z	Body Moments of Inertia (Body Axes)	ft^2-lb(m)
I_r	Rotor Moment of Inertia (Rotor) Axis	ft^2-lb(m)
m	Total Mass of Vehicle	lb(m)
g	Gravitational Constant (32.174)	ft/sec^2
Forces		
F_x,F_y,F_z	Total Translational Forces (Body)	lbs
F_{ax},F_{ay},F_{az}	Aerodynamic Translational Forces	lbs
F_{tx},F_{ty},F_{tz}	Thrust and Propeller Induced Forces	lbs
F_s,F_l,F_d	Side-Slip, Lift, and Drag Forces	lbs

Moments

L, M, N	Total Angular Moments about X,Y,Z	ft-lbs
L_a, M_a, N_a	Aerodynamic Angular Moments	ft-lbs
L_t, M_t, N_t	Thrust and Propeller Induced Moments	ft-lbs
R_r, P_p, Y_y	Roll,Pitch,Yaw (relative to V_{tot})	ft-lbs
h	Angular Momentum of Body	ft-lbs/sec

Servo States

u_a, u_e, u_r, u_t	Input Signals to Servo	volts
$\delta_a, \delta_e, \delta_r, \delta_t$	Output from Servo	radians
T_r	Engine Thrust Force	lbs

Vectors

x(t)/x(k)	Continuous/Discrete Time System States
y(t)/y(k)	Continuous/Discrete Time Output States
$r_c(t)/r_c(k)$	Continuous/Discrete Time Reference Input
$u_c(t)/u_c(k)$	Continuous/Discrete Time Control Input

Matrices

A	Continuous Time System Plant
B	Continuous Time Control Distribution
ϕ	Discrete Time System Plant
Γ	Discrete Time Control Distribution
H	Output Measurement
K	Feedback (continuous and discrete)
W_o	Observability
W_c	Controllability
C	Final State Weighting
Q	Transient State Weighting

R	Control Cost Weighting	
J	Cost Function (Scalar)	

Sampling Quantities

ΔT	Sampling Interval (Period)	seconds
f_s	Sampling Frequency	hertz (Hz)
f_N	System Natural Frequency	hertz (Hz)

Special States

Θ_b, ψ_b	Body-Fixed Pitch and Yaw Angles	radians

ACKNOWLEDGMENT

Especially to Shirley, my wife, whose encouragement and support was, is, and will always be sincerely appreciated.

I. INTRODUCTION

A. WHAT IS AROD?

The U. S. Marine Corps has established the Ground/Air Tele Robotic Systems (GATERS) program to develop, test and field robotic devices for direct use by U. S. Marine infantrymen. These robotic systems will be operated under the concept of *tele robotics* which implies that a man, stationed remotely from the vehicle, will control the device as if he is actually on board.

The Airborne Remotely Operated Device (AROD) is the vehicle being developed through the GATERS program to meet the Marine Corps' needs for an airborne, short-range, direct support remotely piloted vehicle (RPV). The GATERS program office [1] states that, from a tactical perspective:

> The AROD is ... designed to allow the front line commander to see "over the next hill", out to a distance of two kilometers and "around the next corner" in an urban environment.

This tactical requirement has led to a more technical statement of what AROD will be. The GATERS program has stated [2]:

> The AROD will be a ducted-fan, hovering device capable of a forward translation speed of 30 miles per hour. The vehicle will carry a fibre optic data link and on board cameras to support assigned missions out to a distance of 5 kilometers. Normal operating radius is 2 kilometers.

More detailed requirements are listed in Appendix A.

B. AROD AND OPTIMAL CONTROL

The AROD is to be operated by a Marine, untrained and unskilled in aerodynamic flight. Therefore, AROD must be inherently stable and responsive to simple controls such as "go up/down", "rotate right/left", "go forward", "go sideways". These instructions will be commanded from a joystick, through the control uplink to an on-board control system. The control system will interpret the command and perform the necessary tasks to maneuver the AROD. The design of this controller is the major topic of this work. Figure 1.1 is a schematic of the prototype AROD.

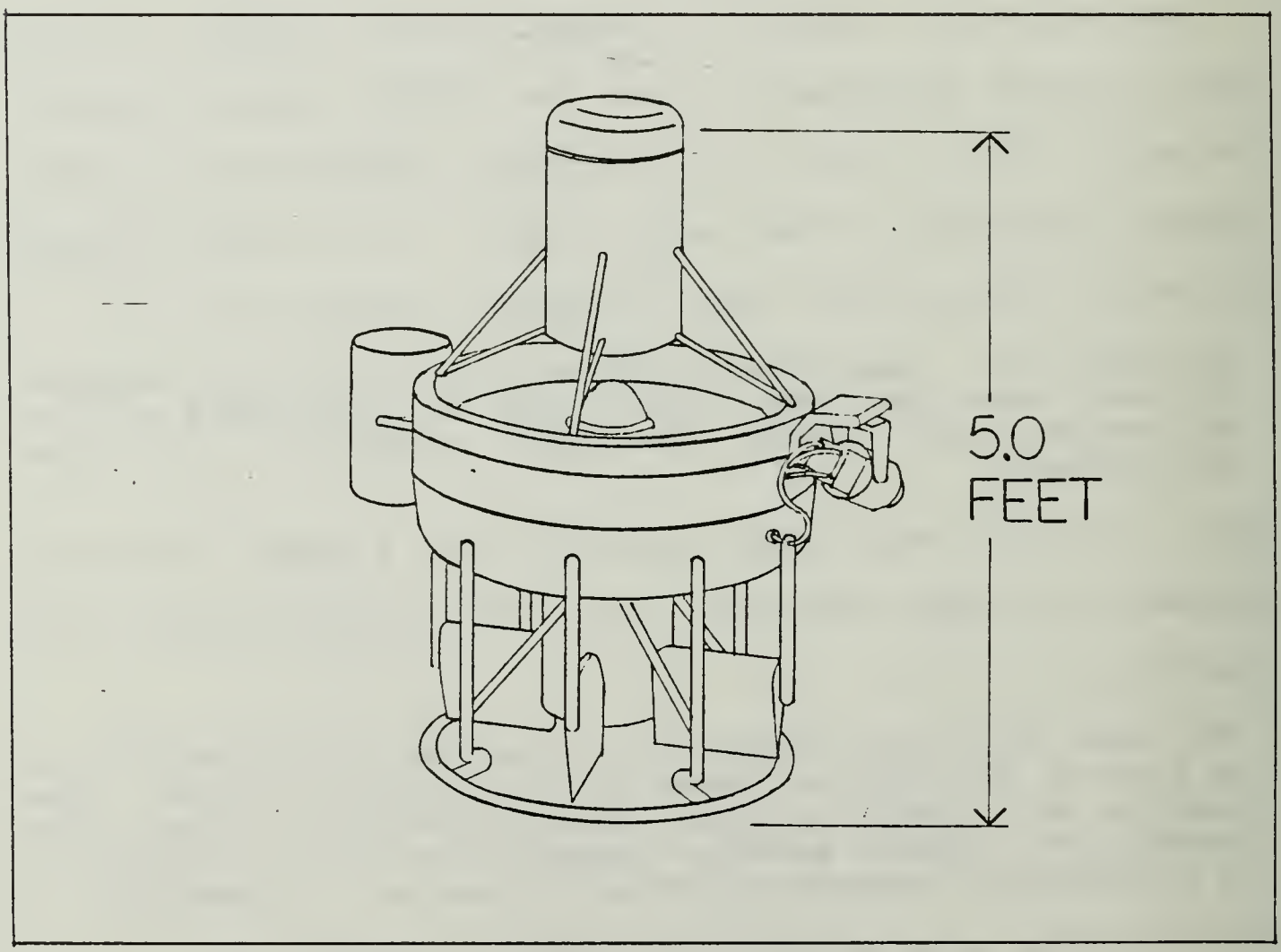

Figure 1.1 Airborne Remotely Operated Device (AROD)

Chapter II discusses the AROD system and the equations which govern its motion. The equations are complex and the system has multiple inputs and multiple outputs. One approach to controller design for such a system is to simplify the equations describing the system as much as possible while retaining as much of the system characteristics as possible. This is the method developed herein.

The complex multiple-input, multiple-output AROD system is appropriately addressed using optimal control techniques with the aid of a digital computer [3]. Optimal control, therefore, is the approach taken and developed in this work to solve the problem of stability and control of the AROD.

C. AROD AND RADIO FREQUENCY TRANSMISSIONS

AROD, as previously described, utilizes a fiber optic tether to pass control information and a video signal from on board observation devices. Therefore, the need for radio frequency (RF) transmissions to or from the vehicle is not immediately obvious. In fact, under ideal tactical conditions, the RF signature, susceptible to hostile electronic countermeasures, would be a most undesirable characteristic for a flying vehicle to have. Nevertheless, the fiber optic tether will be subject to damage and a back-up system must be considered for vehicle control, and for sending back the video signal as well. Most importantly, training must be conducted prior to any conflict or situation in which AROD

is to be used. The fiber optic cable, not immediately reusable by the lower echelon ground forces, is expensive and, again, susceptible to damage. Therefore, it is desirable to provide a low cost method for training operators and tactical commanders in the use of the AROD; hence the need for an alternative to a fiber optic tether.

A back-up RF communications link to provide operator commands to the AROD has already been designed and implemented. However, this is an uplink only and provides no means for the on board cameras to return their wide bandwidth video signal to the ground station. Some consideration of this need has been made in the GATERS program and a transmission frequency in the 800 to 900 megahertz range has been tentatively approved.[2] It has also been recognized that a video signal via RF might be adequate even though it was somewhat degraded relative to the high bandwidth video signals possible with fiber optics. With these assumptions in mind, Chapter IV deals with the design of an on board antenna suitable for transmitting a video signal from AROD to the ground station.

D. SCOPE

In summary, this work will address two different problems associated with AROD:

(1) Design of a control system for stable flight.

(2) Design of a radio frequency antenna for the AROD.

1. Controller Design

System design of the vehicle has been previously undertaken by AROD project engineers. The prototype AROD has been built and pertinent information is listed in Appendix A. In Chapter II, the model describing AROD is developed. Design of the proposed control system is undertaken in Chapter III.

2. Antenna Design

Chapter IV deals exclusively with design and analysis of an RF antenna proposed for AROD. The design approach is to analyze the requirements and determine a basic design which can be refined gradually until an acceptable solution is found. The computer program Numerical Electromagnetics Code (NEC), developed by the Naval Ocean Systems Center is used extensively to aid in the design. No attempt is made to recommend specific hardware components in order to implement the antennas.

II. AROD DYNAMIC SIMULATION

The theory behind the equations governing aerodynamic flight is well developed. Procedures exist which make the modelling of complicated, multiple engine, highly maneuverable aircraft almost a step by step task. Unfortunately, the dynamics which characterize AROD differ considerably from the standard flight model at a very basic level. Like all flying vehicles, AROD has six degrees of freedom of motion: three linear displacements and three angular rotations, but here the similarities end. This ducted fan device has no lift producing surfaces other than the propeller which accounts for 100 percent of its lift and 100 percent of its complexity. This chapter traces the development of a suitable dynamic model of the AROD, concentrating first on the significant gyroscopic contribution of its propeller, and then on the complete vehicle. The goal is to provide a computer simulation with which an experimental control algorithm may be integrated for the purpose of analysis and improvement. [4:pp.2-22]

A. THE GYROSCOPIC AROD

AROD is a gyroscope. The single propeller rotates about the longitudinal vehicle axis to produce a downwash or jet

of air through the duct which makes up the AROD body. This jet is directed by pitching the body forward, backward, or side to side so that the vehicle moves away from the jet in the direction desired. To appreciate the control effort required to pitch the vehicle in a specific direction without causing undesired effects (coupling) in the other five degrees of freedom, the equations governing a gyroscope need to be understood.

Figure 2.1 pictures a gyroscope which rotates in the same plane as the AROD propeller relative to the coordinate system described. This axis orientation will also serve to define symbols for later use. For illustration, the body-fixed and earth-fixed axes do not coincide in Figure 2.1. X,Y,Z and P,Q,R are the body-fixed descriptive geometry for linear displacement and angular rotation rate. P,Q, and R will also be referred to as roll, pitch, and yaw. X',Y',Z' and φ,Θ,ψ, are the corresponding earth-fixed displacements and rotations. X' can be thought of as altitude. φ,Θ, and ψ are the Euler angles. Velocities will be denoted by U,V, and W for rate of displacement in the X,Y, and Z directions, and U',V',W' for X',Y',Z'. Pictured also for use in later discussion are L,M,N (rolling, pitching, and yawing moments) and F_x, F_y, F_z (applied force components).

Angular momentum, h, due to the propeller is defined as

$$h_r = I_r \omega_r = i h_{rx} + j h_{ry} + k h_{rz} \qquad (2.1)$$

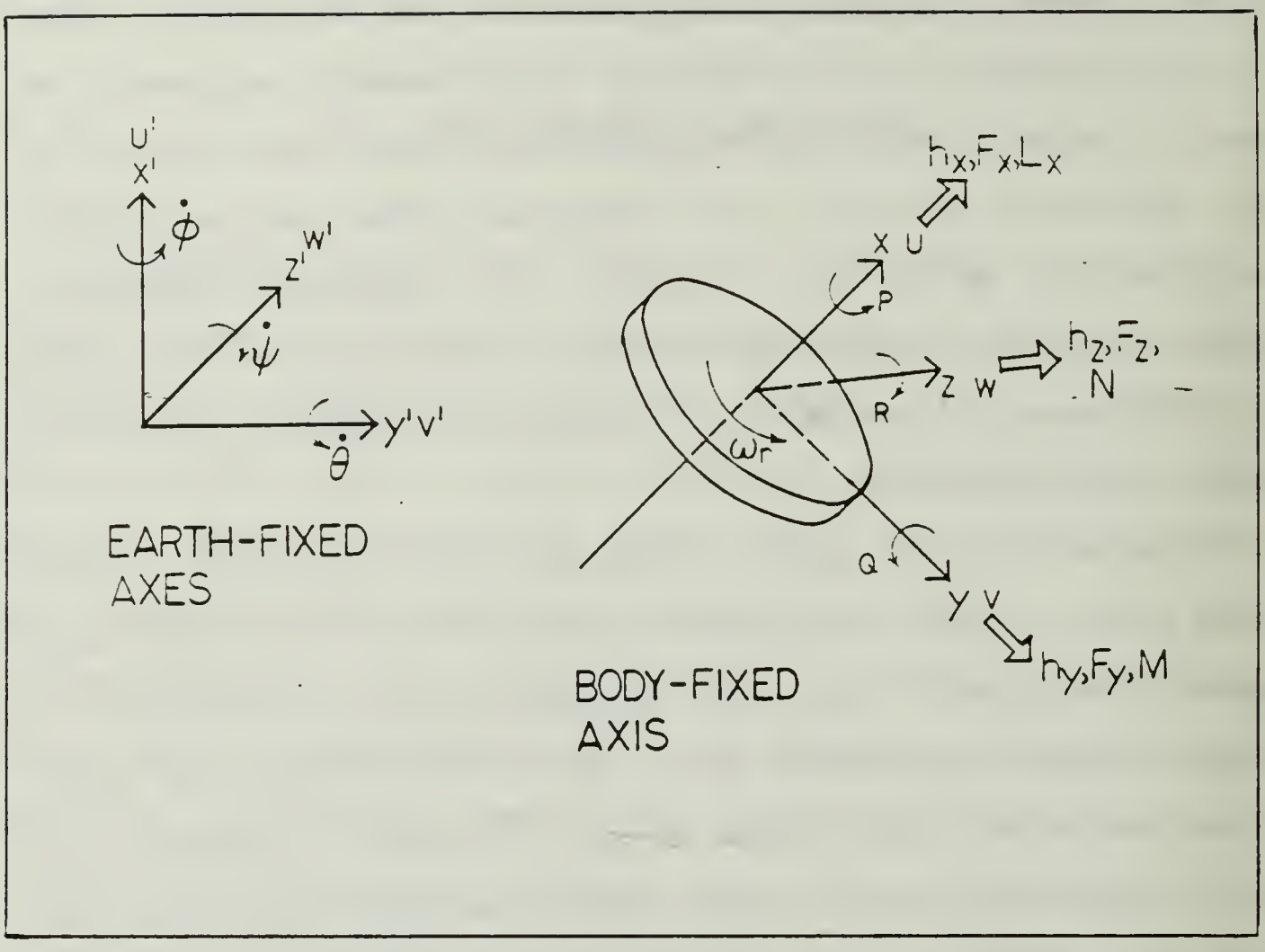

Figure 2.1 Gyroscope and Axes Orientation

The rotor lies in the YZ plane of the body coordinates. Since the coordinate axes have been chosen so that the rotor spins symmetrically about the X-axis, h_r is directed only along X and $h_{ry} = h_{rz} = 0$. Equation 2.1 becomes

$$h_r = I_r \omega_r = i\, h_{rx} \qquad (2.2)$$

At this point, a simple calculation will illustrate the significant influence the rotor has over the AROD. Reference 4 states that in developing the equations of motion for aircraft with rotors which exert gyroscopic moments on the

body "more often than not, such gyroscopic moments turn out to be negligible." In the AROD case, however, I_r = .015 ft^2-lb(mass) and hover speed of the propeller is ω_r = 7200 rpm = 753.98 rad/sec. From Eq. 2.2, h_r = 11.3 ft^2-lb(m)/sec. Compared with a nominal total mass of 2.64 lb(m) (85 lb weight), it is clear that the angular momentum imparted by the rotor is significant and that gyroscopic effects will play a large part in modelling the dynamic behavior of AROD.

Complications arising from these gyro effects can also be illustrated. If the AROD body and rotor are considered a complete gyroscopic system, then the angular momentum of the body must be included in the formulation. Angular momentum due to a rotating body is noted as $h_b = i\,h_{bx} + j\,h_{by} + k\,h_{bz}$. With the orientation of Figure 2.1, Eq. 2.1 becomes

$$h = i\,(h_{bx} + h_{rx}) + j\,h_{by} + k\,h_{bz} \qquad (2.3)$$
$$= i\,(PI_x + I_r\omega_r) + j\,QI_y + k\,RI_z$$

where h is the combined angular momentum of the rotor and body.

Angular moments about the axes of a gyro are discussed in the next section and defined by Euler [5:p. 93] as

$$L = \dot{h}_x - h_y R + h_z Q \qquad (2.4)$$
$$M = \dot{h}_y - h_z P + h_x R$$
$$N = \dot{h}_z - h_x Q + h_y P$$

A simulation of this simple gyro model is given in Appendix B. Results are shown in Figure 2.2 for the case of

a disturbance about the Y axis (pitch). Note that the actual moments of inertia, listed in Appendix A, were used

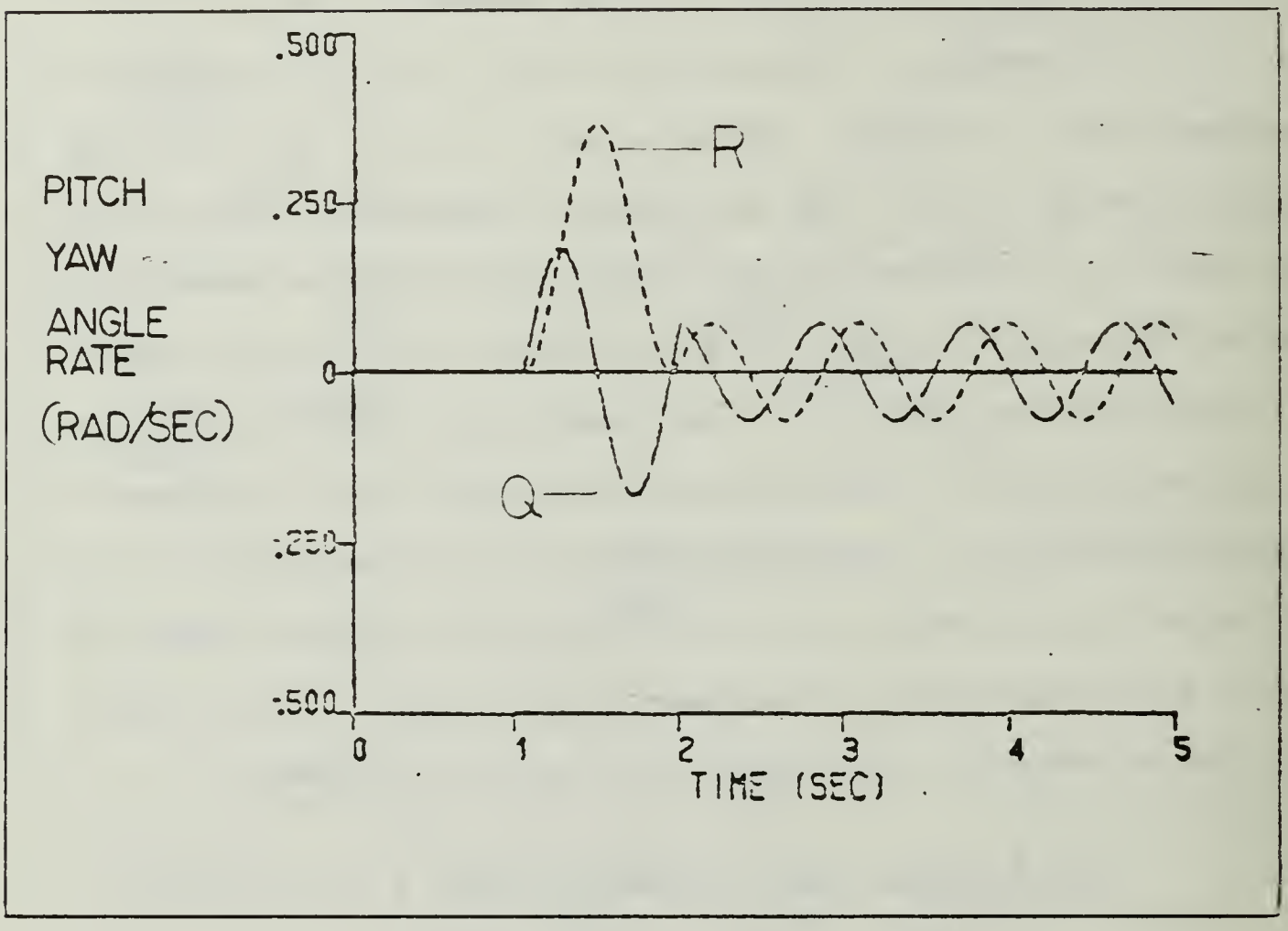

Figure 2.2 Gyroscopic Coupling Effects

in this first step computer simulation. The time response shown here is for the simple case with no rotor acceleration term ($\dot{\omega}_r = 0$) and is the result of a one secon step for an angular moment, M, beginning at time = 1 second. The amplitude is unimportant and has no effect on the time response except to scale the result. The purpose of the input was to pitch over the coordinate system by applying a torque about the Y axis (Q). Ideally, a stable, well

behaved device would simply pitch over and maintain its new attitude. This is not the case for AROD and Figure 2.2 illustrates the precession and nutation due to a severe coupling of the pitch(Q) and yaw(R) axes. These gyroscopic effects, then, are the reason a "simple" device such as AROD presents such a complex controls problem to the designer.

B. EQUATIONS OF MOTION

The basic equations of motion are developed for a typical aircraft in References 4 and 5. A combination of the two approaches is taken here to arrive at the set of equations describing AROD.

The Euler equations of motion for a free flying rigid vehicle with six degrees of freedom are derived from Newton's second law. For angular moments applied to the coordinate axes, we have

$$L = i\frac{dh}{dt} \qquad (2.5)$$

$$M = j\frac{dh}{dt}$$

$$N = k\frac{dh}{dt}$$

where $h = i h_x + j h_y + k h_z$ and is the vehicle's total angular momentum.

For linear or translational forces applied along the axes,

$$F_x = i m\frac{dV}{dt} \qquad F_y = j m\frac{dV}{dt} \qquad F_z = k m\frac{dV}{dt} \qquad (2.6)$$

where $v = iv + jv + kv$ and is the total linear translational velocity of the center of mass(m) of AROD.

The dynamic characteristics of AROD are represented by Equations 2.5 and 2.6. Other relationships are required to solve for each unknown and for each physical force and moment acting on the body. The development of a complete model is undertaken now for the specific case of AROD using actual measurements and experimental data from the prototype.

1. Angular Momentum

Equation 2.4 is expanded to become

$$\dot{h}_x = i\,(I_x\dot{P} + I_r\dot{\omega}_r) + j\,(I_x PR + I_r\omega_r R) - k\,(I_x QP + I_r\omega_r Q) \qquad (2.7)$$

$$\dot{h}_y = -i\,I_y RQ + j\,I_y\dot{Q} + k\,I_y PQ$$

$$\dot{h}_z = i\,I_z QR - j\,I_z PR + k\,I_z\dot{R}$$

where

$$\dot{h} = \frac{\delta h}{\delta t} + \omega \times h$$

$$h = i\,(I_x P + I_r\omega_r) + j\,I_y Q + k\,I_z R$$

$$\omega = iP + jQ + kR$$

Combining Equations 2.4 and 2.7, the AROD angular moment equations are:

$$L = I_x\dot{P} + (I_z - I_y)QR + I_r\dot{\omega}_r \qquad (2.8)$$

$$M = I_y\dot{Q} + (I_x - I_z)PR + RI_r\omega_r$$

$$N = I_z\dot{R} + (I_y - I_x)PQ - QI_r\omega_r$$

The rolling, pitching and yawing moments (L, M, and N) may be induced by the aerodynamics of the body and environment

or by control inputs through the control vanes and are referred to as the "applied moments". They are discussed in a later section. Equation 2.8 is next rearranged so that the unknown variables (dynamic states of interest) may be determined. Roll, pitch, and yaw rates are:

$$\dot{P} = \frac{1}{I_x}[(I_y - I_z)QR - I_r\dot{\omega}_r - L] \qquad (2.9)$$

$$\dot{Q} = \frac{1}{I_y}[(I_z - I_x)PR - RI_r\omega_r - M]$$

$$\dot{R} = \frac{1}{I_z}[(I_x - I_y)PQ + QI_r\omega_r - N]$$

Already obvious is the mathematical explanation for the coupling that was observed in the last section. Every combination of pitch, roll, and yaw are present in Equation 2.9. Pitch, roll, and yaw are each "coupled" to the others. Additionally, coupling of the rotor angular acceleration with roll will cause the throttle controlling the propeller speed to influence these states and further complicate the system.

2. Force Equations

The expressions describing the translational forces are developed from the body accelerations which are

$$\dot{v}_x = i\dot{U} + jRU - kQU \qquad (2.10)$$

$$\dot{v}_y = -iRV + j\dot{V} + kPV$$

$$\dot{v}_z = iQW - jPW + k\dot{W}$$

where $v = iv_x + jv_y + kv_z$ and is the total body velocity vector.

Equations 2.6 and 2.10 are combined and rearranged to obtain the differential equations containing force terms,

$$\dot{U} = (RV - QW) + \frac{F_x}{m} \qquad (2.11)$$

$$\dot{V} = (PW - RU) + \frac{F_y}{m}$$

$$\dot{W} = (QU - PV) + \frac{F_z}{m}$$

where m is the mass of the vehicle.

Equations 2.11 contain nonlinear terms as did Equation 2.9. These nonlinearities are in the form of products of states. The force components F_x, F_y, F_z consist of lift from the propeller (F_t), other aerodynamic influences (F_a), and gravity (g). F_t and F_a depend largely on experimental data in this development and are taken up later.

Gravity is a constant acceleration causing a constant force in the -X' direction (earth-fixed). Note that small changes in weight due to fuel loss are neglected. As the body rotates, the body-fixed axes change relative to the earth-fixed axes. Therefore, a coordinate translation is needed to relate gravity to each of the X,Y,Z axes (g_X, g_Y, g_Z). The gravity components are given by

$$i'g = i g_x + j g_y + k g_z \qquad (2.12)$$

Any translation from earth-fixed to body-fixed axes can be described by a rotation first about the Euler angle φ, then

Θ, and lastly ψ. Figure 2.3 illustrates these three rotations and the resulting relationships between coordinate systems. From Figure 2.3 and Eq. 2.12, the gravity components are

$$g_x = g(\cos\psi \cos\Theta) \qquad (2.13)$$

$$g_y = -g(\sin\psi \cos\Theta)$$

$$g_z = g(\sin\Theta)$$

The first-order differential equation for translational velocities can now be written as

$$\dot{U} = (RV - QW) + g_x + \frac{F_x}{m} \qquad (2.14)$$

$$\dot{V} = (PW - RU) + g_y + \frac{F_y}{m}$$

$$\dot{W} = (QU - PV) + g_z + \frac{F_z}{m}$$

We now have equations describing the six degrees of freedom of AROD and the foundation for the model has been laid.

3. Kinematic Equations of Motion

The coordinate translation through the Euler angles φ,Θ,ψ resulted in an expression for relating gravity to the rotating body. However, the price paid for this necessary convenience is the addition of three more variables (φ,Θ,ψ) to the equations. Therefore, three more equations are needed and, if possible, the three variables φ,Θ,ψ should be expressed in terms of the existing force or moment variables. Fortunately a relationship can be found in the

Figure 2.3 Earth to Body-Fixed Coordinate Transformation

equation describing the body angular rotations. Angular movement of AROD has been expressed in terms of the body-fixed angular rates P,Q,R. It can also be described in terms of the Euler rates φ, Θ, and ψ as

$$\omega = iP + jQ + kR = i'\dot{\varphi} + j'\dot{\Theta} + k'\dot{\psi} \qquad (2.15)$$

A coordinate transformation similar to the one illustrated in Figure 2.3 is possible to relate pitch, roll, and yaw with the Euler angle rates. However, some simplifications can be made with each rotation since φ,Θ,ψ are, in fact, the variables of interest. The resulting transformation is called the kinematic equations of motion:

$$\begin{bmatrix} \dot{\varphi} \\ \dot{\Theta} \\ \dot{\psi} \end{bmatrix} = \begin{bmatrix} 1 & \sin\varphi & \cos\varphi\tan\Theta \\ 0 & \cos\varphi & -\sin\varphi \\ 0 & \frac{\sin\varphi}{\sin\Theta} & \frac{\cos\varphi}{\cos\Theta} \end{bmatrix} \cdot \begin{bmatrix} P \\ Q \\ R \end{bmatrix} \qquad (2.16)$$

4. Summary of Equations of Motion

Nine equations and nine unknowns have been developed that completely describe the dynamic behavior of AROD. P,Q,R, and U,V,W represent the six degrees of freedom and φ,Θ,ψ, relate the constant force exerted by gravity to the body-fixed coordinates. Through the Euler angles, the behavior of AROD can also be observed relative to the Earth. Specifically, the translational velocities for the earth-fixed system U',V',W' can be determined from body-fixed velocities U,V,W and φ,Θ,ψ using the coordinate transforma-

tion of Equation 2.13. The applied forces and moments are made up of external forces and commanded inputs, and are represented by F_x, F_y, F_z, and L, M, N. AROD can be pictured as the block diagram in Figure 2.4. The external influences are taken up next.

C. APPLIED FORCES AND MOMENTS

The applied forces and moments are a result of the commanded inputs and the movement of AROD through the air. The commanded inputs can change the rotor speed causing a change in the lift generated and a torque on the body. Commands can also come in the form of control surface displacements which steer the AROD and cause the body to rotate about its axes. The movement of AROD through the air will create drag. Drag forces can also apply both translational forces and angular moments on the body and are a result of AROD's aerodynamic characteristics.

1. Aerodynamic Characteristics

Two methods exist for determining the aerodynamic forces and moments on a vehicle [4:p.111]: (1) by experiment or empirical analysis and (2) by theoretical development. The great advantage of (1) is accuracy and the advantage of (2) is low cost. The fact that AROD is a ducted fan causes a complex interaction of the rotor with the body, and the downwash with the control surfaces. Hence, the ducted fan compounds the accuracy problem and empirical means for

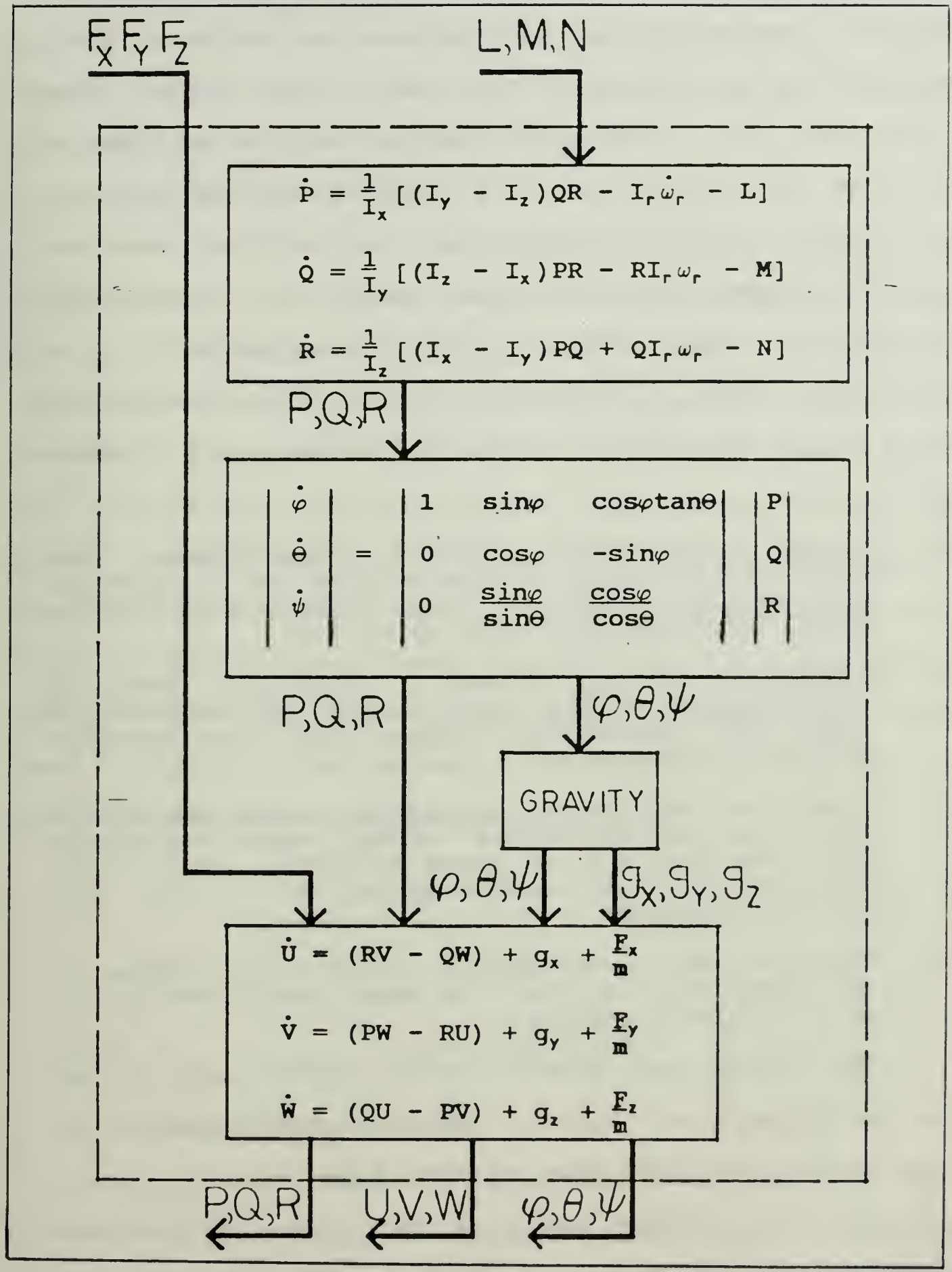

Figure 2.4 Block Diagram of AROD Equations of Motion

determining the forces and moments is the most suitable approach. Sandia National Laboratories has built a prototype AROD and has collected data based on wind tunnel tests of the AROD [6]. This data consists of tabular results describing the aerodynamic drag coefficients and downwash swirl effect; stability derivatives; and physical measurements of constants such as weight, moments of inertia, and servo gains. This data is listed in Appendix A. The tabular data forms a basis from which applied forces and moments may be determined once the following flight information is known:

(1) Weight ratio of actual AROD to 85 lb prototype. The data was originally obtained with an 85 lb prototype and must be scaled for other weights such as the model discussed here which is 76.5 lb.

(2) Propeller angular speed. Propeller speed is determined by setting a hover speed (this model 7200 rpm) and calculating changes from the throttle setting of the engine.

(3) Propeller angular acceleration. Acceleration is based on the difference between speed calculated from the throttle and speed at hover. This is an experimental approximation arrived at by AROD project engineers.

(4) Translational speed U,V,W. Aerodynamic forces on the body are based on the speed and direction of AROD (angle of attack).

The forces and moments which result are of two types: aerodynamic and thrust. The forces and moments due to the aerodynamic data are referred to as F_{ax}, F_{ay}, F_{az}, and L_a, M_a, N_a. Those due to thrust and propeller considerations are F_{tx}, F_{ty}, F_{tz}, and L_t, M_t, N_t.

No attempt is made in this work to verify the data. The relationships leading to the forces and moments discussed in this section are taken verbatim from the information supplied by AROD project engineers.

a. Angle of Attack

The tabular data (aerodynamic drag coefficients and downwash swirl) result in forces and moments relative to the total velocity vector, V_{tot}, of the body. A relationship is needed to transform these forces and moments to body-fixed axes forces and moments. Angles of attack (α,β) are the standard relationship for this purpose. Angle of attack (α) is normally defined as the angle in the XZ plane between V_{tot} and the X axis. Angle of attack (β) is the angle in the XY plane between V_{tot} and the X axis (sometimes referred to as the side slip angle).[4] The angle of attack used in this model is defined and illustrated in Figure 2.5. The resulting relationships are given by

$$\sin\alpha = \frac{W}{V_{tot}} \qquad (2.17)$$

$$\sin\beta = \frac{V}{V_{tot}}$$

where $$V_{tot} = \sqrt{U^2 + V^2 + W^2}$$

b. Aerodynamic Forces

The forces associated with the tabulated data are lift (F_l), drag (F_d), and side force (F_s). They are also depicted in Figure 2.5. The transformation from lift,

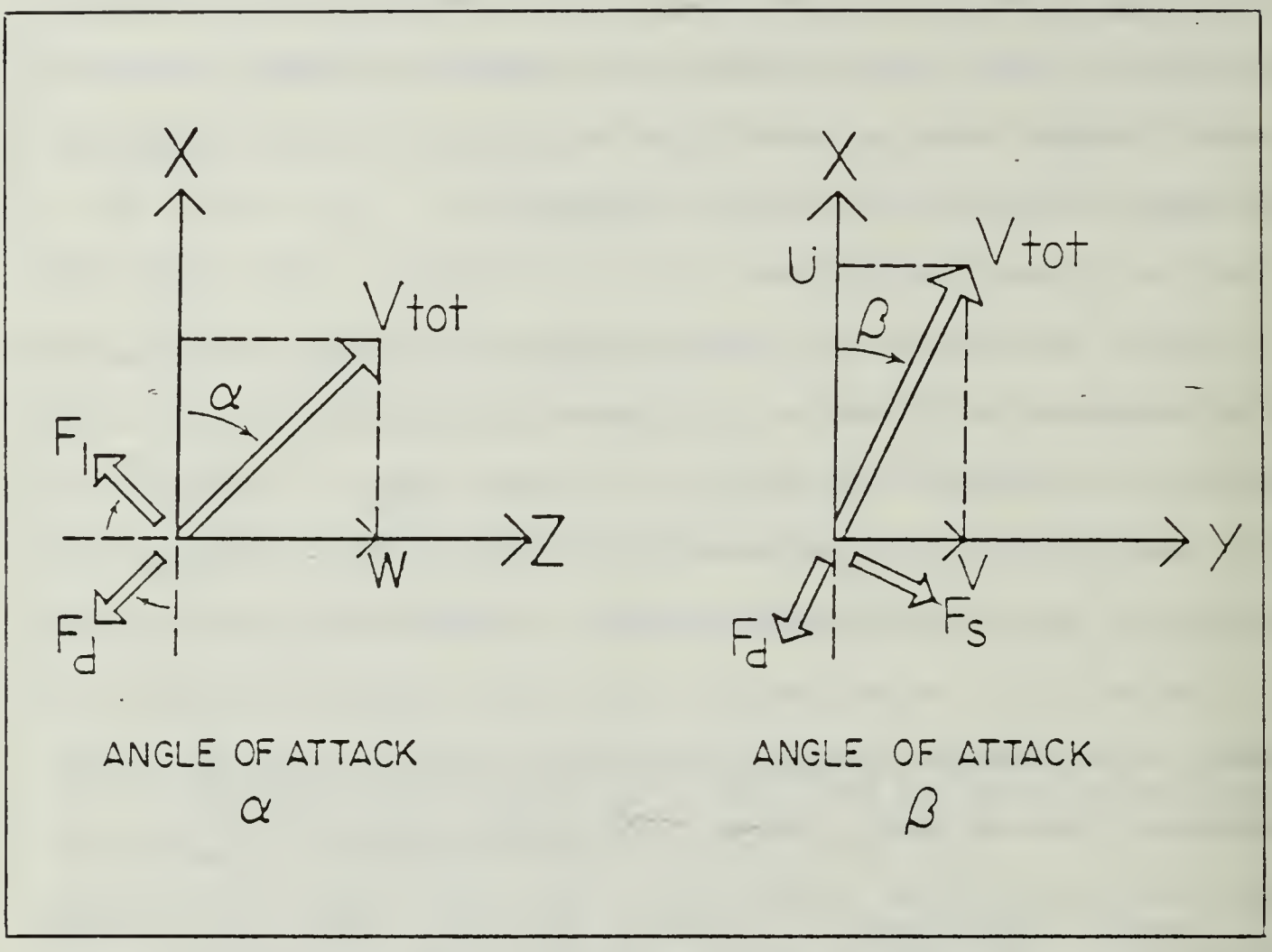

Figure 2.5 Angle of Attack Illustration

drag, and side force is accomplished in like manner to the transformation in Figure 2.3 and results in

$$\begin{bmatrix} F_{ax} \\ F_{ay} \\ F_{az} \end{bmatrix} = \begin{bmatrix} \sin\alpha\cos\beta & -\cos\alpha\cos\beta & \sin\beta \\ -\sin\alpha\sin\beta & \cos\alpha\sin\beta & \cos\beta \\ -\cos\alpha & -\sin\alpha & 0 \end{bmatrix} \begin{bmatrix} F_l \\ F_d \\ F_s \end{bmatrix} \qquad (2.18)$$

c. Aerodynamic Moments

In similar fashion to the aerodynamic forces, the moments applied to the body axes as a result of AROD's movement through air can be derived. These moments are

referred to as the aerodynamic angular moments of roll, pitch, and yaw (L_a, M_a, N_a) and are given as

$$\begin{bmatrix} L_a \\ M_a \\ F_a \end{bmatrix} = \begin{bmatrix} \sin\alpha\cos\beta & -\cos\alpha\cos\beta & \sin\beta \\ -\sin\alpha\sin\beta & \cos\alpha\sin\beta & \cos\beta \\ -\cos\alpha & -\sin\alpha & 0 \end{bmatrix} \begin{bmatrix} Y_y \\ R_r \\ P_p \end{bmatrix} \qquad (2.19)$$

where

Y_y is the yaw moment relative to V_{tot},
R_r is the roll moment relative to V_{tot},
P_p is the pitch moment relative to V_{tot}.

2. Forces and Moments for Control

The forces and moments previously discussed are based on observation of an AROD prototype and are external to the system being designed. A second category is those forces and moments which are a direct result of the commanded inputs. As mentioned earlier, the inputs control (1) the rotor speed and (2) the displacement of the control surfaces.

a. Moment Due to Ducted Fan Effects

The AROD in hover (constant rotor speed) closely resembles a gyroscope. A gyroscope imparts no torque on its axis if it spins with a constant angular rotation. If the rotor accelerates (speeds up or slows down) a torque is applied to the axis. This torque is accounted for in Equation 2.8. However, AROD is also a ducted fan and the drag between the rotor tip and the inside body wall creates a moment about the X axis (P, roll). The project engineers

for AROD have determined an approximation for this moment based on experiment which is given as

$$L_{Tr} = .0729\ (\Delta\omega_r^2) \quad \text{(ft-lbs)} \qquad (2.20)$$

where $\Delta\omega_r$ is the difference between the rotor speed and hover, Subscript Tr refers to a dependence on the throttle, and .0729 is a constant due to the duct and is referred to as K_{duct} in Appendix A.

b. Moments Due to Control Surface Displacement

Command inputs also include the ability to displace the four control vanes into the downwash from the duct. As these surfaces are displaced, they impart moments about the body axes. The vanes are arranged symmetrically as in Figure 2.6. The vanes are displaced by a servo mechanism connected directly to the top of each surface. Vanes (1) and (3) are operated together as "elevators" and impart a moment about the Y-axis (pitch). Vanes (2) and (4) together are the "rudder" and contribute a moment about the Z-axis (yaw). Vanes (1) and (3) displaced in opposite directions and (2) and (4) displaced oppositely work as "ailerons" to impart a moment about the X-axis (roll). Throughout this work, the term aileron, rudder, and elevator will be used as defined here. The actual torque applied by each combination of vanes was determined experimentally and "constants of effectiveness" were calculated by the AROD project engineers.

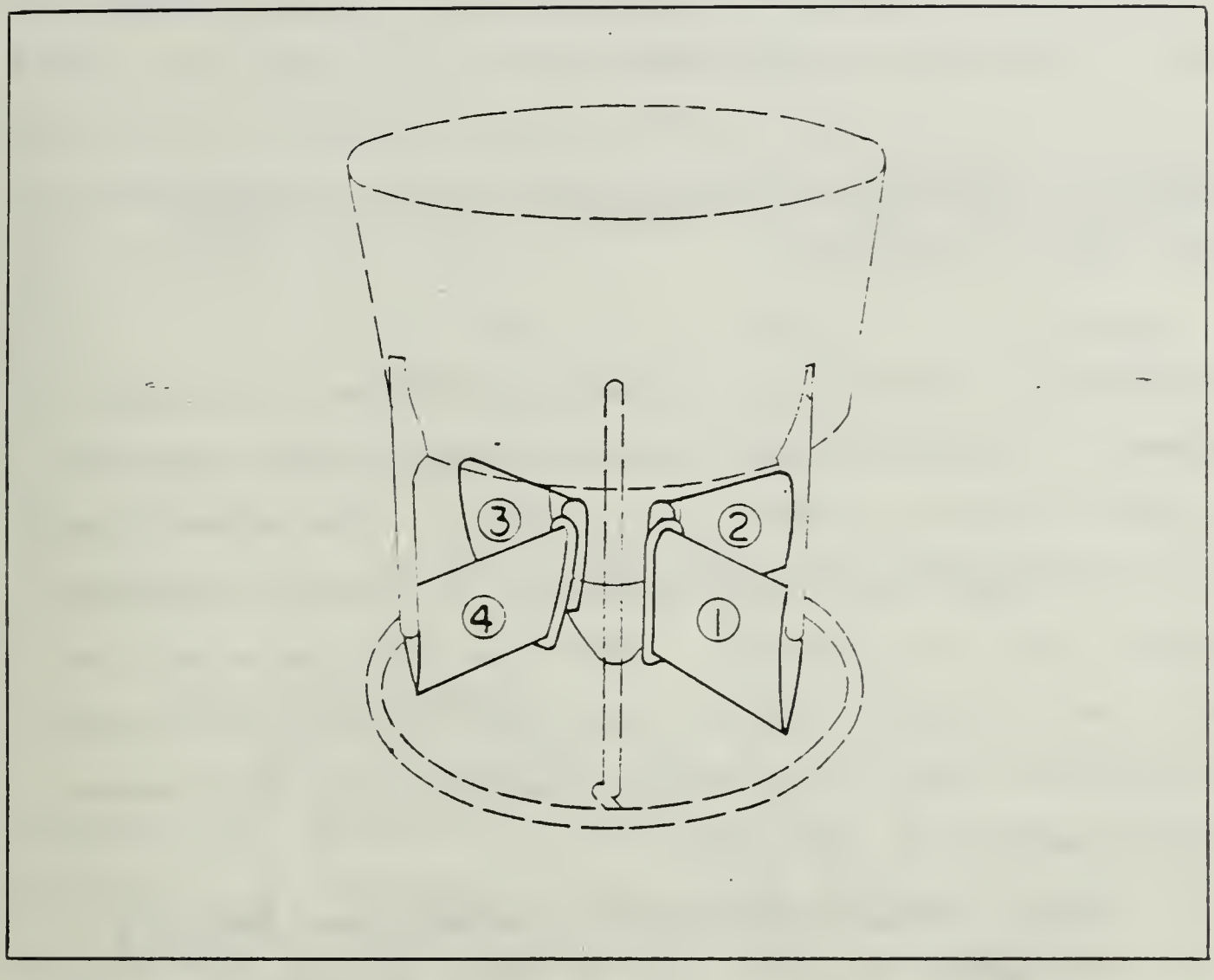

Figure 2.6 AROD Control Vanes

The constants of effectiveness are referred to as dimensional stability derivatives when developed theoretically. They are given the symbols $L_{\delta e}$, $M_{\delta e}$, $N_{\delta e}$, for their contribution of moments about the roll, pitch, and yaw axes due to a displacement by the ailerons, elevators, and rudder. They can be thought of as acceleration quantities per radian of control surface displacement. The resulting relationships, concluding in moments about the three body axes, are

$$L_t = L_{ae}\delta_a \qquad (2.21)$$

$$M_t = M_{ee}\delta_e$$

$$N_t = N_{re}\delta_r$$

where δ is the displacement of the aileron, elevator or rudder into the rotor downwash. L_{ae}, M_{ee}, and N_{re} are given in Appendix A.

Theoretically, each set of control surfaces will yield a constant of effectiveness about each axis (three constants for each aileron, elevator, and rudder). The symmetry of AROD causes negligible cross coupling of control surfaces, however, and it is ignored. Note also that the effectiveness of each control vane was determined for one rotor speed and that the change in downwash associated with the changes in rotor speeds is also ignored.

3. Servo Equations for Control Surfaces and Throttle

Commanded inputs sent to AROD include "go forward/backward", "go side to side", "turn around", and "go up/down". These commands can be satisfied by pitching the AROD forward or sideways (pitch and yaw) for translational flight, turning the AROD about its centerline (roll) for turning about, and changing the propeller speed for altitude control (throttle). Second order servo motors are used to displace each control vane as well as the throttle.

a. Control Surface Servos

The servos for each control surface are identical. Three equations will describe the operation of the

elevators, rudders and ailerons. For each of these equations, at least two servos are actually operating at the same time on different control vanes. Each servo receives a command input (voltage) and results in an angular position for the servo.

$$\ddot{\delta}_a = -H_1\dot{\delta}_a - H_2\delta_a + H_2 u_a \qquad (2.22)$$

$$\ddot{\delta}_e = -H_1\dot{\delta}_e - H_2\delta_e + H_2 u_e$$

$$\ddot{\delta}_r = -H_1\dot{\delta}_r - H_2\delta_r + H_2 u_r$$

where

H_1 and H_2 are servo gain constants,
u_a, u_e, and u_r are the servo input.

b. Throttle Servos

The servo motor used to open and close the throttle is identical to the ones used for the control surfaces. An additional first order system describes the relationship between the throttle position and the power delivered to the rotor (thrust, T_r). The complete third order system is

$$\ddot{\delta}_t = -H_1\dot{\delta}_t - H_2\delta_t + H_2 u_t \qquad (2.23)$$

$$\dot{T}_r = -T_r + .5(\delta_t)$$

The power delivered to the rotor, T_r, directly relates to both the change in rotor speed, $\Delta\omega_r$, and the force in the X direction. These relationships are

$$\Delta\omega_r = T_r * Pr_{ef} \qquad (2.24)$$

$$\Delta F_{tx} = T_r$$

where Pr_{ef} is a constant relating the rotor speed to the power delivered by the engine.

D. ASSEMBLING THE MODEL: PROGRAMMING

In this section, the equations of motion and the force/moment relationships are represented in a block diagram of the AROD model developed earlier, and the flow chart used to program the model is illustrated.

1. The Complete Block Diagram

Figure 2.7 is a block diagram of the complete model. For a more detailed explanation of the experimental aerodynamic forces and moments, Appendices A and B should be consulted.

2. Program Flow Chart

The logic flow chart developed to program the equations and the aerodynamic data is pictured in Figure 2.8. The IBM Dynamic Simulation Language (DSL/VS) source code used is given in Appendix B [7].

E. SIMULATION RESULTS

Graphical illustration of time response is shown here. The four inputs u_a, u_e, u_r, and u_t are applied alternately as step inputs to the AROD model. A caution to the reader interpreting these results is appropriate here. The body-fixed angle rates P, Q, and R are the dynamic states of interest in the control problem. Emphasis should be placed on the response of <u>these</u> rates to control input and <u>not</u> on the earth-fixed Euler angles φ, Θ, and ψ. The Euler angles are shown here only as a reference for the reader who wishes

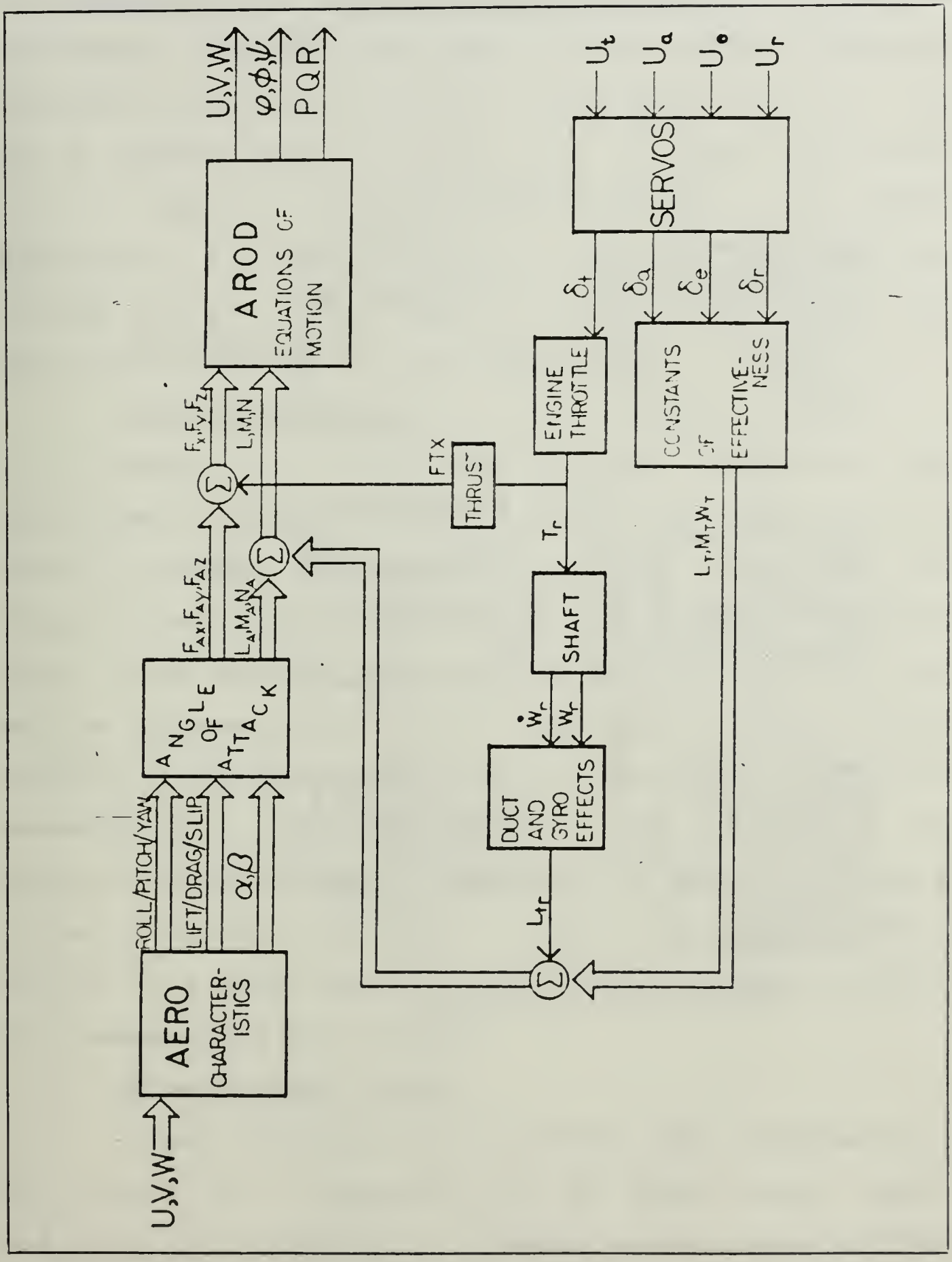

Figure 2.7 AROD Model Block Diagram

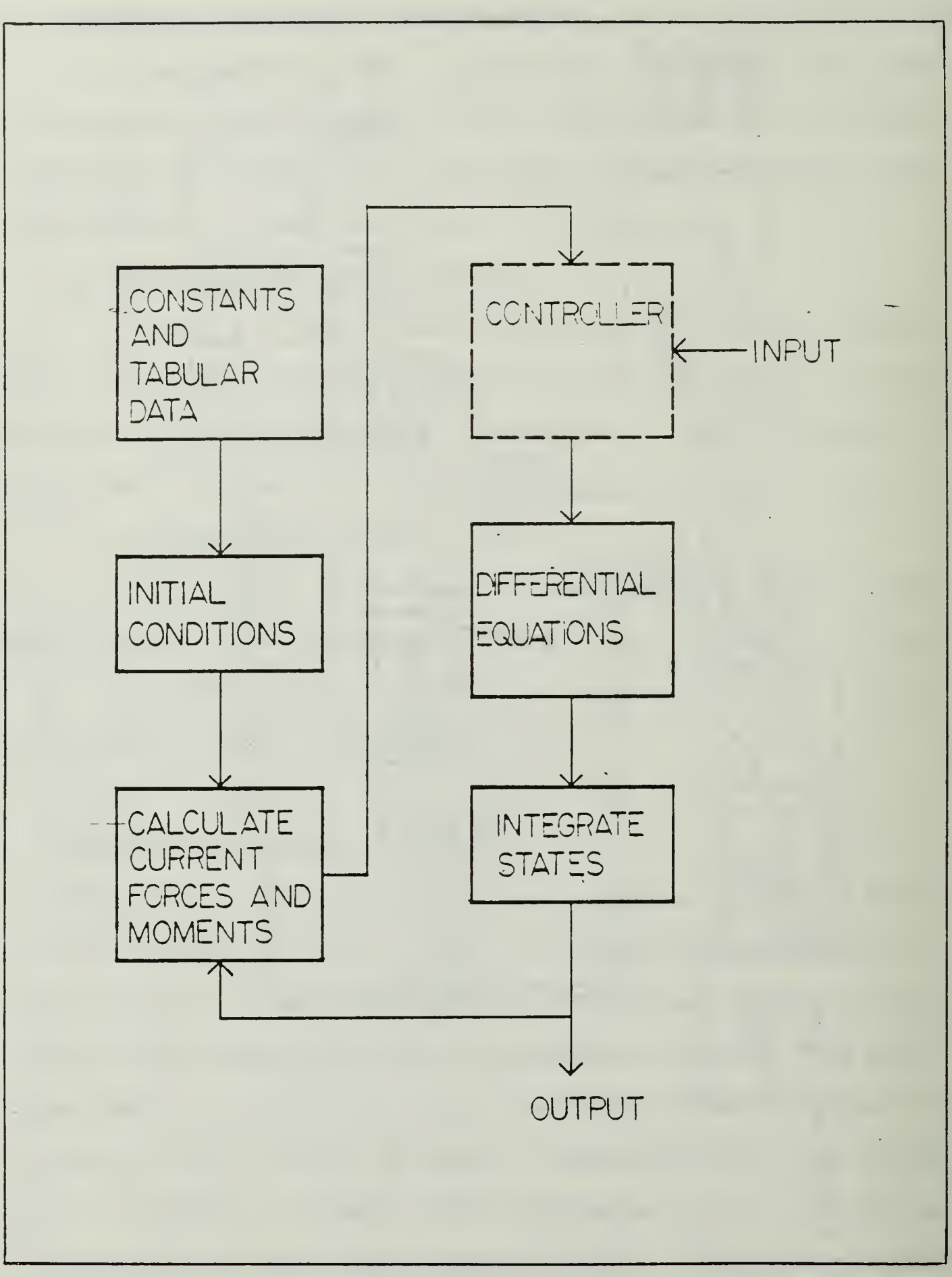

Figure 2.8 AROD Simulation Logic Flow Chart

to picture what the vehicle's behavior would be relative to the Earth. Confusion can result if one tries to directly associate these angles with the roll, pitch, and yaw. By way of example (refer to Figure 2.1), the time derivatives of φ, Θ, and ψ are equal to roll(P), pitch(Q), and yaw(R) only when $\varphi = 0$ and Θ and ψ are small. If the body has rotated 90° ($\varphi = 90$), then Q actually approximates the derivative of ψ and R the derivative of Θ.

1. Zero Input Response

Figure 2.9 is the resulting time response of the model when all control inputs are zero. For zero input, all control surfaces are parallel with the X-axis and not displaced into the downwash. The throttle is set for hover speed. Note that the pitch and yaw axes remain stable and zero as expected, but the roll axis spins opposite to the rotation of the propeller. This precession is a result of downwash swirl which was measured and included in the tabular aerodynamic data. The propeller downwash is not a linear flow of air but has a pattern of vortices which results in a force applied to the control surfaces leading to a moment about the roll axis.

2. Aileron Input

Figure 2.10(a) is the resulting time response when the aileron (δ_a) is displaced and all other control inputs are zero as in Figure 2.9. Figure 2.10(a) indicates that the ailerons can be positioned to counteract the swirl

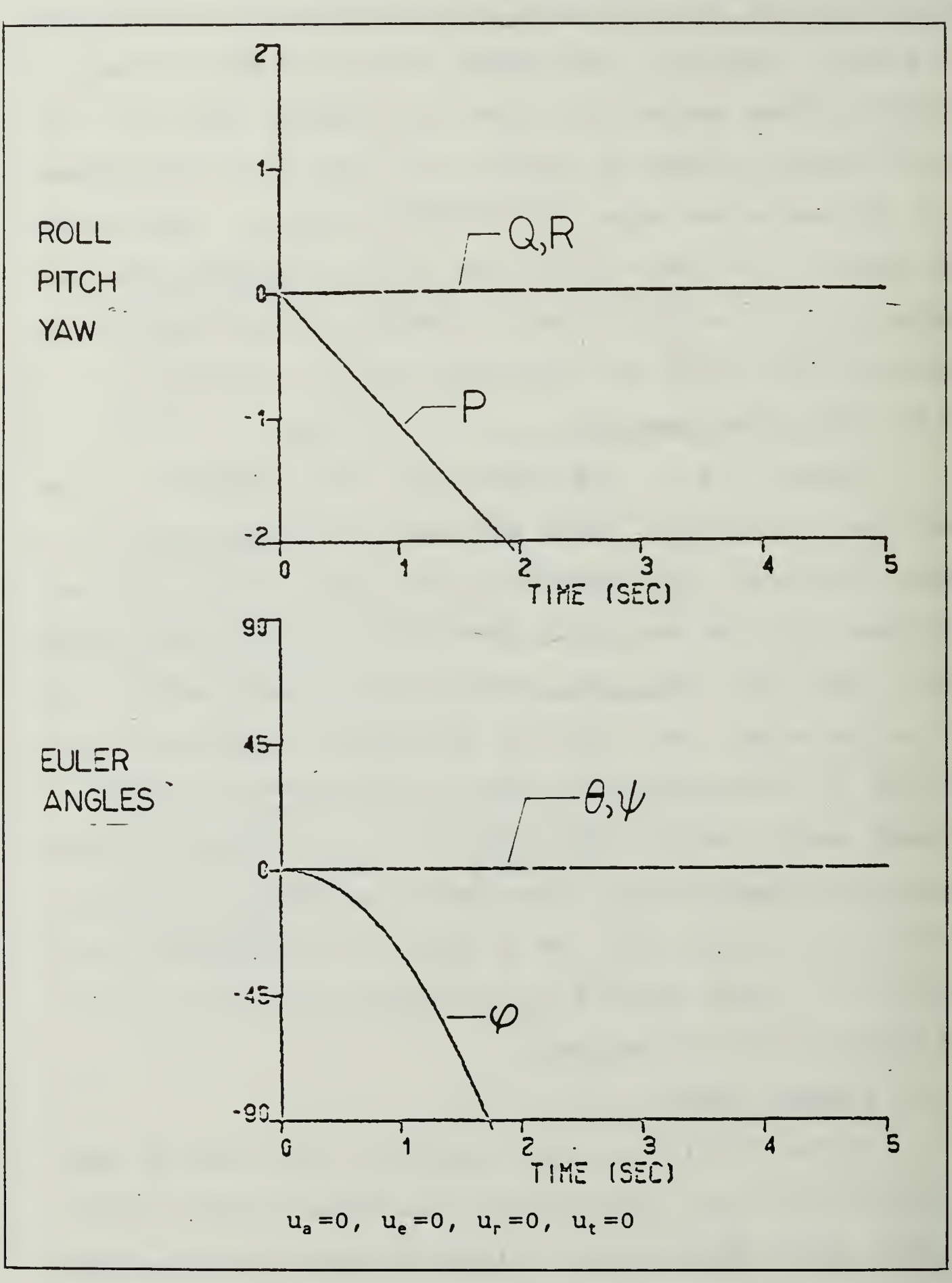

Figure 2.9 Time Response to Zero Input

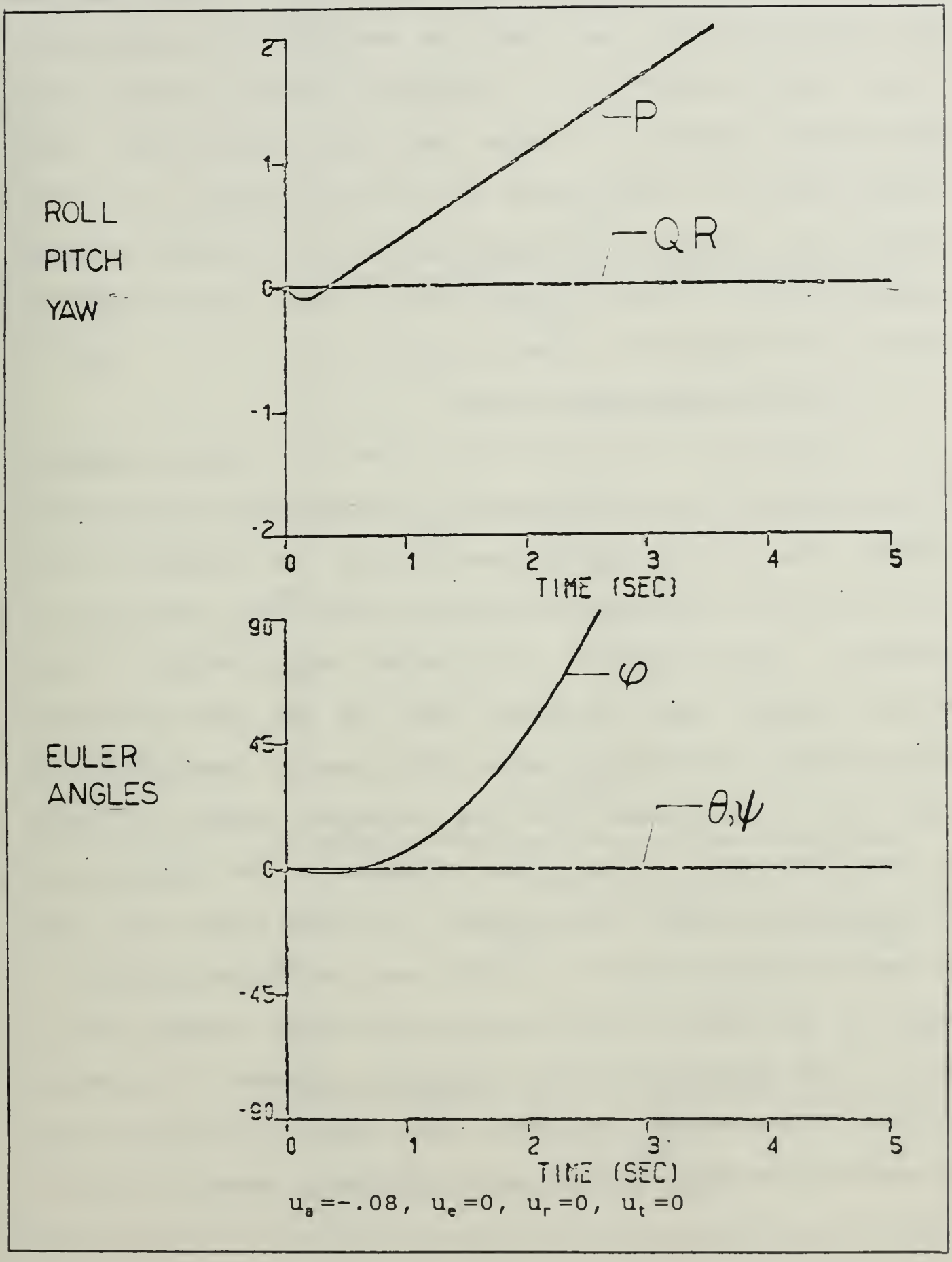

Figure 2.10 (a) Time Response to Aileron Input

effect and actually roll the AROD oppositely. These results also affirm that the roll axis is uncoupled from the pitch and yaw axes as Equation 2.9 suggests. Figure 2.10(b) is an illustration intended to show that the roll can be controlled and set to zero when no roll is desired. In this example, an initial displacement of $\delta_a = -.0499$ on the aileron control vanes is used and a bias equal to this initial displacement is added to u_a.

3. Elevator and Rudder Input

Figure 2.11 is the result when the rudder combination of vanes (δ_r) is displaced into the downwash and the ailerons are set as in Figure 2.10(b) to minimize roll. Note the severe coupling between the pitch and yaw axes, as expected. This coupling is a major complication to the control process and is dealt with in the next chapter. Figure 2.12 is the result when the elevator combination of vanes (δ_e) is displaced into the downwash, rudder is reset to zero, and the ailerons set as above. The results are similar to the rudder observations. In both cases, the roll has been affected by the pitch and yaw disturbances, a result of the tabular aerodynamic data which changes with α and β. The amplitude of the elevator, however, is greater than the illustration with the rudder and more clearly shows the serious problems that these aerodynamic moments present.

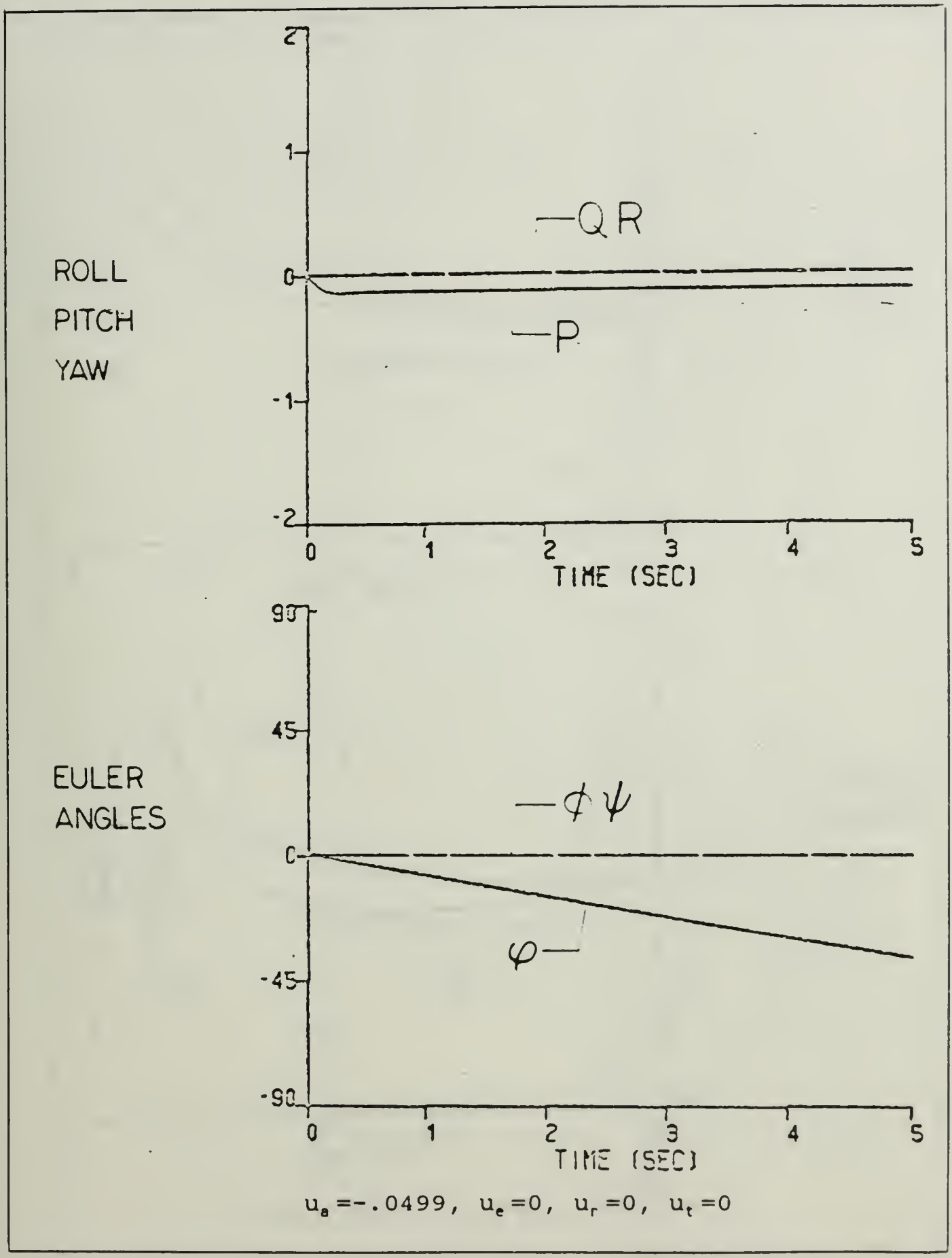

Figure 2.10 (b) Time Response: Aileron Displaced to Eliminate Swirl Effect

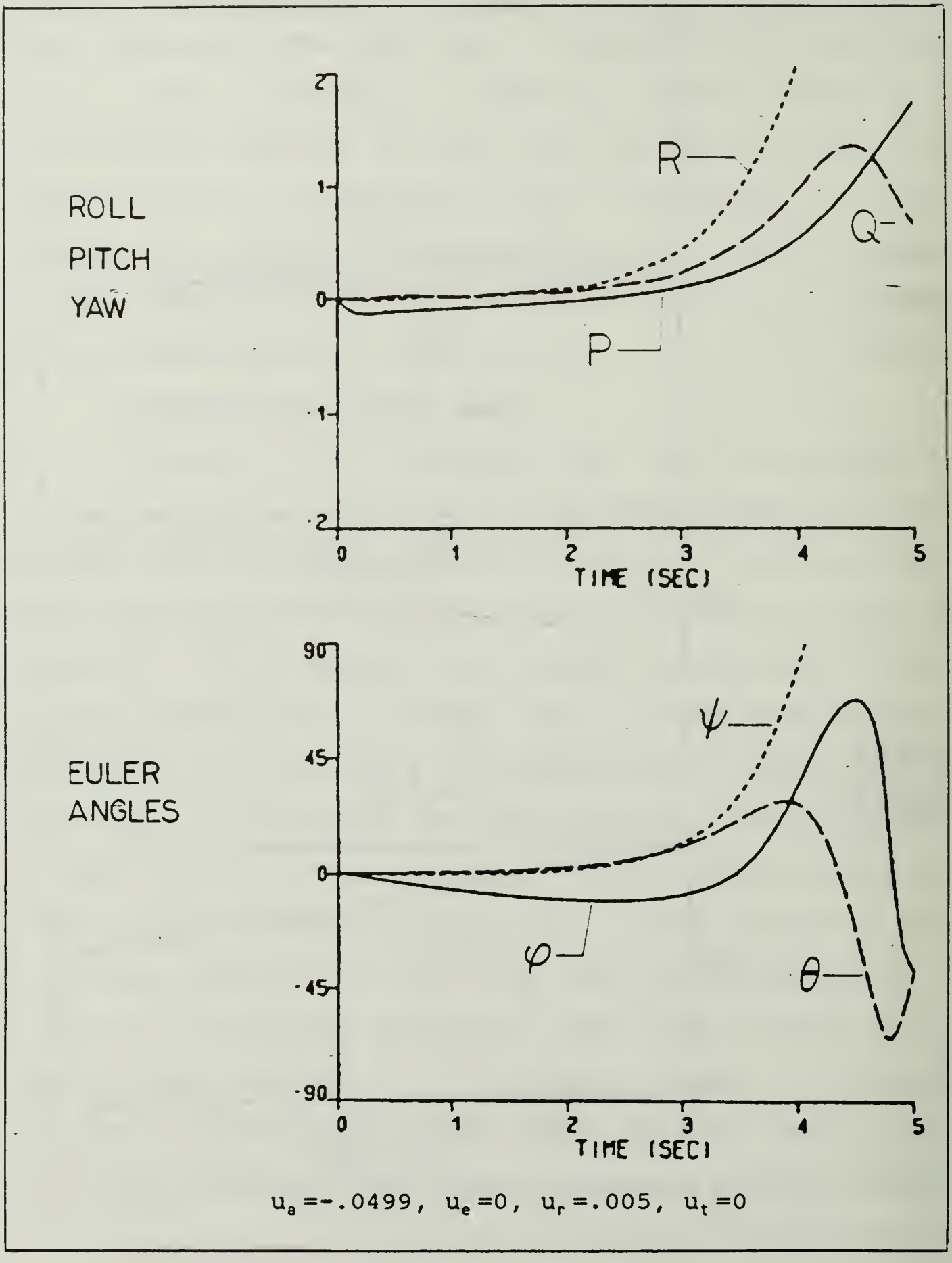

Figure 2.11 Time Response to Rudder Displacemnt

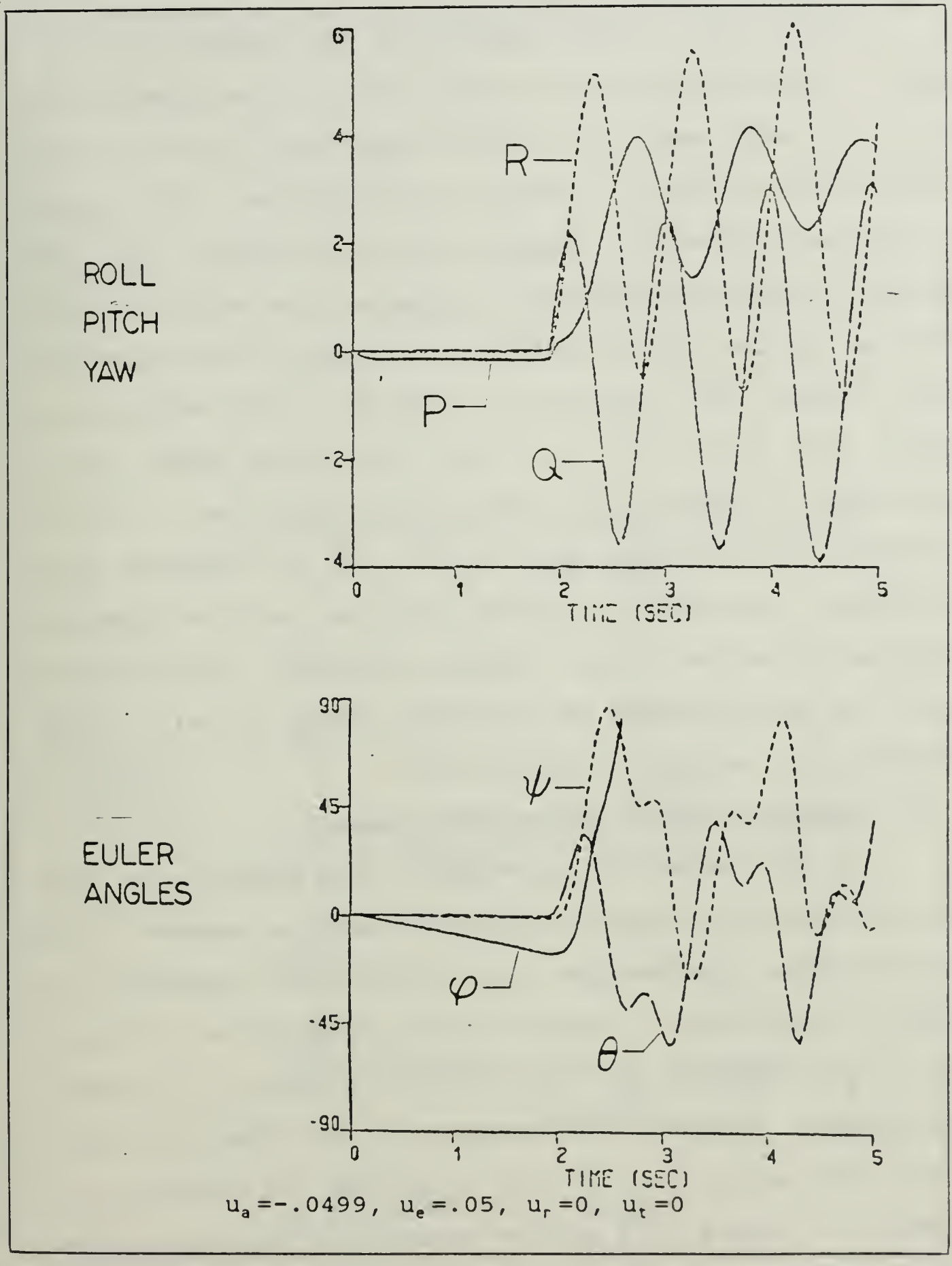

Figure 2.12 Time Response to Elevator Displacement

4. Throttle Input

Figure 2.13 is the result when the throttle (δ_t) is opened to increase the rotor speed and all other inputs are zero. The rotor applies a torque about the roll axis and, indeed, this influence is seen in the results. The torque is directed oppositely to the spin direction (-P) and results in a less negative roll. However, the equations for pitch (Q) and yaw (R) include terms coupled to the propeller speed through the aerodynamic moments. The aerodynamic moments are determined by angle of attack which is a relationship between the body-fixed velocities. As U increases, the coupling with pitch and yaw becomes more pronounced, the angle of attack changes, and the moments determined from the tables change radically. The discontinuity is best observed by the sharp change in roll, pitch and yaw at .75 seconds in Figure 2.13.

5. Response Without Aerodynamic Moments

It is insightful to observe the behavior of the model with the troublesome aerodynamic moments removed. The system behavior without the wind tunnel data supplying the moments is much more in keeping with expectations. Figure 2.14 is the response of this modified system to a rudder displacement. Note the similarities of the nutation (Q and R) and precession (ψ) to the gyroscope illustration of Figure 2.2. Figure 2.15 is the response of the same system to an opening of engine throttle. This smooth system

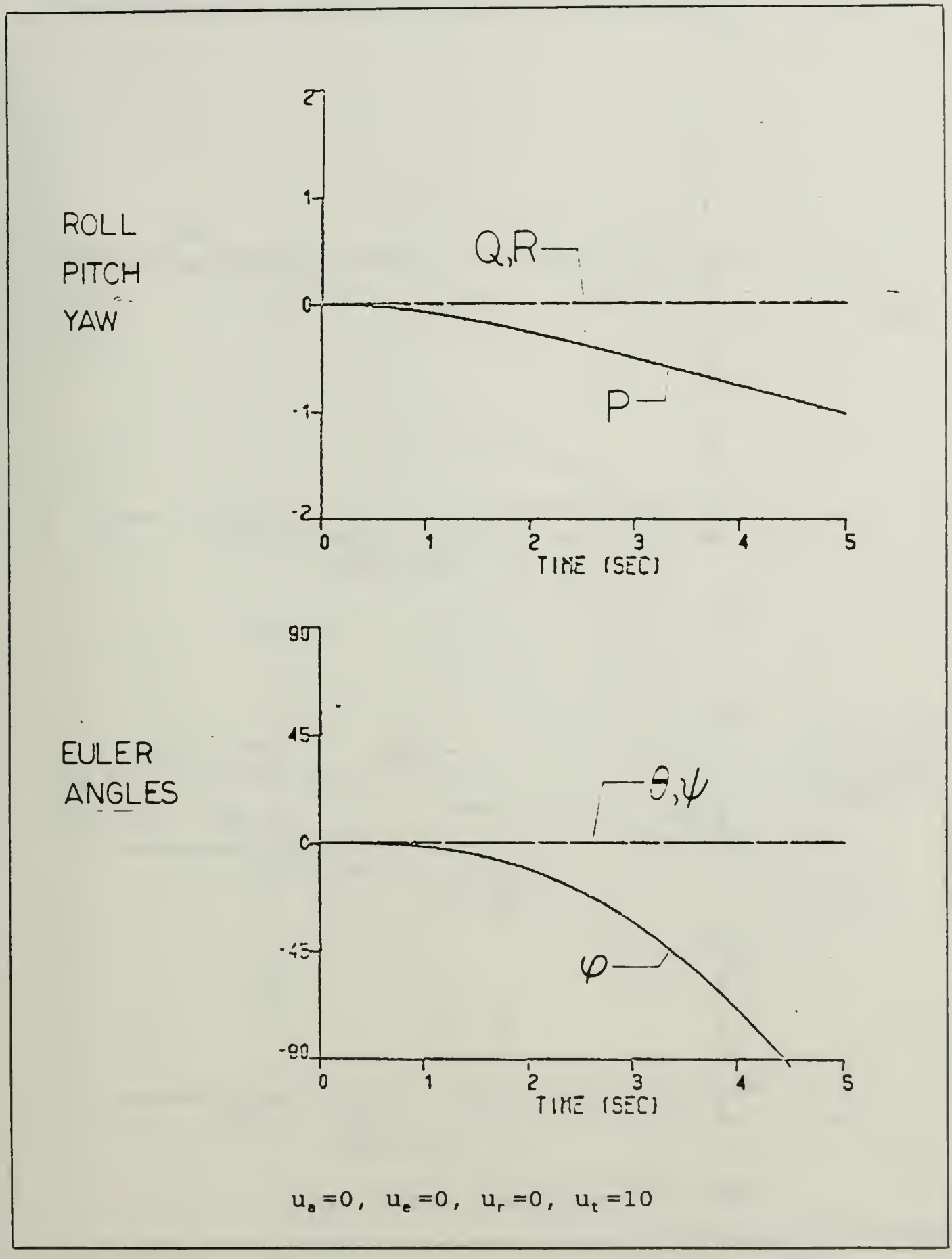

Figure 2.13 Time Response to Throttle Input

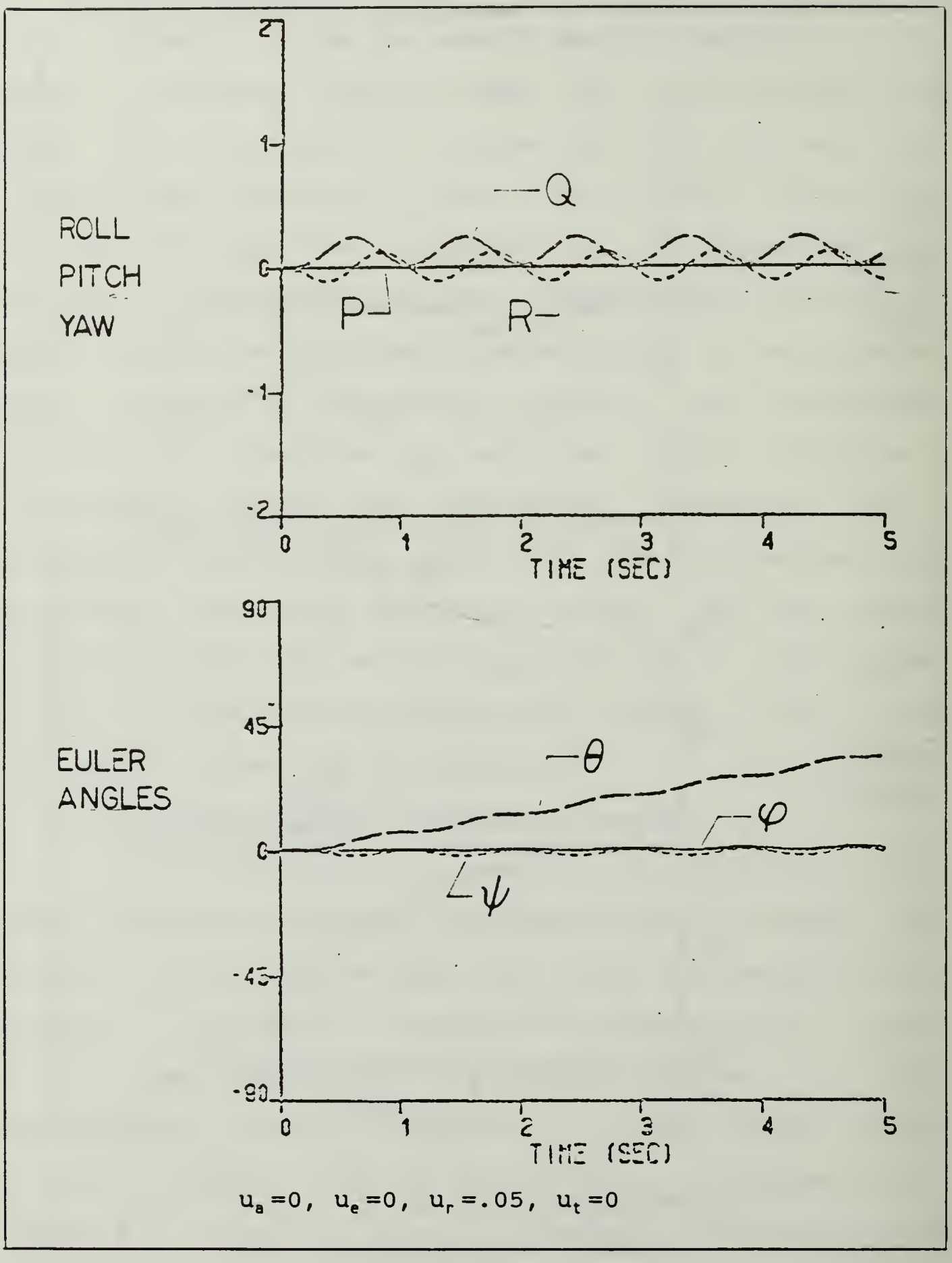

Figure 2.14 Time Response to Rudder Control
Aerodynamic Moments Removed

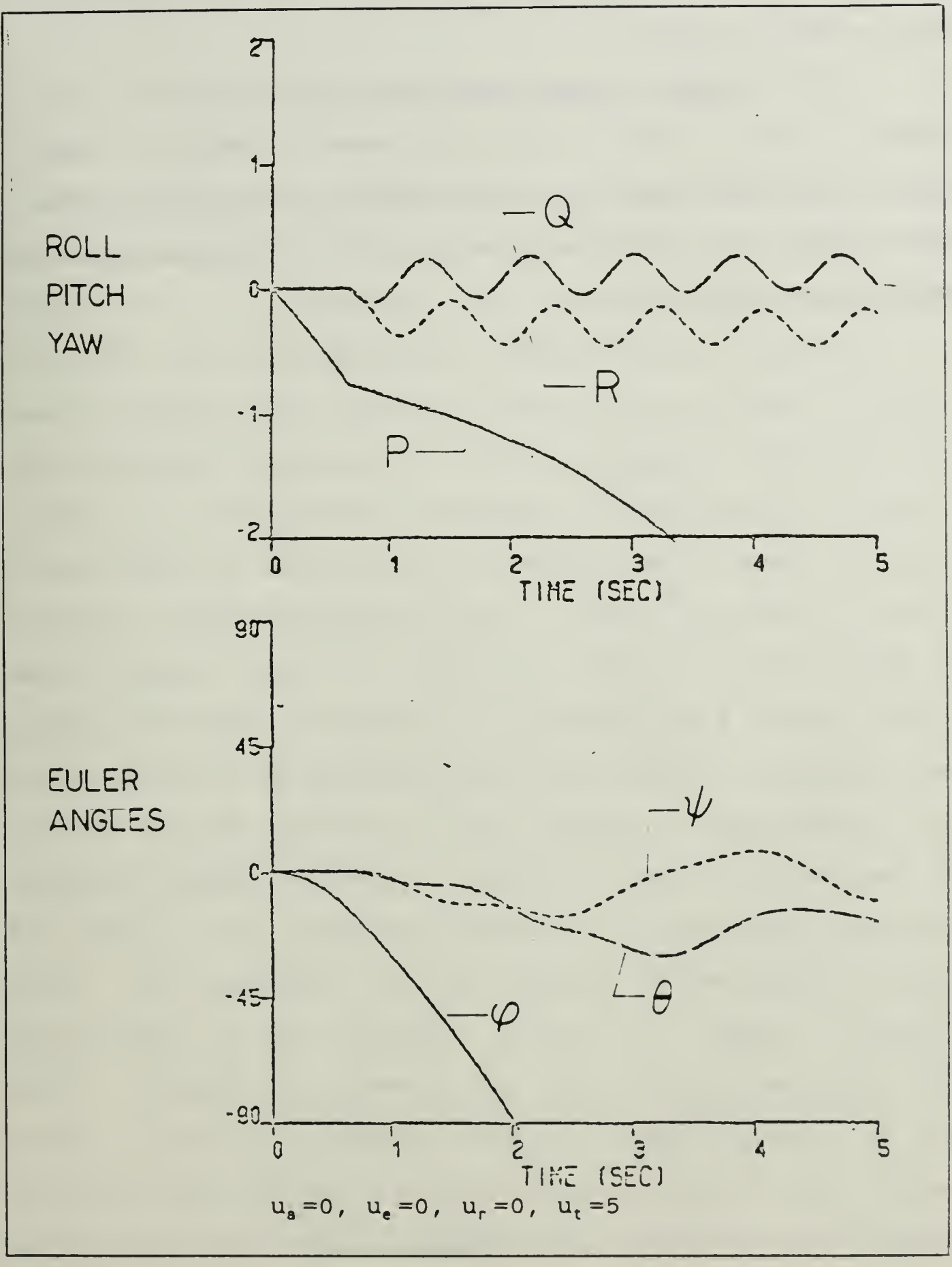

Figure 2.15 Time Response to Throttle Input
Aerodynamic Moments Removed

response is clearly more in keeping with how we expect the actual system to behave.

The validity of the data was not able to be confirmed nor is it being challenged here. However, these results do suggest that the application of the data to the system model is a problem that is best addressed by the engineers who derive it.

III. STABILITY AND CONTROL OF AROD

The equations of motion describing AROD and the forces and moments which act on AROD were developed in detail in Chapter II. A computer simulation of these equations indicated solid stability in hover, but an inability to remain stable once disturbed from the hover state. Therefore, a method is needed to maintain stability and drive the system to a steady-state condition. Additionally, once a steady-state is achieved, it is necessary to steer the AROD up/down, forward/backward, side to side, and make it turn about its axis (roll). Hence, a method is also needed to control the AROD and cause it to change from a given initial steady-state to another desired steady-state. Stability and control are the topics of this chapter. Specifically, an algorithm based on optimal control theory is developed in the form of the regulator problem to address the stability issue. The regulator is then adapted to the control issue formulated as the tracking problem of control theory. First, however, a summary of the entire stability and control issue is offered. Then, a simplification of the complete AROD system is made so that standard, well founded methods may be used to address the stability and control dilemma.

A. SUMMARY OF THE CONTROL PROBLEM

The task is to provide an algorithm on which to base a control system for AROD. The control system intended for AROD relies on inputs provided by an operator to command desired outputs. This section discusses the control problem based on the inputs, the outputs, and the equations which relate them.

1. Summary of the Complete AROD System

The result of Chapter II was 18 first order differential equations which are listed in Table 3.1. Also listed are the equations for useful quantities which were derived in modelling the system.

Figure 3.1 is a simple, open loop block diagram of the AROD system. The block labelled "AROD" represents all

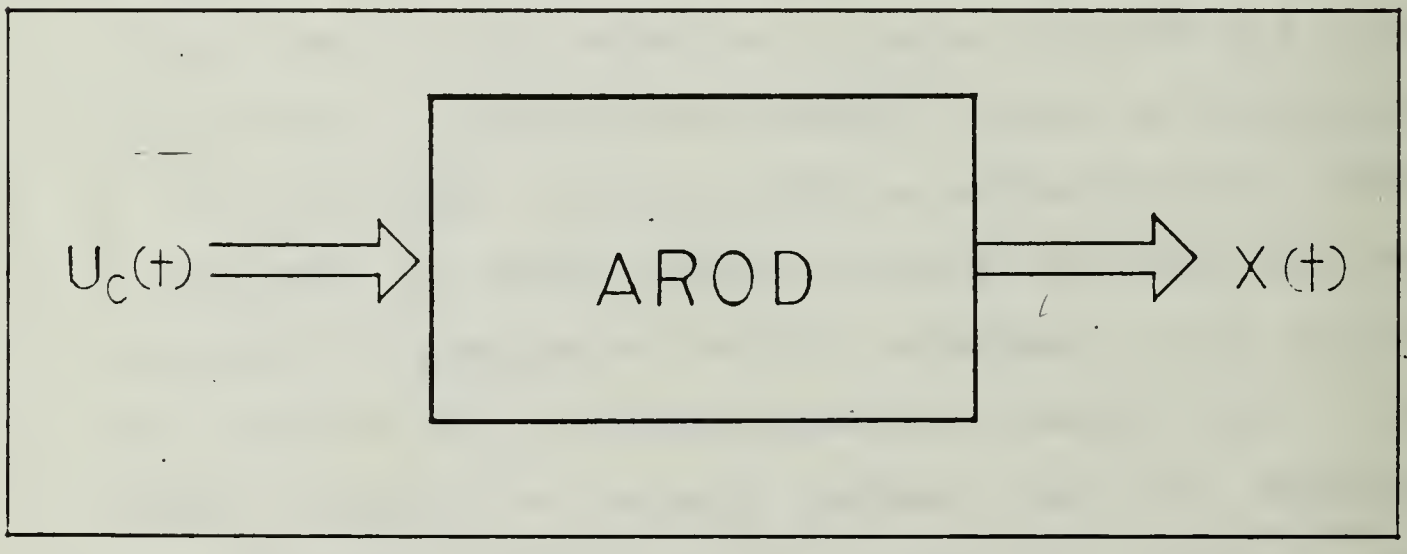

Figure 3.1 AROD Open Loop Model

the equations listed in Table 3.1. The forces, including gravity, and moments acting on the block are external influences and are variables in the equations over which the designer has no control. The inputs of interest are u_a, u_e,

TABLE 3.1

AROD DIFFERENTIAL EQUATIONS

State

$$\dot{P} = [(I_y - I_z)QR - I_r\dot{\omega}_r + \acute{L}_a + \acute{L}_t]/I_x$$

$$\dot{Q} = [(I_z - I_x)PR - RI_r\omega_r + \acute{M}_a + \acute{M}_t]/I_y$$

$$\dot{R} = [(I_x - I_y)PQ + QI_r\omega_r + \acute{N}_a + N_t]/I_z$$

$$\dot{U} = (RV - QW) + \acute{F}_{ax}/m + F_{tx}/m$$

$$\dot{V} = (PW - RU) + \acute{F}_{ay}/m + F_{ty}/m$$

$$\dot{W} = (QU - PV) + \acute{F}_{az}/m + F_{tz}/m$$

$$\dot{\varphi} = P + Q\sin\varphi + R\cos\varphi\tan\Theta$$

$$\dot{\Theta} = Q\cos\varphi - R\sin\varphi$$

$$\dot{\psi} = Q\frac{\sin\varphi}{\sin\Theta} + R\frac{\cos\varphi}{\cos\Theta}$$

$$\dot{T}_r = -T_r + .5(\delta_t)$$

$$\ddot{\delta}_a = -H_1\dot{\delta}_a - H_2\delta_a + H_2 u_a$$

$$\ddot{\delta}_e = -H_1\dot{\delta}_e - H_2\delta_e + H_2 u_e$$

$$\ddot{\delta}_r = -H_1\dot{\delta}_r - H_2\delta_r + H_2 u_r$$

$$\ddot{\delta}_t = -H_1\dot{\delta}_t - H_2\delta_t + H_2 u_t$$

u_r, and u_t. These inputs are voltages applied to servos and determine the position of the control vanes in the rotor downwash and the throttle position. The outputs of interest are φ,Θ,ψ, and U. If these outputs can be manipulated at will, then the rest of the equations, which are derivatives of these, can be controlled as well.

2. Optimal Feedback Control

Control systems may be divided into two basic categories: open loop and closed loop systems. Open loop control was attempted in Chapter II and is pictured in Figure 3.1. Step inputs for pitch(Q) and yaw(R) resulted in severe nutation and oscillations. Open loop control is not suited to the AROD application. Closed loop (feedback) control, then, is the direction taken in this work.

A feedback control system is one which tends to maintain a controlled variable at a fixed steady-state value [8]. Therefore, a control system must be able to sense variations in the system variables of interest in order to apply control to them. For AROD, the outputs are the controlled system variables. A scheme to relate the output to the input is the feedback loop and is pictured in Figure 3.2. The feedback matrix, K, must be determined so that a given control input always results in the same desired output. Note that the reference control vector, r_c, does not match the commanded input vector, u_c, except in steady-state. The time when $r_c \neq u_c$ is called the transient response time and is also the time it takes the output to reach the desired state. It follows that transient response time should be as short as possible. Note also that the difference, $r_c - u_c$, should be greatest when r_c is first applied and should decay to zero as the outputs reach their desired state. This will result in a smooth transition of

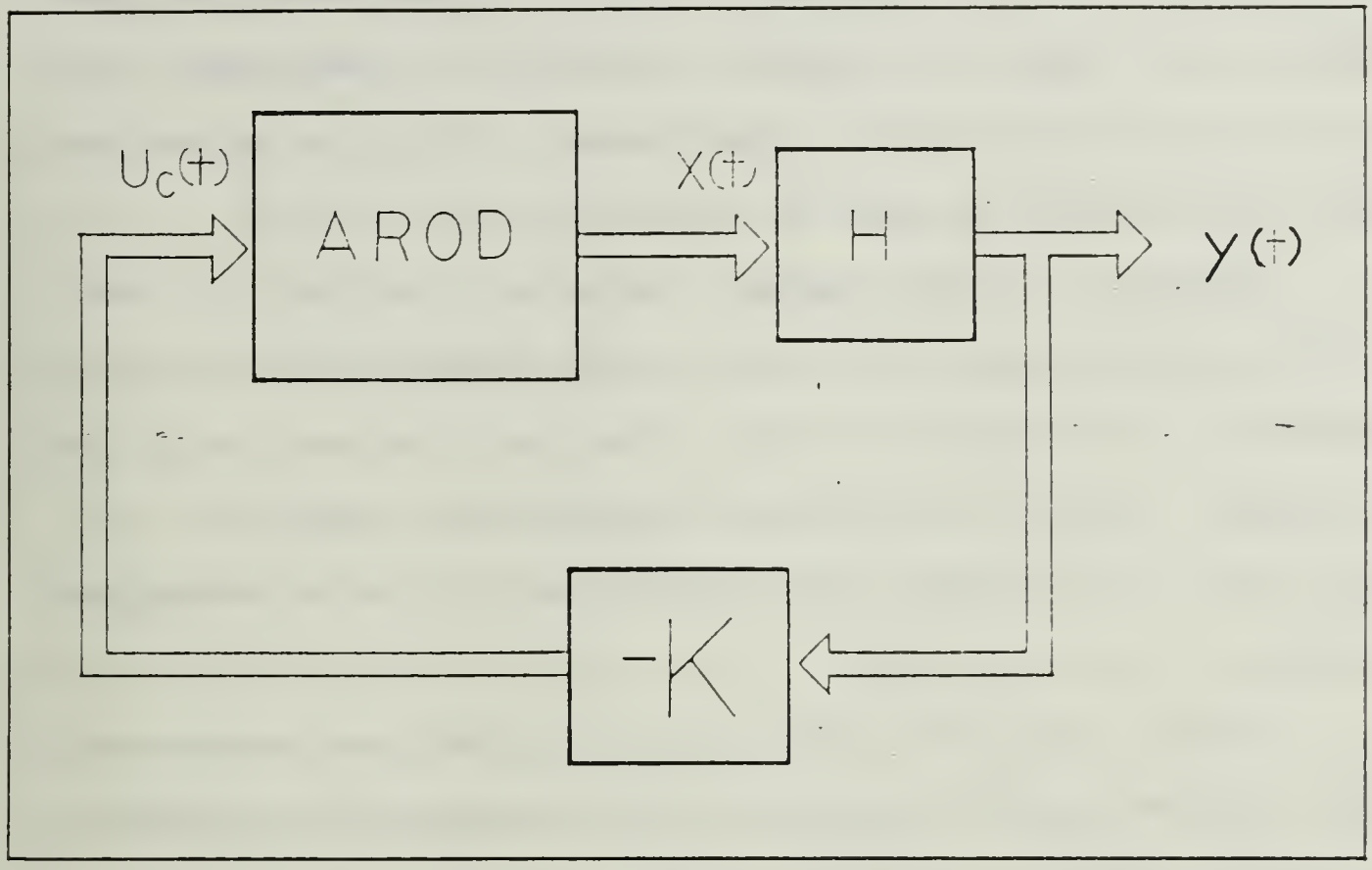

Figure 3.2 Output Feedback Model

the output states from beginning to end. In other words, there should be little or no overshoot of the desired state by the transient states. A good feedback control will minimize both the transient response time and the overshoot of the desired state.

A method of feedback control that might minimize both the transient response time and the overshoot is optimal control. Its name suggests that optimal control may provide the optimum solution to the problem of feedback control for AROD. However, it is more than semantics which drives the choice of controllers.

First, optimal control lends itself nicely to a discrete time solution of the control problem. AROD will

employ an on board, digital computer to perform inflight stability and control. While a continuous time controller can be easily discretized in many cases, design of a sampled data controller will simplify the procedure.

Second, optimal control is ideally suited to state variable techniques. A state-space approach is desired because of the enormity of the system and the complexity of equations. Matrix manipulation utilizing computers will prove far less tedious than traditional transfer function methods.

Third, and by far the most important reason to select optimal control analysis over classical methods is the unique ability of optimal control theory to accommodate multiple-input, multiple-output systems such as AROD [3]. Four inputs and four outputs have been identified. It will be shown in the next section that, although some separation of states is possible, severe coupling between other states precludes a reduction of the system to single-input, single-output systems.

Fourth and last, optimal control is known to provide robust and insensitive solutions to the feedback control problem. Assuming that an appropriate performance measure is chosen to determine the optimal feedback gain matrix, K, the solution can be expected to have a fair degree of tolerance to plant model inaccuracies. This section develops an approximation of the full AROD model so that

troublesome nonlinearities can be dealt with. Therefore, some inaccuracies are bound to appear in the new, linear model compared with the nonlinear system of Table 3.1. Clearly, robustness is not only a desired property of the controller, it is an absolute necessity if the controller is to be applicable to both the linear and nonlinear model of AROD.

With the advantages of optimal control comes a certain drawback: optimal control requires the availability of all system states [3:p. 22]. Therefore, the feedback scheme pictured in Figure 3.2 must be modified to include all system states in the feedback loop. Figure 3.3 satisfies this requirement. However, if the system states

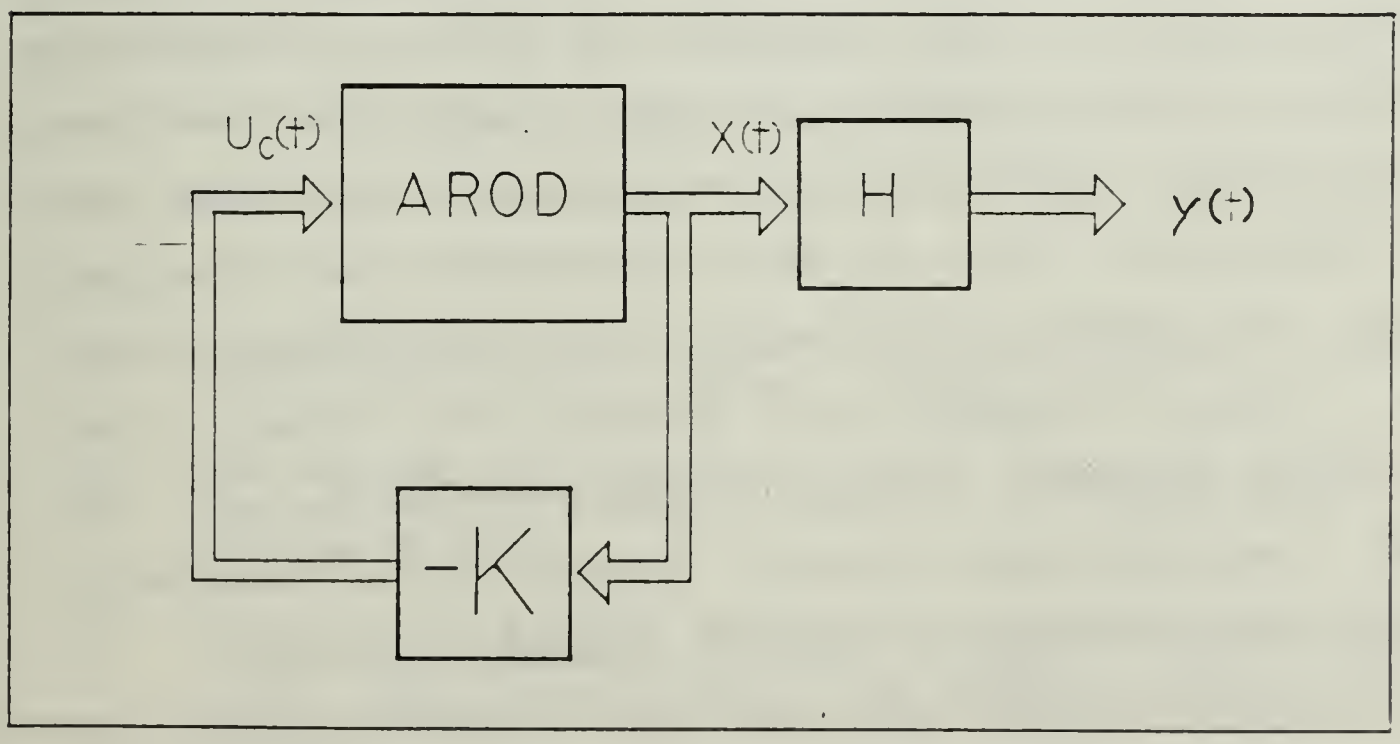

Figure 3.3 Full State Feedback Model

are not available from sensor measurements or other means, computational observers must also be included to provide an

estimate of the hidden states. Observers add an extra computational task to the onboard computer, but otherwise present no problem to the control designer.

B. LINEARIZING THE AROD MODEL

Throughout model development in Chapter II, nonlinear relationships were identified. These nonlinearities fall into two categories: nonlinear combination of states (e.g. Equation 2.8) and discontinuous functions (e.g. table look-up of aerodynamic force/moment coefficients).

A linear approach to controller design is much preferred over a nonlinear analysis. Three major reasons drive this preference. First, the theoretical basis for controllers of linear systems is well developed and easier to implement. Second, in airplane design, the use of linear approximations for nonlinear systems has yielded good results for the case of steady-state flight and small disturbances therefrom [5]. Third, the optimal control solution, K, can often be reduced to a single, constant gain schedule for linear, time-invariant systems. A constant gain matrix, K, will mean that a minimum amount of memory storage will be required of the on board computer for control implementation [9].

In this section, the equations of Table 3.1 will be replaced with linear approximations based on the small-disturbance theory, steady-state assumptions, and selected physical approximations where necessary.

1. The Small-Disturbance Theory

A straight forward discussion of the small disturbance theory is contained in [5:p. 106]. Essentially, if AROD is assumed to be in a certain steady-state reference condition, then motion of the vehicle consists of small deviations from the reference. If this steady-state is hover (all translational and angular movement is zero) then each of the states in Table 3.1 will be zero or nearly zero. This is not a bad assumption in the case of AROD. The flight condition in which AROD will spend most of its time is the hover. Only small deviations from the hover will be necessary to effect translational or angular movement. For example, a translational velocity forward (along the Z' axis) of four miles per hour requires only a 15 degree pitch of the body. The small-disturbance theory and the steady-state hover assumption result in the following simplifications:

(1) Products of states are zero since the product of two small values is an extremely small value.

(2) Derivatives of states are zero since the time derivative of a small valued time function is extremely small.

(3) The sine of a state is equal to the state and the cosine of a state is equal to one. This is the small angle approximation for angles less than 15 degrees.

Table 3.2 is the set of equations which result when the above assumptions are applied to Table 3.1. Note that much of the coupling between states and all of the nonlinear

TABLE 3.2

SIMPLIFIED EQUATIONS (SMALL-DISTURBANCE THEORY)

State

$$\dot{\varphi} = P$$

$$\dot{\Theta} = Q$$

$$\dot{\psi} = R$$

$$\dot{P} = -(I_r/I_x)\dot{\omega}_r + (L_a + L_t)/I_x$$

$$\dot{Q} = -(I_r/I_y)\omega_r R + (M_a + M_t)/I_y$$

$$\dot{R} = (I_r/I_z)\omega_r Q + (N_a + N_t)/I_z$$

$$\dot{U} = g + F_{ax}/m + F_{tx}/m$$

$$\dot{V} = F_{ay}/m + F_{ty}/m$$

$$\dot{W} = F_{az}/m + F_{tz}/m$$

$$\ddot{\delta}_a = -H_1\dot{\delta}_a - H_2\delta_a + H_2 u_a$$

$$\ddot{\delta}_e = -H_1\dot{\delta}_e - H_2\delta_e + H_2 u_e$$

$$\ddot{\delta}_r = -H_1\dot{\delta}_r - H_2\delta_r + H_2 u_r$$

$$\ddot{\delta}_t = -H_1\dot{\delta}_t - H_2\delta_t + H_2 u_t$$

products of states have been eliminated. Note that the derivative term of rotor velocity, $\dot{\omega}_r$, remains in the equation for roll (P). The term is kept because $\dot{\omega}_r$ is not a state and because it is easily approximated. We wish to keep as much similarity between the linear and nonlinear models as possible, so physical approximations of troublesome quantities are important.

2. Physical Approximations of Forces and Moments

The force and moment terms in Table 3.2 are made up, in part, of functions of aerodynamic coefficients measured at discrete AROD flight attitudes in a wind tunnel. The data, listed in Appendix A, follow no linear pattern and, instead, are discontinuous functions of angle of attack. The relationships used to include these data in the non-linear model were discussed in Chapter II. If a steady-state condition is assumed, then some simplification of these forces and moments is possible.

It is not desirable to exclude the aerodynamic data completely from the simplified model. An analysis of the magnitude of the forces and moments which result reveals that they are significant in all flight attitudes. However, if a constant hover is assumed then only one set of coefficients need be considered. Hover condition is defined by AROD project engineers as $\alpha=90^{o}$ and $\beta=0^{o}$ [6]. In hover condition, the forces and moments become those listed in Table 3.3. Note that, for the purpose of Table 3.3, the total body-fixed velocity is reduced to U. V and W are assumed zero.

Table 3.3 indicates that each force and moment in hover flight can be reduced to a linear function of a state, with one exception. Recall from Chapter II, we concluded that the rotor downwash created a swirl resulting in a force on the control vanes and a moment about the roll

TABLE 3.3

HOVER STATE FORCES AND MOMENTS

Forces	Moments
Aerodynamic	**Aerodynamic**
$F_{ax} = 0$	$L_a = U(.036) - T_r(.045) - 1.62$
$F_{ay} = U(.0729)$	$M_a = U(.81)$
$F_{az} = -U(1.08)$	$N_a = -U(.18)$
Thrust	**Thrust**
$F_{tx} = (76.5) + T_r(2.125)$	$L_t = -T_r(.5) - \delta_a(21.29)$
$F_{ty} = 0$	$M_t = -\delta_e(14.51)$
$F_{tz} = 0$	$N_t = -\delta_r(16.68)$
Useful Approximations	
$\omega_r = 753.98$ rad/sec	
$\dot{\omega}_r = T_r(10.472)$	

axis. This moment was illustrated in Figure 2.10(a). This same constant moment appears in the equation for roll moment, L_A, in Table 3.3. The compensating factor of .0499, determined experimentally in the last chapter, can be derived by dividing the constant moment, -1.06, by the aileron control vane effectiveness, L_{ae} (-21.29). This constant moment will be eliminated in the linear model, but will be included in the resulting controller as a constant addition to the aileron control, u_a. The aerodynamic moments about the pitch and yaw axes are zero in hover flight. While this poses no problem to the linearizing

goal, it means that moments in other flight attitudes have not been approximated. Thus the controller resulting from the linear model will not consider these external moments.

3. The Linear Model Assembled

The complete, linearized equations are listed in Table 3.4. Numerical values for the constant quantities

TABLE 3.4

LINEARIZED HOVER STATE EQUATIONS

State

$$\dot{\varphi} = P$$

$$\dot{\Theta} = Q$$

$$\dot{\psi} = R$$

$$\dot{P} = U(.0236) - T_r(3.738) - \delta_a(21.29)$$

$$\dot{Q} = U(.4831) - R(6.75) - \delta_e(14.51)$$

$$\dot{R} = U(.108) + Q(6.78) - \delta_r(16.68)$$

$$\dot{U} = T_r(.894)$$

$$\ddot{\delta}_a = -H_1\dot{\delta}_a - H_2\delta_a + H_2 u_a$$

$$\ddot{\delta}_e = -H_1\dot{\delta}_e - H_2\delta_e + H_2 u_e$$

$$\ddot{\delta}_r = -H_1\dot{\delta}_r - H_2\delta_r + H_2 u_r$$

$$\ddot{\delta}_t = -H_1\dot{\delta}_t - H_2\delta_t + H_2 u_t$$

were taken from Appendix A. The next section will assemble the equations in a form suitable to determine the optimal gain matrix, K.

C. FORMULATING THE CONTROL PROBLEM

1. State Space Representation

The control system of Figure 3.3 is called a regulator. As discussed earlier, the goal of this regulator system is to obtain a stable closed loop system which will force any arbitrary initial states to zero. The first task, then, is to assemble the state equations in a form suitable for control analysis. The form desired is given by

$$\dot{x}(t) = Ax(t) + Bu_c(t) \qquad (3.1)$$

where

$x(t)$	is the state vector,
A	is the plant matrix,
B	is the control matrix,
$u_c(t)$	is the control vector.

Note that the A and B matrices do not vary with time. A time-invariant system greatly simplifies controller design.

The 18 states listed in Table 3.4 are the complete states of the equations of motion for AROD. However, some of the states are unnecessary to the control issue and some additional assumptions will aid in determining the best control scheme.

The control problem can be simplified if it is recognized that translational velocities over the ground (V' and W' in the earth-fixed horizontal plane) are accomplished by pitching the AROD forward/backward or side to side. Therefore, the states important to this task are roll(P), pitch(Q), and yaw(R) along with their associated angles.

The only translational velocity of interest is the earth-fixed vertical velocity or altitude rate. For small pitch and yaw angles, then, body-fixed V and W are equivalent to earth-fixed V' and W' and will be eliminated from the equations. Also, the earth-fixed vertical velocity (altitude rate) will be approximated by the body-fixed velocity, U.

A caution about the angles φ,Θ,ψ, is appropriate here. The linearized equations conveniently eliminated any dependence on the earth-fixed Euler angles. While this may be a valid assumption for determining the control solution, it changes the meaning of the angle states Θ and ψ. φ depends only on the angles Θ and ψ which will be kept small in the hover condition, but Θ and ψ both depend on the roll(heading) angle, φ, which can range from 0 to 360^{o}. Therefore, the linearized angles Θ_b and ψ_b will be used from here on to remind us that these are body-fixed pitch and yaw angles and no longer relate the vehicle to the earth-fixed coordinate system.

The complete, linearized system can now be put in the form of Eq. 3.1 and is listed in Table 3.5. Figure 3.4 is the complete signal flow graph for the linear system.

2. Stability, Observability, and Controllability

a. Stability

A gyroscope is a stable, open loop device. Small, bounded disturbances of the roll, pitch, or yaw axes

TABLE 3.5

STATE-SPACE LINEARIZED SYSTEM

$$x(t) = [\varphi, \Theta_b, \psi_b, U, P, T_r, Q, R, \delta_a, \delta_e\ \delta_r, \delta_t, \dot{\delta}_a, \dot{\delta}_e, \dot{\delta}_r, \dot{\delta}_t]^t$$

$A(t) =$

$$\begin{bmatrix}
0 & 0 & 0 & 0 & 1 & 0 & 0 & 0 & 0 & 0 & 0 & 0 & 0 & 0 & 0 & 0 \\
0 & 0 & 0 & 0 & 0 & 0 & 1 & 0 & 0 & 0 & 0 & 0 & 0 & 0 & 0 & 0 \\
0 & 0 & 0 & 0 & 0 & 0 & 0 & 1 & 0 & 0 & 0 & 0 & 0 & 0 & 0 & 0 \\
0 & 0 & 0 & 0 & 0 & .894 & 0 & 0 & 0 & 0 & 0 & 0 & 0 & 0 & 0 & 0 \\
0 & 0 & 0 & .024 & 0 & -3.74 & 0 & 0 & -21.29 & 0 & 0 & 0 & 0 & 0 & 0 & 0 \\
0 & 0 & 0 & 0 & 0 & -1 & 0 & 0 & 0 & 0 & 0 & .5 & 0 & 0 & 0 & 0 \\
0 & 0 & 0 & .483 & 0 & 0 & 0 & -6.75 & 0 & -14.51 & 0 & 0 & 0 & 0 & 0 & 0 \\
0 & 0 & 0 & .108 & 0 & 0 & 6.78 & 0 & 0 & 0 & -16.68 & 0 & 0 & 0 & 0 & 0 \\
0 & 0 & 0 & 0 & 0 & 0 & 0 & 0 & 0 & 0 & 0 & 0 & 1 & 0 & 0 & 0 \\
0 & 0 & 0 & 0 & 0 & 0 & 0 & 0 & 0 & 0 & 0 & 0 & 0 & 1 & 0 & 0 \\
0 & 0 & 0 & 0 & 0 & 0 & 0 & 0 & 0 & 0 & 0 & 0 & 0 & 0 & 1 & 0 \\
0 & 0 & 0 & 0 & 0 & 0 & 0 & 0 & 0 & 0 & 0 & 0 & 0 & 0 & 0 & 1 \\
0 & 0 & 0 & 0 & 0 & 0 & 0 & 0 & -157.9 & 0 & 0 & 0 & -17.77 & 0 & 0 & 0 \\
0 & 0 & 0 & 0 & 0 & 0 & 0 & 0 & 0 & -157.9 & 0 & 0 & 0 & -17.77 & 0 & 0 \\
0 & 0 & 0 & 0 & 0 & 0 & 0 & 0 & 0 & 0 & -157.9 & 0 & 0 & 0 & -17.77 & 0 \\
0 & 0 & 0 & 0 & 0 & 0 & 0 & 0 & 0 & 0 & 0 & -157.9 & 0 & 0 & 0 & -17.77
\end{bmatrix}$$

$$B(t) = \begin{bmatrix}
0 & 0 & 0 & 0 & 0 & 0 & 0 & 0 & 0 & 0 & 0 & 0 & 157.9 & 0 & 0 & 0 \\
0 & 0 & 0 & 0 & 0 & 0 & 0 & 0 & 0 & 0 & 0 & 0 & 0 & 157.9 & 0 & 0 \\
0 & 0 & 0 & 0 & 0 & 0 & 0 & 0 & 0 & 0 & 0 & 0 & 0 & 0 & 157.9 & 0 \\
0 & 0 & 0 & 0 & 0 & 0 & 0 & 0 & 0 & 0 & 0 & 0 & 0 & 0 & 0 & 157.9
\end{bmatrix}^t$$

Note: t is the transpose operator.

produce bounded outputs. The outputs may be in the form of nutation or oscillations, but it will not grow with time once the disturbance is removed. This stability was illustrated for AROD in Figure 2.14 where the yaw axis was disturbed. The results compared favorably to the response of a gyroscope.

The open loop linearized system may be tested for stability also. Since it is linear time-invariant, the

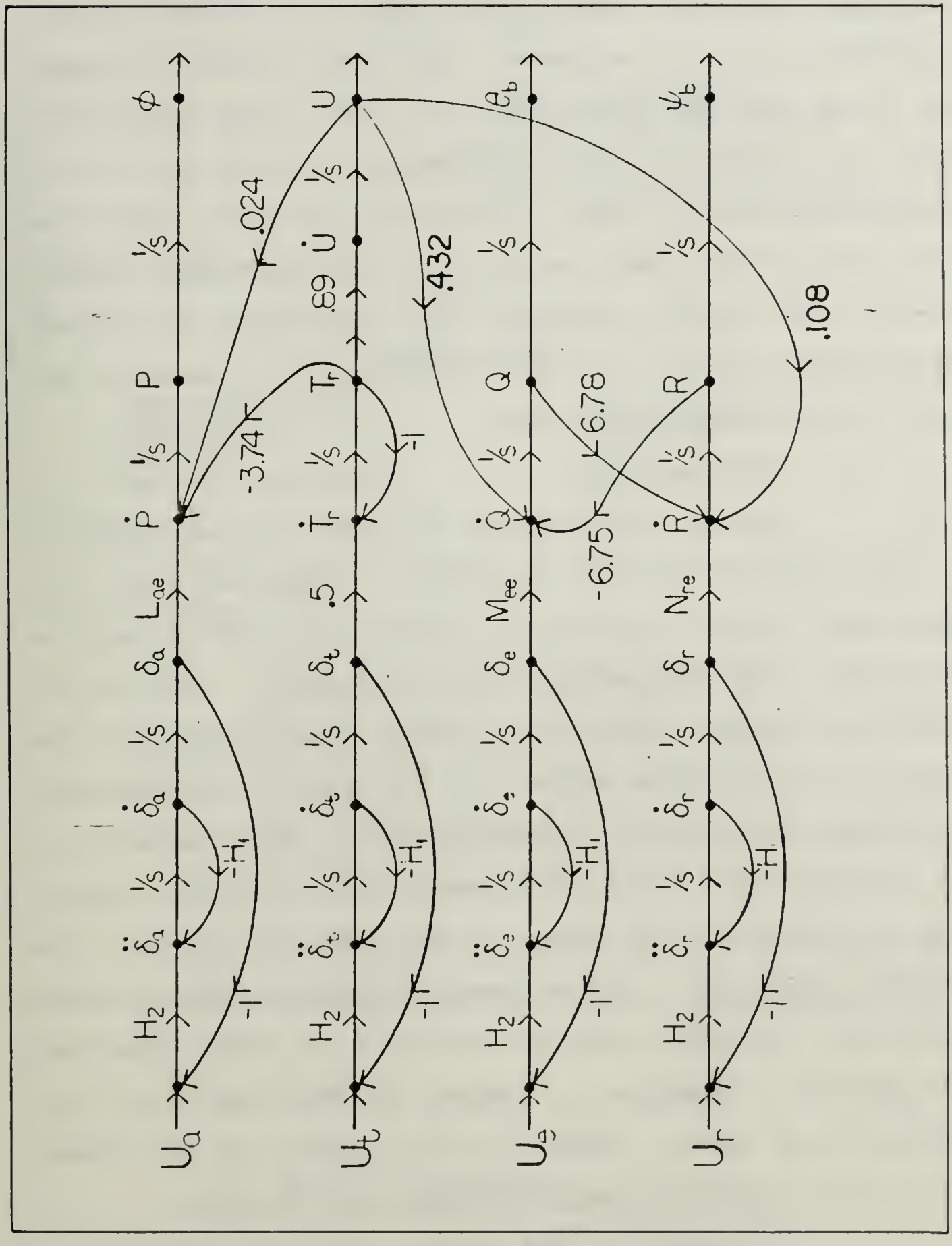

Figure 3.4 Signal Flow Graph of the Linear System

simplified system of Table 3.5 is stable if and only if the eigenvalues of the continuous time plant matrix, A, have real parts all less than zero [10]. Our system fails this test for stability since it results in seven out of 16 eigenvalues equal to zero. Therefore, the linear model has lost some of the characteristics of the nonlinear model. However, the control algorithm that stabilizes the linear system and minimizes the time response and overshoot may still be applicable to the AROD.

b. Observability

Another relationship to test the applicability of the linearized plant to AROD is observability. An observable system is one for which all states may be determined from observations of the output. This is an important concept since an optimal controller will be useless if any system states are not known. To determine the observability of our linearized plant, the outputs which are available from direct measurement must be known. Reference 2 indicates that three single axis rate gyros, one vertical rate gyro, a magnetometer (magnetic heading) and a barometric altimeter will be available on AROD. Control vane position based on a history of the input is also assumed to be known. Table 3.6 is a listing of the states which will be measured and the device used for each.

The output of the linear, time-invariant system is given by

$$y(t) = Hx(t) \qquad (3.2)$$

where

y(t) is the output vector,
H is the measurement matrix dimensioned o × n,
n is the number of states,
o is the number of measurements.

TABLE 3.6

MEASURED STATES

Measurement Device	State Obtained
Magnetometer	φ (heading)
Rate Gyro	U, P, Q, R
Control History(Servo)	δ_a, δ_e, δ_r, δ_t

and from Table 3.6

$$H = \begin{bmatrix} 1&0&0&0&0&0&0&0&0&0&0&0&0&0&0&0 \\ 0&0&0&1&0&0&0&0&0&0&0&0&0&0&0&0 \\ 0&0&0&0&1&0&0&0&0&0&0&0&0&0&0&0 \\ 0&0&0&0&0&0&1&0&0&0&0&0&0&0&0&0 \\ 0&0&0&0&0&0&0&1&0&0&0&0&0&0&0&0 \\ 0&0&0&0&0&0&0&0&1&0&0&0&0&0&0&0 \\ 0&0&0&0&0&0&0&0&0&1&0&0&0&0&0&0 \\ 0&0&0&0&0&0&0&0&0&0&1&0&0&0&0&0 \\ 0&0&0&0&0&0&0&0&0&0&0&1&0&0&0&0 \end{bmatrix}$$

Observability of a system due to its measured states can be determined from the observability matrix, W_o, given by [11]

$$W_o = [H \;,,\; HA \;,,\; HA^2 \;,,\; \ldots \;,,\; HA^{n-1}] \qquad (3.3)$$

where

W_o is a n × mn matrix,
m is the number of states measured.

The rank of W_o (the number of independent columns) must equal n if all of the states are observable from output

measurements. For the 16 state, linearized AROD system of Table 3.5, W_o has rank 10. Although a control solution might still be found assuming all states were available, it would not be a realizable controller. Therefore, a different approach must be taken.

Figure 3.4 reveals that the roll(P) and the throttle(T_r) coupled together and the pitch(Q) and yaw(R) states are likewise coupled as expected from the gyroscope analogy. However, these two subsystems are coupled only through a force/moment relationship dependent on the total velocity of the body, V_{tot}. In the last section, V_{tot} was approximated by U. A further simplification assumes that the moment on the pitch and yaw axis due to vertical speed, U, is negligible. The complete 16 state linear system can now be considered two independent subsystems of eight states each as pictured in Figure 3.5. State space representation of the two subsystems is listed in Table 3.7.

Each subsystem has an observability matrix of rank eight. Therefore, the states required in the subsystem configuration can be obtained from the measurements.

c. Controllability

A final test of the linearized model, before any effort is expended in actual controller design, is to determine whether it is even possible to find a control sequence such that a desired final state may be reached. This concept is known as controllability [10:p. 205]. The control-

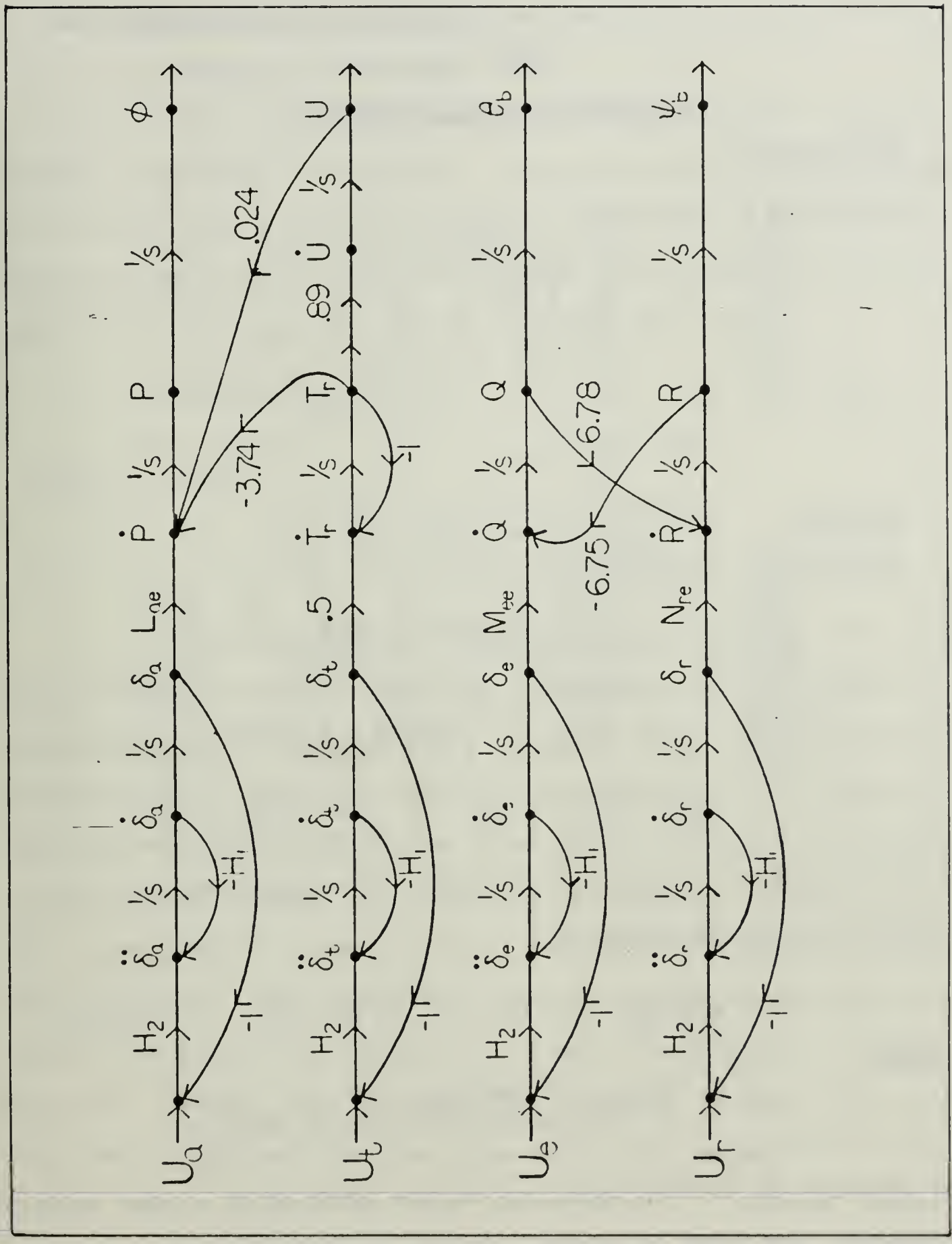

Figure 3.5 Linear Subsystem Signal Flow Graphs

TABLE 3.7

STATE-SPACE LINEAR SUBSYSTEMS

Roll/Throttle

$$x_{PT}(t) = \begin{bmatrix} \varphi \\ U \\ P \\ T_r \\ \delta_a \\ \delta_t \\ \dot{\delta}_a \\ \dot{\delta}_t \end{bmatrix} \qquad A_{PT} = \begin{bmatrix} 0 & 0 & 1 & 0 & 0 & 0 & 0 & 0 \\ 0 & 0 & 0 & .894 & 0 & 0 & 0 & 0 \\ 0 & .02 & 0 & -3.7 & -21.29 & 0 & 0 & 0 \\ 0 & 0 & 0 & -1 & 0 & .5 & 0 & 0 \\ 0 & 0 & 0 & 0 & 0 & 0 & 1 & 0 \\ 0 & 0 & 0 & 0 & 0 & 0 & 0 & 1 \\ 0 & 0 & 0 & 0 & -157.9 & 0 & -17.77 & 0 \\ 0 & 0 & 0 & 0 & 0 & -157.9 & 0 & -17.77 \end{bmatrix}$$

$$B_{PT} = \begin{bmatrix} 0 & 0 & 0 & 0 & 0 & 0 & 157.91 & 0 \\ 0 & 0 & 0 & 0 & 0 & 0 & 0 & 157.91 \end{bmatrix}^t$$

Pitch/Yaw

$$x_{QR}(t) = \begin{bmatrix} \Theta_b \\ \psi_b \\ Q \\ R \\ \delta_e \\ \delta_r \\ \dot{\delta}_e \\ \dot{\delta}_r \end{bmatrix} \qquad A_{QR} = \begin{bmatrix} 0 & 0 & 1 & 0 & 0 & 0 & 0 & 0 \\ 0 & 0 & 0 & 1 & 0 & 0 & 0 & 0 \\ 0 & 0 & 0 & -6.75 & -14.51 & 0 & 0 & 0 \\ 0 & 0 & 6.78 & 0 & 0 & -16.68 & 0 & 0 \\ 0 & 0 & 0 & 0 & 0 & 0 & 1 & 0 \\ 0 & 0 & 0 & 0 & 0 & 0 & 0 & 1 \\ 0 & 0 & 0 & 0 & -157.9 & 0 & -17.77 & 0 \\ 0 & 0 & 0 & 0 & 0 & -157.9 & 0 & -17.77 \end{bmatrix}$$

$$B_{QR} = \begin{bmatrix} 0 & 0 & 0 & 0 & 0 & 0 & 157.9 & 0 \\ 0 & 0 & 0 & 0 & 0 & 0 & 0 & 157.9 \end{bmatrix}^t$$

lability matrix is given by

$$W_c = [B,\ AB,\ A^2B,\ \ldots\ ,\ A^{n-1}B] \qquad (3.4)$$

where

W_c is a n×in matrix,
i is the number of control inputs.

The measure of controllability is the rank of W_c. For each subsystem, the rank is eight. Hence, a control sequence can be found for the linearized system.

3. Discretizing the System

a. Sampling Frequency

We wish to obtain a discrete time, digital control algorithm. Therefore, the system of Table 3.7 must be converted to a sampled system. A basis for determining the sampling interval, ΔT, is needed. The sampling theorem, based on the Nyquist criterion requires that [11]:

$$f_s = \frac{1}{\Delta T} \geq 2f_N \qquad (3.5)$$

where

f_s is the sampling frequency,
ΔT is the sampling period,
f_N is the natural frequency of the system.

Multiple-input, multiple-output systems do not have a single natural frequency. However, if the system is considered a set of several single-input, single-output systems then a number of different bandwidths are observed. The highest bandwidth can be used as the natural frequency of the entire system for sampling purposes. In this way, four independent systems, with coupled terms set to zero, are extracted. The frequency domain transfer functions are listed in Table 3.8 along with their bandwidths. A Bode analysis yields the frequencies listed. Each of the transfer functions also has the describing equation of the second order servo in the denominator. Second order analysis yields a servo natural frequency of 2 Hz. Since the servo frequency is the highest, it will be considered

TABLE 3.8

SIMPLIFIED TRANSFER FUNCTIONS AND BANDWIDTHS

		Natural Frequency
Roll	$\frac{\varphi(s)}{u_a(s)} = \frac{La_e H2}{s^2(s^2+H_1 s+H_2)}$	.74 hz
Pitch	$\frac{\Theta(s)}{u_e(s)} = \frac{Me_e H2}{s^2(s^2+H_1 s+H_2)}$	.61 hz
Yaw	$\frac{\psi(s)}{u_r(s)} = \frac{Nr_e H2}{s^2(s^2+H_1 s+H_2)}$	.65 hz
U	$\frac{U(s)}{u_t(s)} = \frac{-.89H2}{s(s^2+H_1 s+H_2)(s+1)}$	.03 hz

the natural frequency, f_N, of the multiple system. The sampling frequency is now given as

$$f_s > 2f_N = 4 \text{ Hz} \qquad (3.6)$$

Equation 3.6 is a lower bound on the sampling frequency that will allow the continuous time system to be reconstructed once sampled. Selection of the actual sampling rate is based on engineering judgment which calls for a factor of 10 between the highest frequency component and the sampling frequency [12]. A rate of 25 Hz meets this criteria and yields a sampling period of $\Delta T=.04$ seconds.

b. Analog to Digital Conversion

The process of conversion is illustrated in Figure 3.6. The block labelled D-A is a digital to analog signal converter. The block labelled A-D is an analog to digital signal converter. The AROD block is the nonlinear

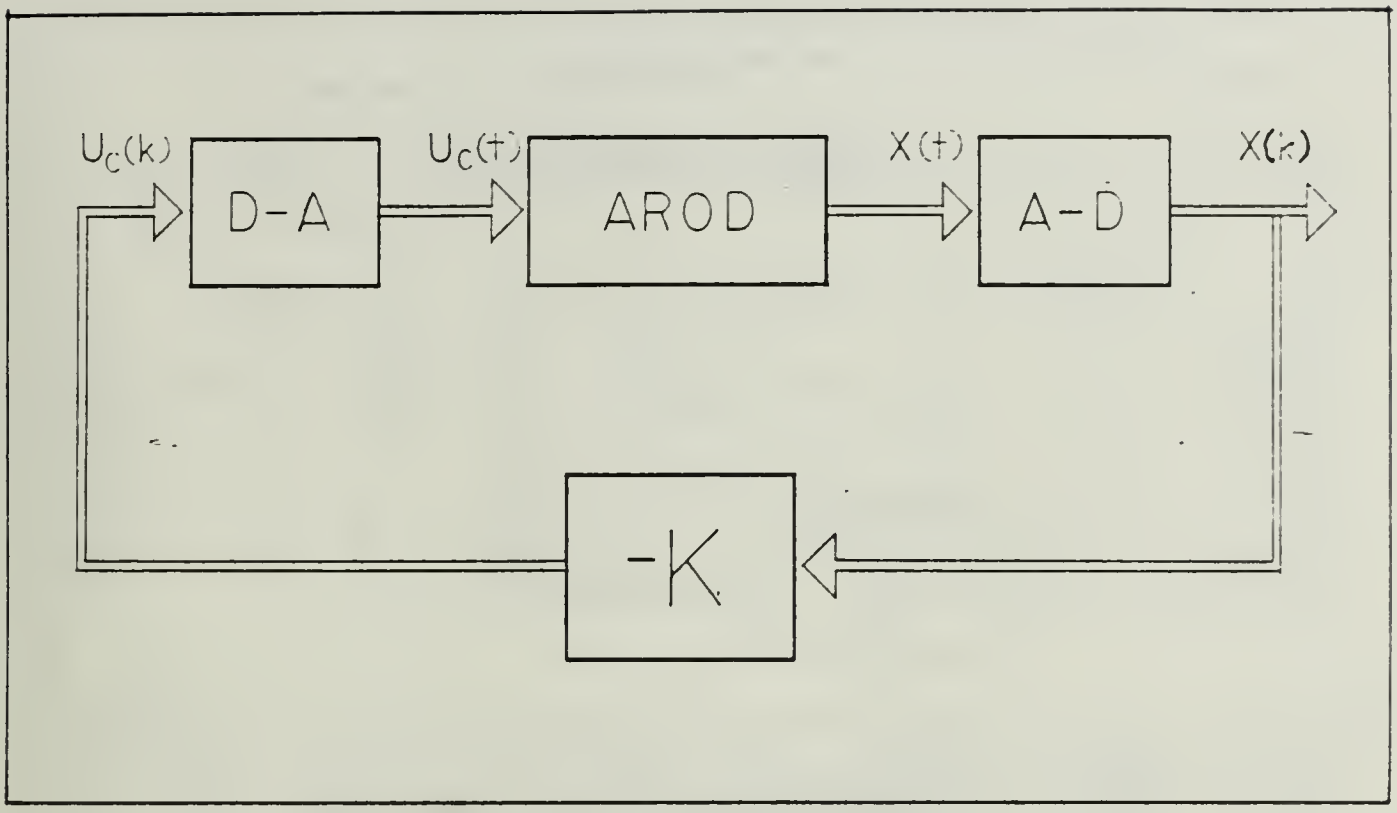

Figure 3.6 Digital System Feedback Scheme

model which has been linearized here. The next step is to combine the D-A, linear AROD model, and the A-D to obtain a discrete time representation of the linear, time-invariant system. Since the present linear model consists of two subsystems, the task is to convert the two systems and determine two control systems separately. The discrete version of the closed loop system is pictured in Figure 3.7. The discrete form of the system Equation 3.1 is given by

$$x(k+1) = \phi x(k) + \Gamma u_c(k) \qquad (3.7)$$

where

$k = k\Delta T$,
$k+1 = k\Delta T + \Delta T$,
ΔT is the sampling period,
ϕ is discretized A plant matrix,
Γ is discretized B control distribution.

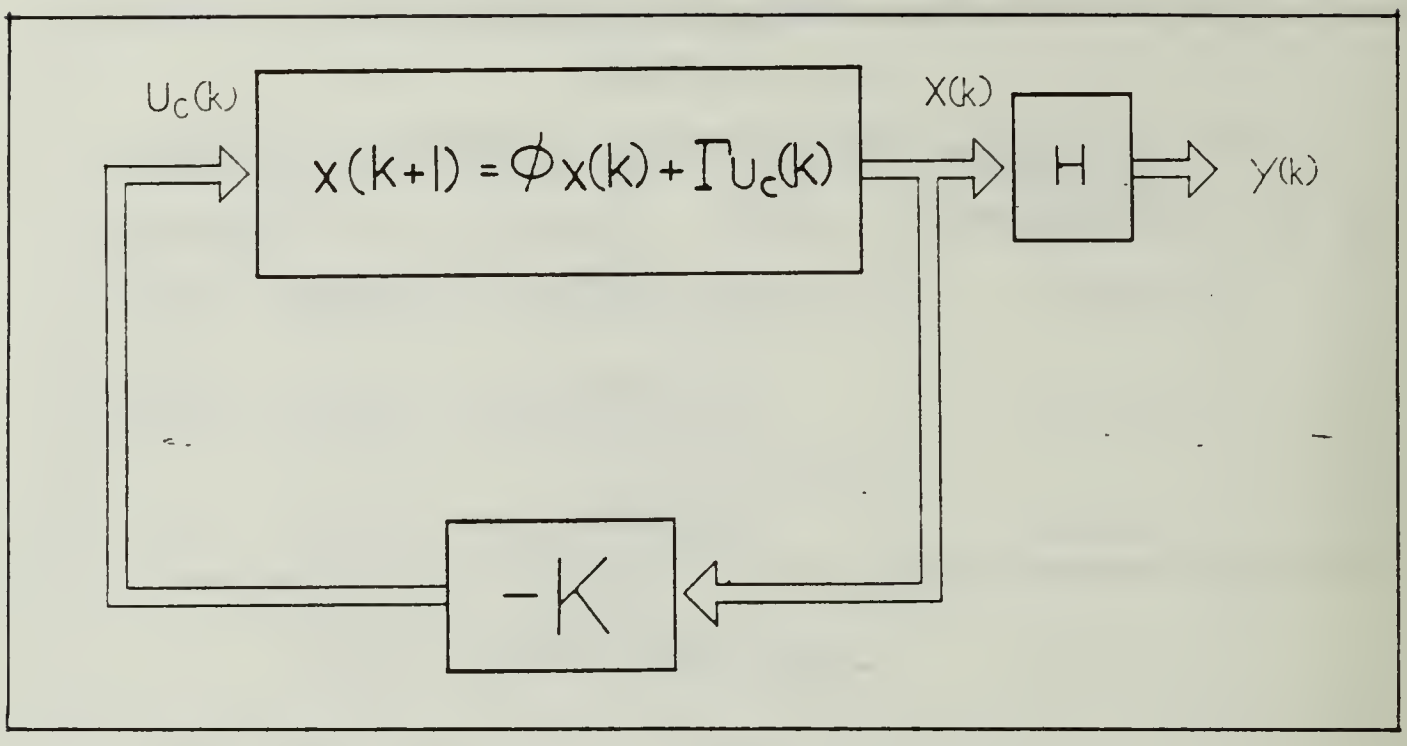

Figure 3.7 Discretized AROD Feedback

The discrete plant and control distribution matrices are given by [11]

$$\Phi = e^{A\Delta T} \qquad (3.8)$$

$$\Gamma = \int_0^{\Delta T} e^{As}\, ds B$$

where

e is the natural logarithm operator,
s is the Laplace operator,
ds is the derivative with respect to s.

Equation 3.8 can be solved by using a series expansion of the matrix exponential and integrated using a numerical scheme on a digital computer. The program called ORCONV [13] is used to obtain the discrete time system matrices of Table 3.9.

TABLE 3.9

DISCRETIZED SUBSYSTEMS

Φ_{PT} =

$$\begin{bmatrix}
1 & 0 & .0400 & -.0030 & -.0167 & 0 & -.0002 & 0 \\
0 & 1 & 0 & .0350 & 0 & .0004 & 0 & 0 \\
0 & .0009 & 1 & -.1466 & -.8217 & -.0015 & -.0134 & 0 \\
0 & 0 & 0 & .9608 & 0 & .0189 & 0 & .0003 \\
0 & 0 & 0 & 0 & .9010 & 0 & .0275 & 0 \\
0 & 0 & 0 & 0 & 0 & .9010 & 0 & .0275 \\
0 & 0 & 0 & 0 & -4.334 & 0 & .4132 & 0 \\
0 & 0 & 0 & 0 & 0 & -4.334 & 0 & .4132
\end{bmatrix}$$

Γ_{PT} =

$$\begin{bmatrix}
-.0003 & 0 \\
0 & .00001 \\
-.0299 & -.00003 \\
0 & .0007 \\
.0990 & 0 \\
0 & .0990 \\
4.334 & 0 \\
0 & 4.334
\end{bmatrix}$$

Φ_{QR} =

$$\begin{bmatrix}
1 & 0 & .0395 & -.0054 & -.0113 & .0012 & -.0001 & .00001 \\
0 & 1 & .0054 & .0395 & -.0010 & -.0130 & -.00001 & -.0002 \\
0 & 0 & .9636 & -.2667 & -.5530 & .0879 & -.0090 & .0010 \\
0 & 0 & .2681 & .9636 & -.0768 & -.6357 & -.0009 & -.0104 \\
0 & 0 & 0 & 0 & .9010 & 0 & .0275 & 0 \\
0 & 0 & 0 & 0 & 0 & .9010 & 0 & .0275 \\
0 & 0 & 0 & 0 & -4.334 & 0 & .4132 & 0 \\
0 & 0 & 0 & 0 & 0 & -4.334 & 0 & .4132
\end{bmatrix}$$

Γ_{QR} =

$$\begin{bmatrix}
-.0002 & .00001 \\
-.00001 & -.0002 \\
-.0203 & .0016 \\
-.0014 & -.0234 \\
.0990 & 0 \\
0 & .0990 \\
4.334 & 0 \\
0 & 4.334
\end{bmatrix}$$

D. THE OPTIMAL REGULATOR

A review of the linear control problem is appropriate here. We now have two discrete-time subsystems, each defined by Eq. 3.7. The roll/throttle subsystem is described by the plant matrix Φ_{PT} and control distribution Γ_{PT}. The pitch/yaw subsystem is described by Φ_{QR} and Γ_{QR} These matrices were listed in Table 3.9. We also know that all of the states in each subsystem are available either by direct measurement or computational observers. We wish to find the closed loop feedback matrix, K, in Figure 3.7 such that any

disturbance of any state from the reference hover condition (all states zero) will be damped out, returning the states to zero in minimum time with minimum overshoot. Since each subsystem is controllable, the control law that satisfies these requirements is given by [10:p. 771]

$$u_c^*(k) = -Kx(k) \qquad (3.9)$$

where * denotes optimal in the minimum time, minimum overshoot sense.

Note that K is a constant matrix. We state this goal to reduce to a minimum the amount of computer memory required to store the feedback gains and, in general, to simplify the control algorithm. The validity of this approach is born out by experience with linear time-invariant systems [3]. The applicability of the resulting controller to the nonlinear system, like the previous linearizing assumptions, will be determined by the time response of the full AROD model once K is found. The following paragraphs will provide analytical justification for the steady-state approach.

1. Optimal Control

Optimal control theory is concerned with minimizing a performance criterion chosen by the designer [3:p. 3]. Therefore, the primary focus in developing the controller should be on a performance measure that quantifies the goals of the design effort. These goals are summarized here:

(1) Minimize the transient response time

(2) Minimize the state overshoot

(3) Determine a constant gain schedule, K.

(4) Operate within the physical constraints of the system.

The performance measure typically used in formulating the discrete time optimal regulator control solution is

$$J = \frac{1}{2}x(N)^t Cx(N) + \frac{1}{2}\sum_{k=0}^{N-1}[x(k)^t Q(k)x(k) + u_c(k)^t R(k)u_c(k)] \quad (3.10)$$

where

J	is the cost function,
N	is the final time step ($N\Delta T$),
k	is the time step index,
Q(k)	is the state weighting matrix,
R(k)	is the control cost weighting matrix,
C	is the final state weighting matrix,
t	is the matrix transpose operator.

The proper choice of C, Q(k), and R(k) will ensure that the control schedule, $u_c(k)$, that minimizes J will meet the first two of our design goals and minimize the control effort required.

The solution to Eq. 3.10 for time-invariant systems is found from the recurrence relation

$$K(N-k) = -[R(N-k) + \Gamma^t P(k-1)\Gamma]^{-1} \times \Gamma^t P(k-1)\phi \quad (3.11)$$

and

$$P(k) = M(N-k)^t P(k-1)M(N-k) + K(N-k)^t R(N-k)K(N-k) + Q(N-k)$$

and

$$M(k) = \phi - \Gamma K(N-k)$$

To meet goal (3), a constant K, it is necessary to know that under certain conditions the recurrence relation converges to a steady-state for large enough k. The conditions sufficient for a steady-state convergence are: constant, positive definite weighting matrices Q and R; final state weight C=0; and $u_c(k)$ unconstrained [10]. The final time loses its meaning for the steady-state case since we assume convergence prior to reaching time-step N. Equation 3.10 becomes

$$J = \sum_{k=0}^{k_c} [x(k)^t Q x(k) + u_c(k)^t R u_c(k)] \qquad (3.12)$$

where k_c is the time step when J converges.

The recurrence formula can now be written [13]

$$K = [R + \Gamma^t P \Gamma]^{-1} \Gamma^t P \phi \qquad (3.13)$$

and

$$P = M^t P M + K^t R K + H^t Q H$$

and

$$M = \phi - \Gamma K$$

where the measurement matrix, H, modifies Q so that only states of interest are considered.

The revised performance measure appears to have no dependence on the final state. In fact, the solution, K, is sometimes referred to as a "suboptimal" gain schedule. However, experience shows that for time-invariant systems, the suboptimal gain schedule is often quite satisfactory.[9]

2. Selecting the Performance Measure

The weighting matrices Q and R must be selected to define the cost function used to determine the optimal

gains. For the linear AROD problem, Q and R are both diagonal matrices. Each diagonal element of Q corresponds to a weight placed on the deviation of a particular state from its desired value. Equation 3.13 introduced the idea of weighting only certain states utilizing the H matrix. The states we are interested in weighting are the angle states, the altitude rate, and the control vane displacements and displacement rates. The angle states and altitude rates describe the steady-state of the system. The control vanes are constrained in their movement. Therefore, these are the states with which we are concerned with controlling through the gain schedule. A definition of the measurement matrix, H, strictly for the purpose of the cost function, is

$$H = \begin{bmatrix} 1 & 0 & 0 & 0 & 0 & 0 & 0 & 0 \\ 0 & 1 & 0 & 0 & 0 & 0 & 0 & 0 \\ 0 & 0 & 0 & 0 & 1 & 0 & 0 & 0 \\ 0 & 0 & 0 & 0 & 0 & 1 & 0 & 0 \\ 0 & 0 & 0 & 0 & 0 & 0 & 1 & 0 \\ 0 & 0 & 0 & 0 & 0 & 0 & 0 & 1 \end{bmatrix} \qquad (3.14)$$

where H applies to both subsystems. The non-zero elements correspond to $\varphi, U, \delta_a, \delta_t, \dot{\delta}_a, \dot{\delta}_t$ for roll/throttle and $\Theta_b, \psi_b, \delta_e, \delta_r, \dot{\delta}_e, \dot{\delta}_r$ for pitch/yaw.

Now Q is a 6×6 matrix. If all the states of interest are weighted equally, Q is given by

$$Q = \begin{bmatrix} 1 & 0 & 0 & 0 & 0 & 0 \\ 0 & 1 & 0 & 0 & 0 & 0 \\ 0 & 0 & 1 & 0 & 0 & 0 \\ 0 & 0 & 0 & 1 & 0 & 0 \\ 0 & 0 & 0 & 0 & 1 & 0 \\ 0 & 0 & 0 & 0 & 0 & 1 \end{bmatrix} \qquad (3.15)$$

This reduction in cost states will streamline the iterative design process of the gain matrix in the next section.

Each subsystem has two control inputs: u_a and u_t for roll/throttle, and u_e, u_r for pitch/yaw. A control weight matrix which treats each control cost equally is

$$R = \begin{bmatrix} 1 & 0 \\ 0 & 1 \end{bmatrix} \qquad (3.16)$$

The cost function resulting in the best gain matrix for our purposes may not be the one which weights each state and cost equally. Factors such as the units a particular state is scaled to and system constraints on other states require scaling the diagonal values of the Q and R matrices accordingly. It may also be more important to drive a particular state more rigidly than others because of the dynamics of the system. In the case of AROD, it is most important to drive the angle states and the altitude rate to the desired state because the other states, all derivatives of these, follow. The time response of the angle states and altitude rate is the standard by which the best cost function is selected. Therefore, an iterative approach is taken, altering Q and R as necessary to meet the following specific objectives: settling time of two seconds to less than 10% overshoot, and maintaining constrained states within limitations.

The settling time requirement is chosen for two reasons. First, the servo response time (second order time

constant) is .5 seconds which places a lower limit on the response. The equations are coupled which means action by one state will force a delayed, but proportional reaction by the others. Two seconds for any response on a slow speed hovering vehicle such as AROD is considered adequate. Second, if the erratic behavior observed in Chapter II is to be controlled, then a quick response to disturbances and commands is necessary.

The control vanes are constrained in displacement to $\pm$.5236 radians (30^{o}) and in velocity to $\pm$.8727 radians per second. The throttle is constrained to $\pm$100 radians and $\pm$100 radians per second. The iterative design process must account for these constraints by weighting the corresponding elements of the Q matrix. Appendix A lists constraints.

Constraints on the servo states imply that the rate of change of other states may be restricted as well. A constraint on the output states means a limit must be applied to the disturbances from which we expect the system to recover in the given time. An angular displacement of .1 radians (6^{o}) is a reasonable disturbance to the system. This does not mean that the system is restricted to motions within 6^{o} of the hover condition, only that the response time for which we design applies up to these limits.

4. Iterative Design Process

We are now ready to form cost functions for each subsystem and determine suitable gain matrices. A numerical

algorithm for solving Equation 3.13 is discussed in [3:83]. A computer program for iterating the solution and converging to the steady state is described in [13] and is used to determine the gain matrices in this section.

Once a gain matrix is determined, the time response of the linearized, closed loop system can be tested using the linear system computer simulation in Appendix C. The process repeats until an acceptable time response is obtained.

a. Roll/Throttle SubSystem

Table 3.10 summarizes the results with various cost functions. The values for Q are the diagonals of the Q matrix which are the weights on φ, U, δ_a, δ_t, $\dot{\delta}_a$, and $\dot{\delta}_t$, respectively. The values for R are the weights on u_a and u_t in that order.

Iteration (1) is with a Q normalized to account for scaling differences between states. Results indicate that the normalized cost function is not adequate. A shorter response time is desired.

Iterations (2), (3), (4), and (5) chronicle a trial and error design process where each succeeding cost function is chosen based on the response of the previous ones. A dominant consideration is the coupling between the throttle and roll states. Since is undesirable to have the throttle used to correct the roll angle, a heavy cost is put on maintaining the throttle at the desired state.

TABLE 3.10

ROLL/THROTTLE SUBSYSTEM COST DESIGN ITERATIONS

Cost #	Initial Value	Settling Time φ	Settling Time U	Overshoot %(absolute) φ	Overshoot %(absolute) U	Deviation δ_a	Deviation δ_t	Deviation $\dot{\delta}_a$	Deviation $\dot{\delta}_t$
(1)	φ =.1	4.	6.	0%	(0)	.02	0	.2	0
(2)	φ =.1	1.5	3.	12%	(0)	.03	-.0002	.35	.025
(3)	φ =.1	1.5	2.5	10%	(0)	.03	-.004	.35	.06
(4)	φ =.1	1.	2.	6%	(0)	.07	-.0007	1.2	-.007
(5)	φ =.1	1.	2.	3%	(-.0001)	.055	.0125	.87	.3
	U =.1	2.	1.	(.004)	5%	.045	-3.	.275	-50

Cost Functions

(1) Q	(1) R	(2) Q	(2) R	(3) Q	(3) R	(4) Q	(4) R	(5) Q	(5) R
10	60	20	1	50	1	50	1	50	.1
3	60	1000	.1	2000	.1	2000	.1	2000	.05
60		.1		.01		.01		.01	
60		.1		.01		.01		.01	
30		1		3		.2		.4	
30		.1		.1		.1		.005	

The final iteration results in an acceptable time response and satisfies the state constraints. The optimal gain matrix, K_{PT} converged in 14 iterations at ΔT=.04 seconds per iteration. Hence, the steady-state constant gain schedule is reached after .56 seconds. Since the settling time is 1 and 2 seconds, our assumption that a constant gain schedule would provide the optimal solution is valid.

b. Pitch/Yaw SubSystem

Table 3.11 lists results for the iterative design of the pitch/yaw subsystem gain matrix. The values

for Q are the diagonal elements corresponding to Θ_b, ψ_b, δ_e, δ_r, $\dot{\delta}_e$, and $\dot{\delta}_r$, respectively. u_e and u_r are the control inputs in R.

TABLE 3.11

PITCH/YAW SUBSYSTEM COST DESIGN ITERATIONS

Cost #	Initial Value	Settling Time Θ	Settling Time ψ	Overshoot %(absolute) Θ	Overshoot %(absolute) ψ	Deviation δ_e	Deviation δ_r	Deviation $\dot{\delta}_e$	Deviation $\dot{\delta}_r$
(1)	Θ =.1	2.	1.5	10% (.013)		.035	-.055	.35	-.45
(2)	Θ =.1	.6	1.	8% (.0125)		.08	.045	.6	.5
(3)	Θ =.1	.75	1.5	3% (.0125)		.05	-.065	.7	-.7
	ψ =.1	1.	1.5	(-.012)	2%	.065	.06	.75	.6

Cost Functions

(1)

$$Q = \begin{bmatrix} 100 \\ 100 \\ .01 \\ .01 \\ 2 \\ 2 \end{bmatrix} \qquad R = \begin{bmatrix} 1 \\ 1 \end{bmatrix}$$

(2)

$$Q = \begin{bmatrix} 100 \\ 100 \\ .01 \\ .01 \\ 1 \\ 1 \end{bmatrix} \qquad R = \begin{bmatrix} 1 \\ 1 \end{bmatrix}$$

(3)

$$Q = \begin{bmatrix} 150 \\ 150 \\ .01 \\ .01 \\ 1 \\ 1 \end{bmatrix} \qquad R = \begin{bmatrix} 1 \\ 1 \end{bmatrix}$$

The same procedure as roll/throttle for iterating through various possible cost functions is used for the pitch/yaw subsystem. As in Table 3.10, only selected iterations are listed. Insight gained from the roll/throttle iterations was valuable in reducing the steps needed for the pitch/yaw design.

The final gain matrix, K_{QR}, converged in 13 iterations, or .52 seconds which is less than the settling time of .75 seconds. Therefore, the steady-state gain matrix is an optimal solution for this cost function.

c. Steady-State Gains

Table 3.12 lists the optimal steady-state gain matrices resulting from the iterative design. A test for stability places all eigenvalues of the discrete time closed loop subsystems inside the unit circle. Therefore, the gain matrix, K, has succeeded in stabilizing the open loop plant.

TABLE 3.12

STEADY-STATE GAIN SCHEDULES

Roll/Throttle

$$K_{PT} = \begin{bmatrix} -1.99 & -.603 & -.717 & .274 & 1.75 & .00994 & .140 & .00016 \\ -.585 & 111. & -.205 & 28.9 & .582 & 1.67 & .00962 & .137 \end{bmatrix}$$

Pitch/Yaw

$$K_{QR} = \begin{bmatrix} -1.61 & -1.61 & -.553 & .320 & 1.05 & -.208 & .127 & -.00264 \\ 1.57 & -1.60 & -.305 & -.566 & .107 & 1.23 & .00096 & .130 \end{bmatrix}$$

5. Linear System Optimal Regulator Response

The graphical results discussed here are for the optimal gains of Table 3.12 applied to the linear model with state constraints. The DSL/VS simulation is listed in Appendix C.

Figures 3.8(a), (b), (c), and (d) are the regulator time responses for initial conditions of $\varphi(0)=.1$, $U(0)=.1$, $\Theta_b(0)=.1$, and $\psi_b(0)=.1$, respectively. The design goals for overshoot and settling time are satisfied for the linear

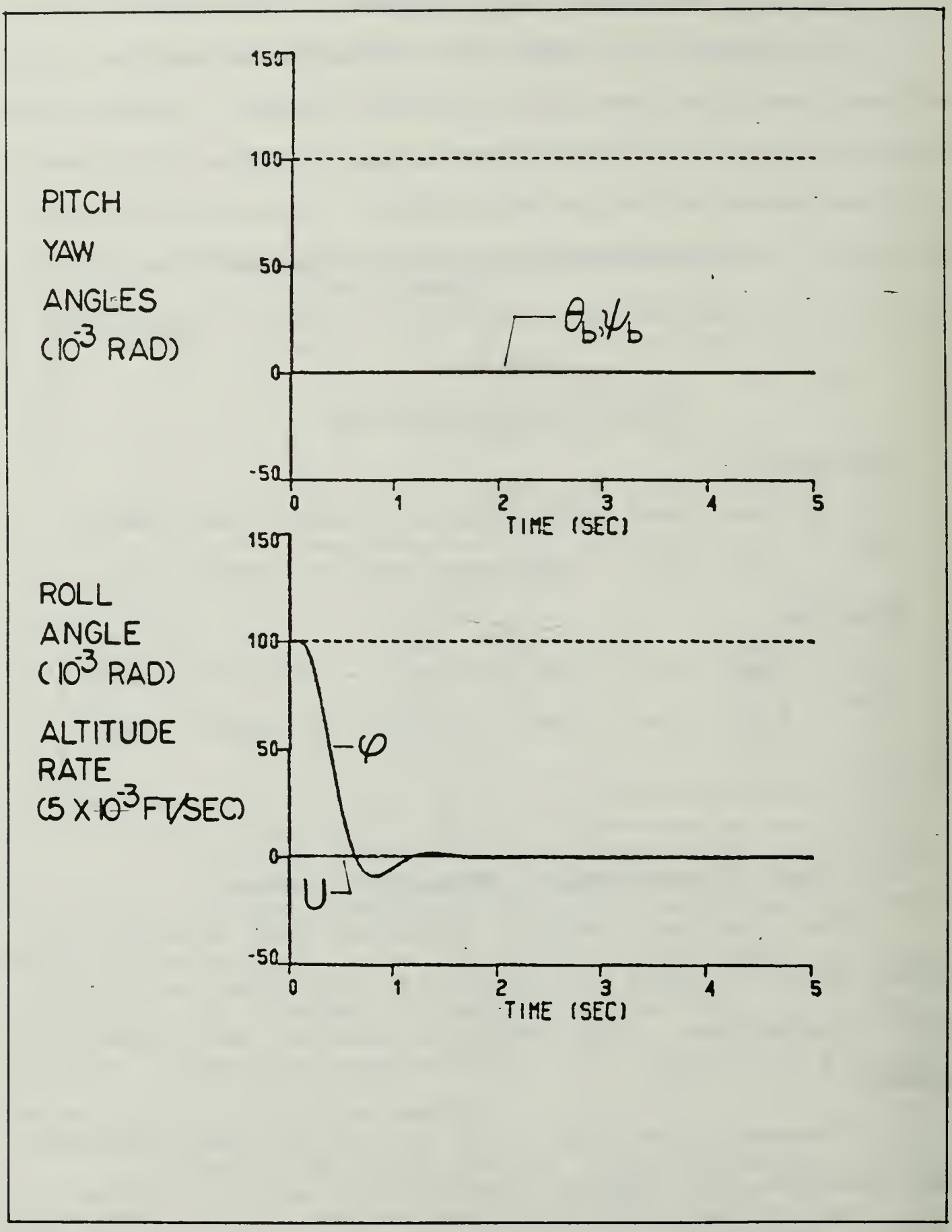

Figure 3.8 (a) Linear System Regulator Time Response with Optimal Gains, $\varphi(0)=.1$

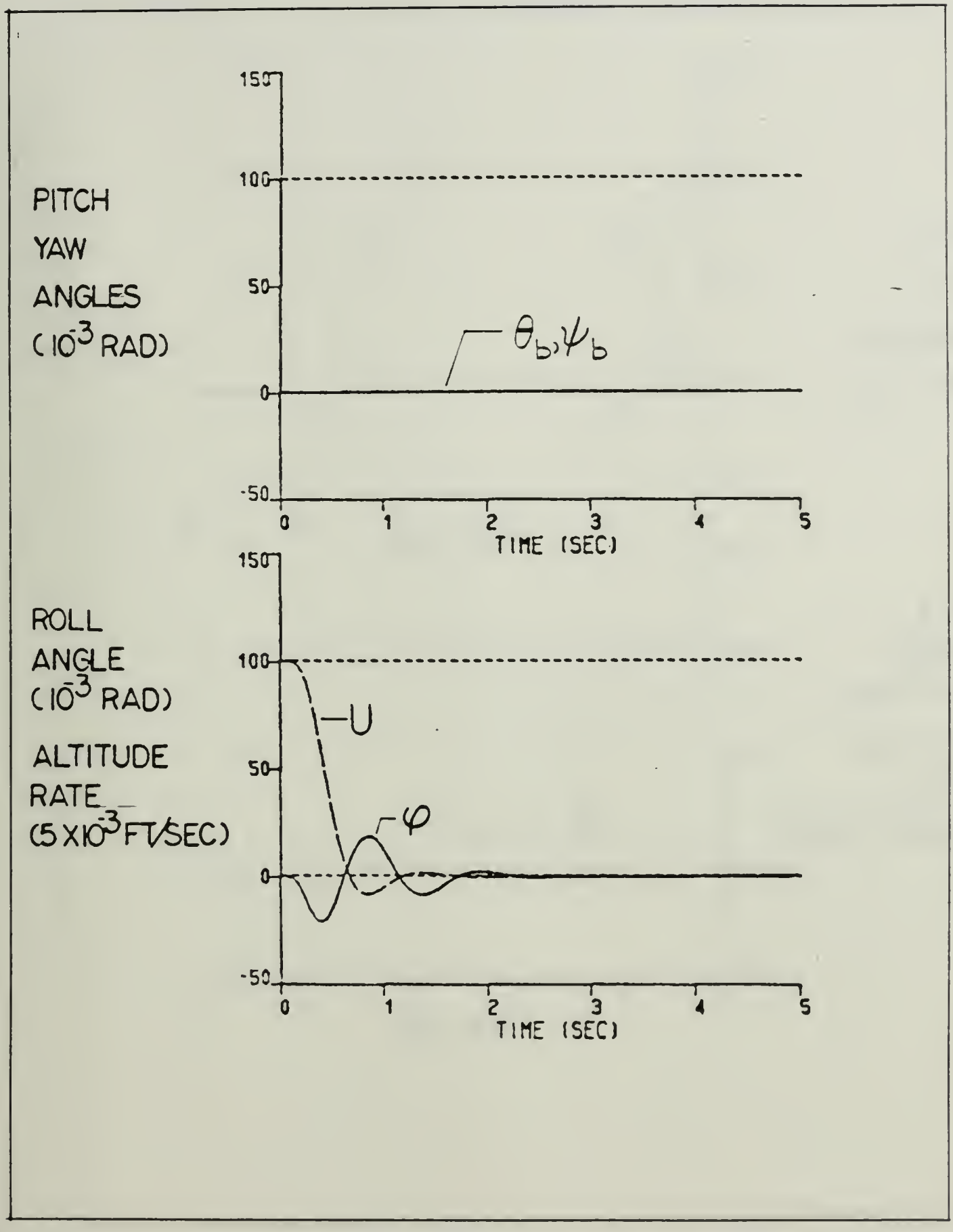

Figure 3.8 (b) Linear System Regulator Time Response with Optimal Gains, U(0)=.1

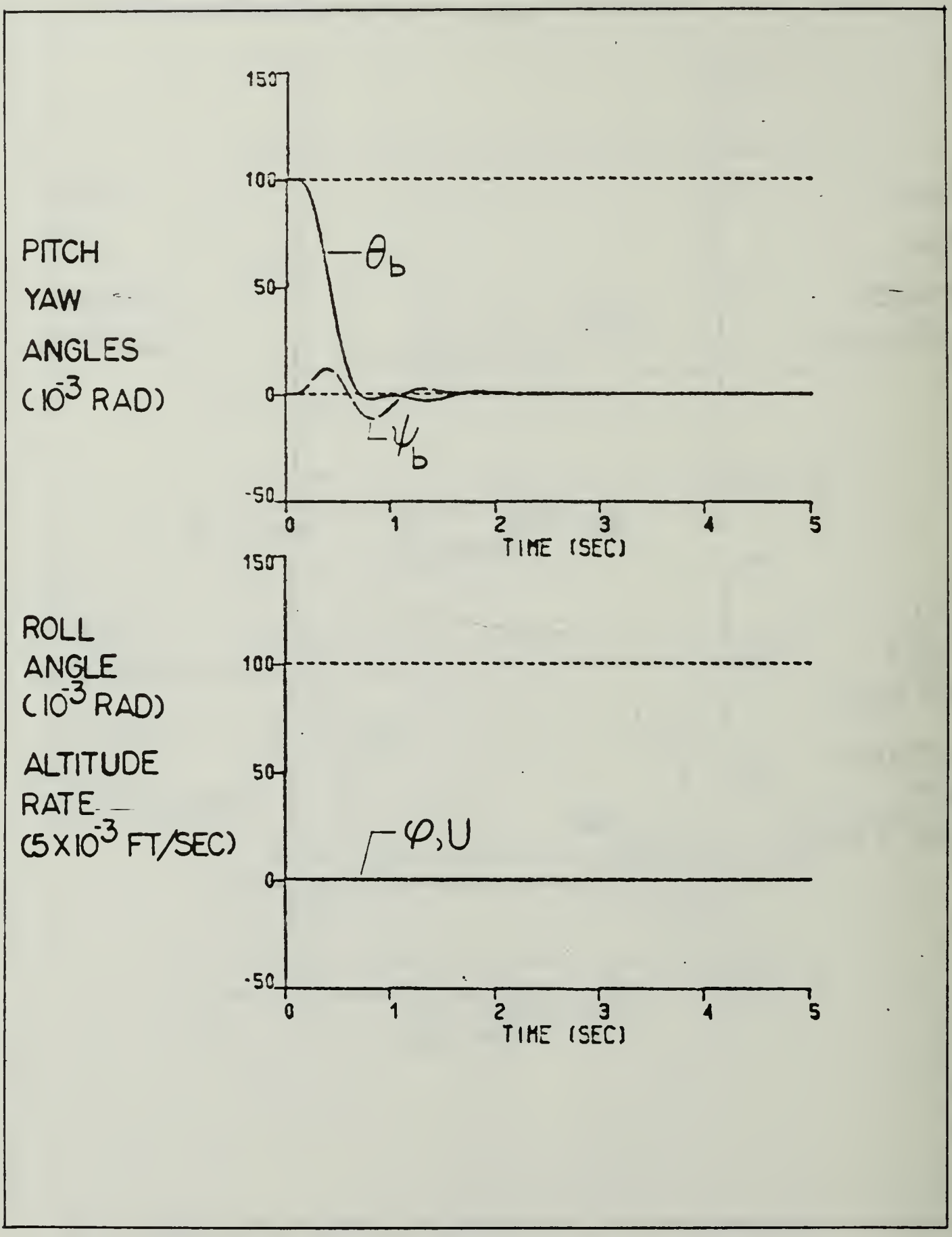

Figure 3.8 (c) Linear System Regulator Time Response with Optimal Gains, $\theta(0)=.1$

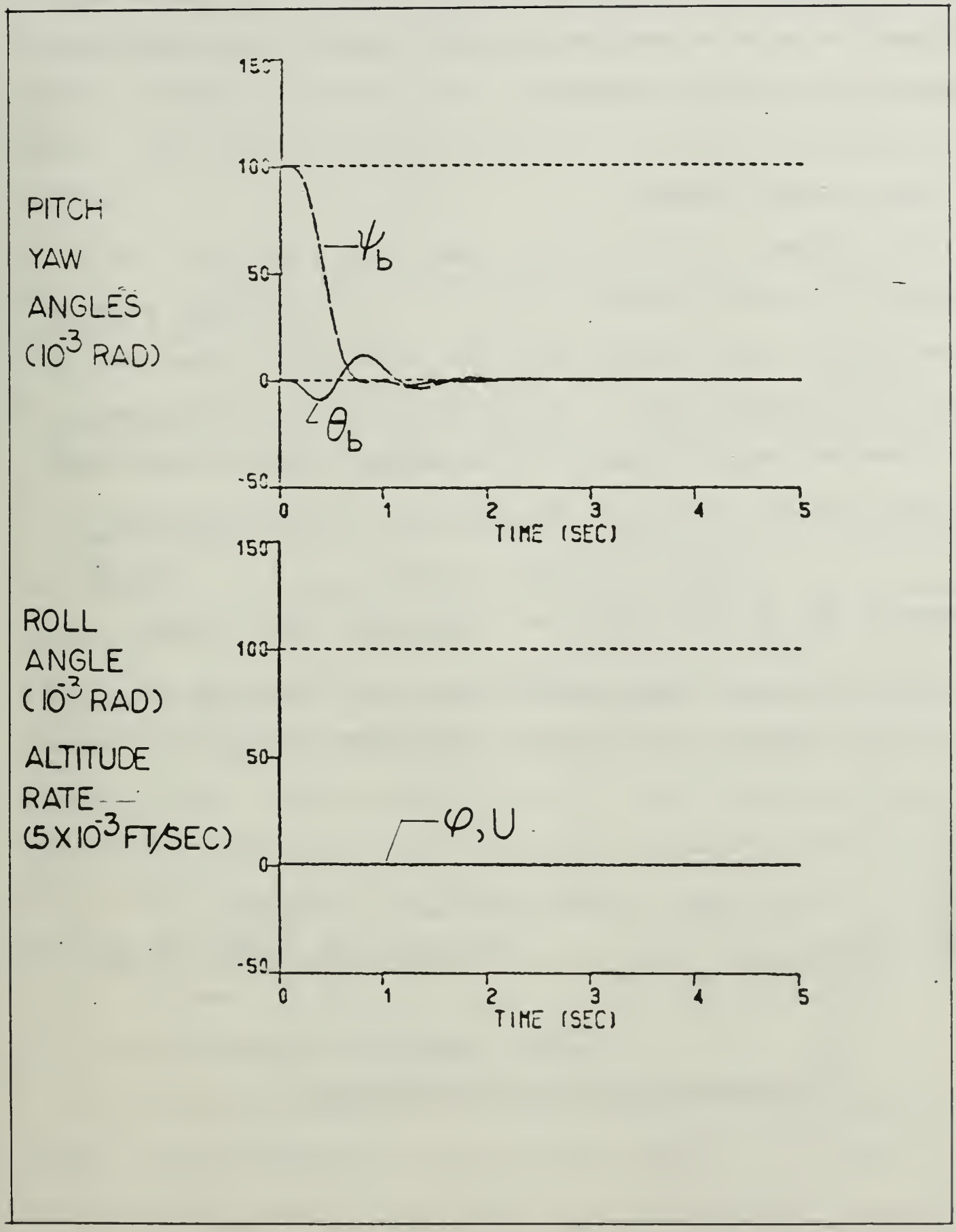

Figure 3.8 (d) Linear System Regulator Time Response with Optimal Gains, $\psi(0)=.1$

system. These results, for which the optimal gains were designed, are a reference to which results with the non-linear system can be compared.

E. THE OPTIMAL TRACKER

The optimal gains derived for the regulator can be extended to the tracking problem. The tracking problem characterizes the command-response relationship desired to steer and maneuver AROD. In theory, several approaches to the tracking problem exist. The method used in this work utilizes the error state. The control law which applies is

$$u_c(k) = -K\{x(k) - r_c(k)\} \qquad (3.17)$$

where $r_c(k)$ is the reference (commanded) state vector.

This control law is pictured in Figure 3.9. The error state

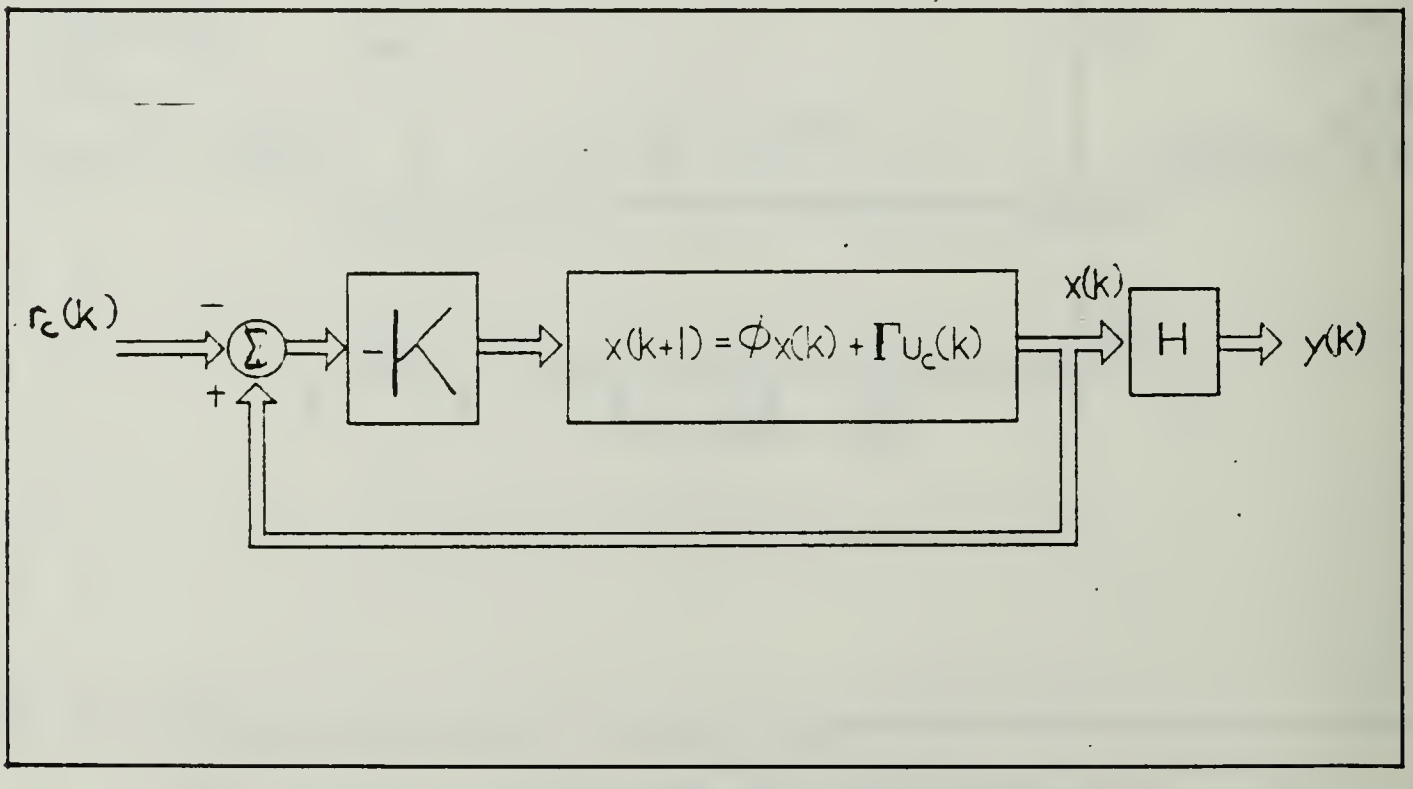

Figure 3.9 Tracker Control Scheme

as it drove the system states to zero in the regulator problem. A full state reference vector is required which means a commanded value must be specified for every system state. The reference vector for the roll/throttle subsystem becomes

$$r_{c_{PT}} = [\varphi_c, U_c, P_c, T_{r_c}, \delta_{a_c}, \delta_{t_c}, \dot{\delta}_{a_c}, \dot{\delta}_{t_c}]^t \quad (3.18)$$

and for pitch/yaw

$$r_{c_{QR}} = [\Theta_c, \psi_c, Q_c, R_c, \delta_{e_c}, \delta_{r_c}, \dot{\delta}_{e_c}, \dot{\delta}_{r_c}]^t \quad (3.19)$$

where the values of the reference vectors may be time varying and are the desired values of the final state.

Application of Eq. 3.17 to the linear model is described in Appendix C. Figure 3.10(a) is the response for desired states $\varphi=\Theta=.1$. The response is within the desired limitations for settling time (2 seconds) and overshoot (10%). Coupling is quite pronounced between the pitch and yaw. Figure 3.10(b) is the response to U=.5 and coupling between the throttle and roll heading is seen. Finally, Figure 3.10 (c) is the response to a step input on yaw ($\psi_b=.1$). The results are within specification.

F. RESULTS WITH THE NONLINEAR SYSTEM

The optimal steady-state gains for the linearized AROD model are determined in the previous section. The goal in designing the control algorithm is to provide fast response to disturbances and command inputs, while maintaining minimum overshoot of the final state. The requirement for

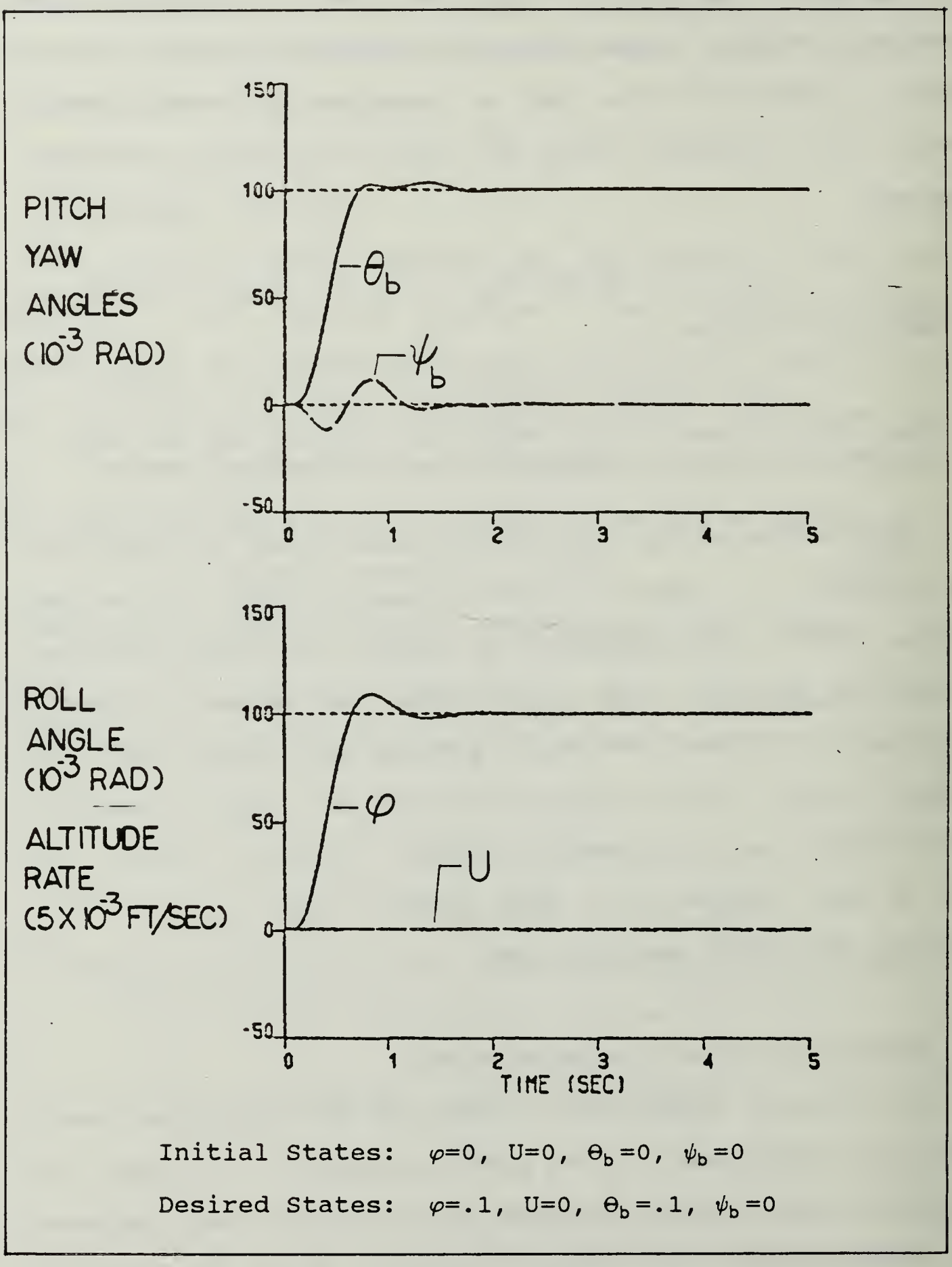

Figure 3.10 (a) Linear System Tracker Time Response with Optimal Gains, Roll and Pitch Command

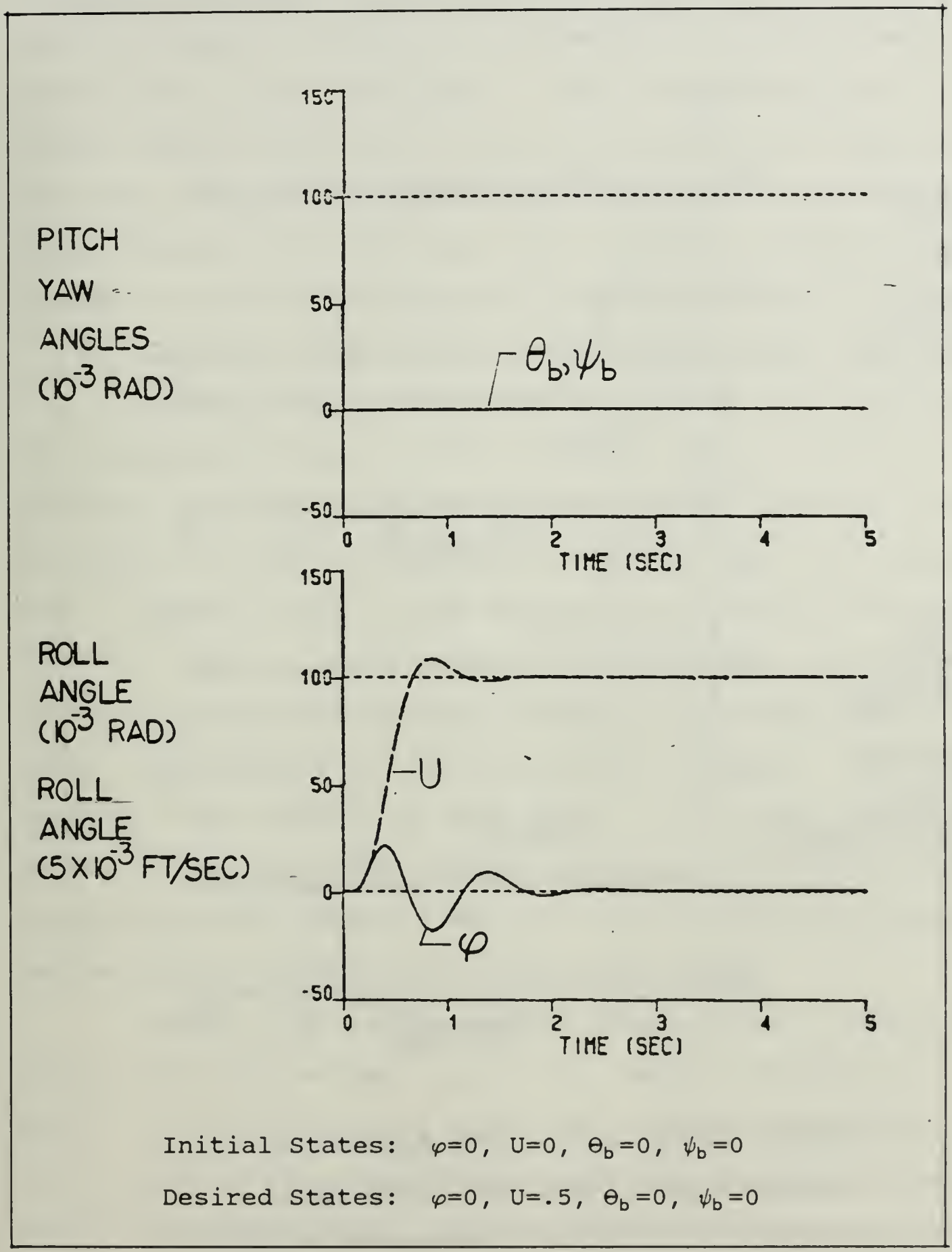

Initial States: $\varphi=0$, $U=0$, $\theta_b=0$, $\psi_b=0$

Desired States: $\varphi=0$, $U=.5$, $\theta_b=0$, $\psi_b=0$

Figure 3.10 (b) Linear System Tracker Time Response with Optimal Gains, Altitude Rate Command

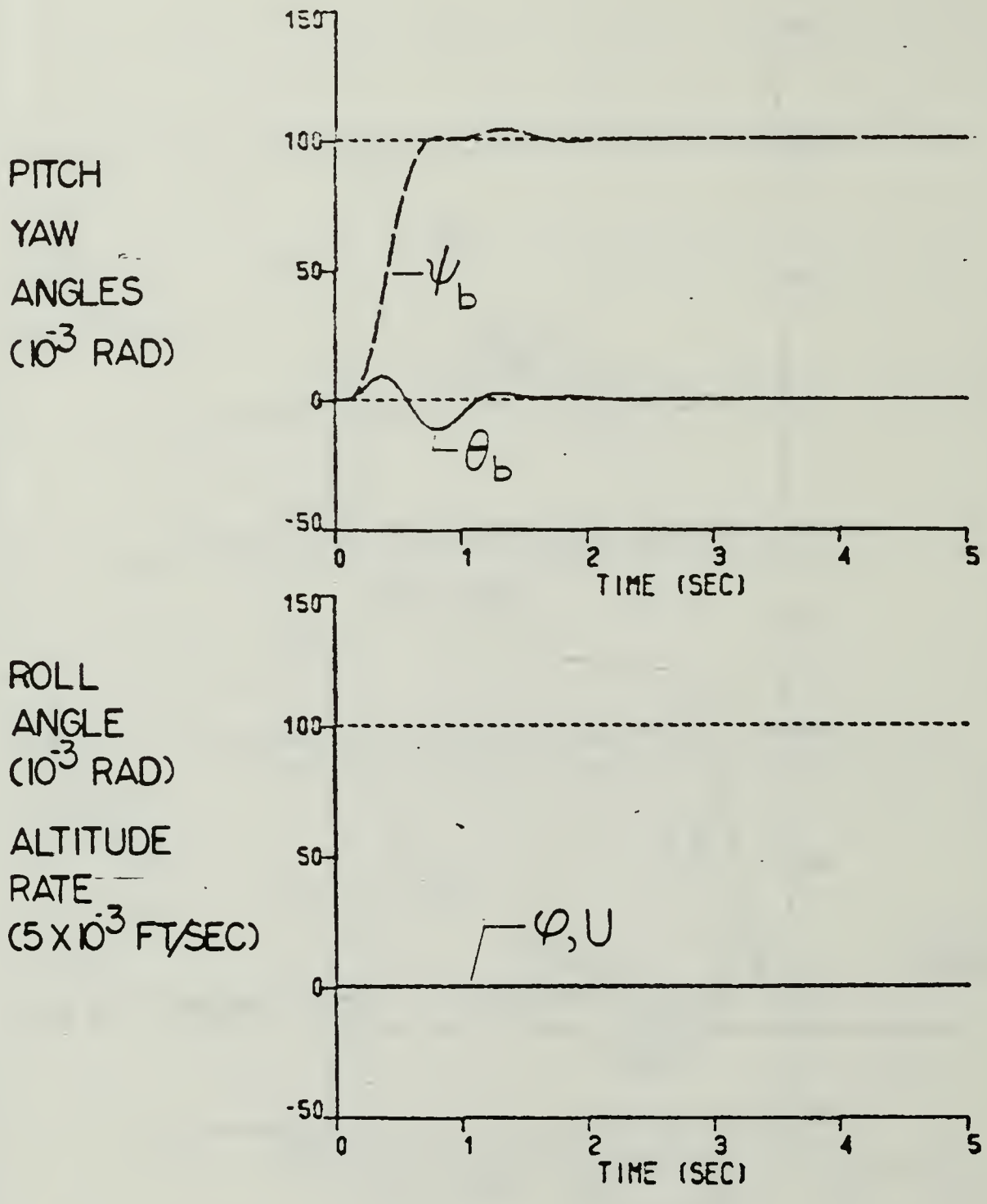

Initial States: $\varphi=0$, $U=0$, $\theta_b=0$, $\psi_b=0$

Desired States: $\varphi=0$, $U=0$, $\theta_b=0$, $\psi_b=.1$

Figure 3.10 (c) Linear System Tracker Time Response with Optimal Gains, Yaw Command

quickness is driven by the erratic behavior of the full model in Chapter II when it is disturbed from the steady-state pitch or yaw positions. This section applies the linear system controller to the nonlinear model. Results are given first for the controller applied to the nonlinear model without the pitch and yaw aerodynamic moments and second to the full model with all moments and forces.

1. Nonlinear Model without Aerodynamic Moments

Figure 3.11(a) is the nonlinear system step response for the heading angle, φ. The settling time is 1.5 seconds which is the same as for the linear system. However, the overshoot is nearly 15% which is larger than the linear case. Figure 3.11(b) is the response to a desired altitude rate, U', of .1. Note that for the nonlinear model, the altitude rate is derived from the Euler angles and it is no longer approximated by the body-fixed velocity, U. The altitude rate settles in less than 1.5 seconds, but the heading angle, disturbed through coupling, settles in 1.75 seconds with .05 radians overshoot. Still, the system does settle quickly and with zero steady-state error.

Figure 3.12 is the system response for a desired state step input on yaw, ψ_b, of .1. Severe coupling to φ and U' is observed, while pitch, Θ_b, behaves as expected. The reality of the linearizing assumptions becomes evident here. The results simply indicate that as the body is

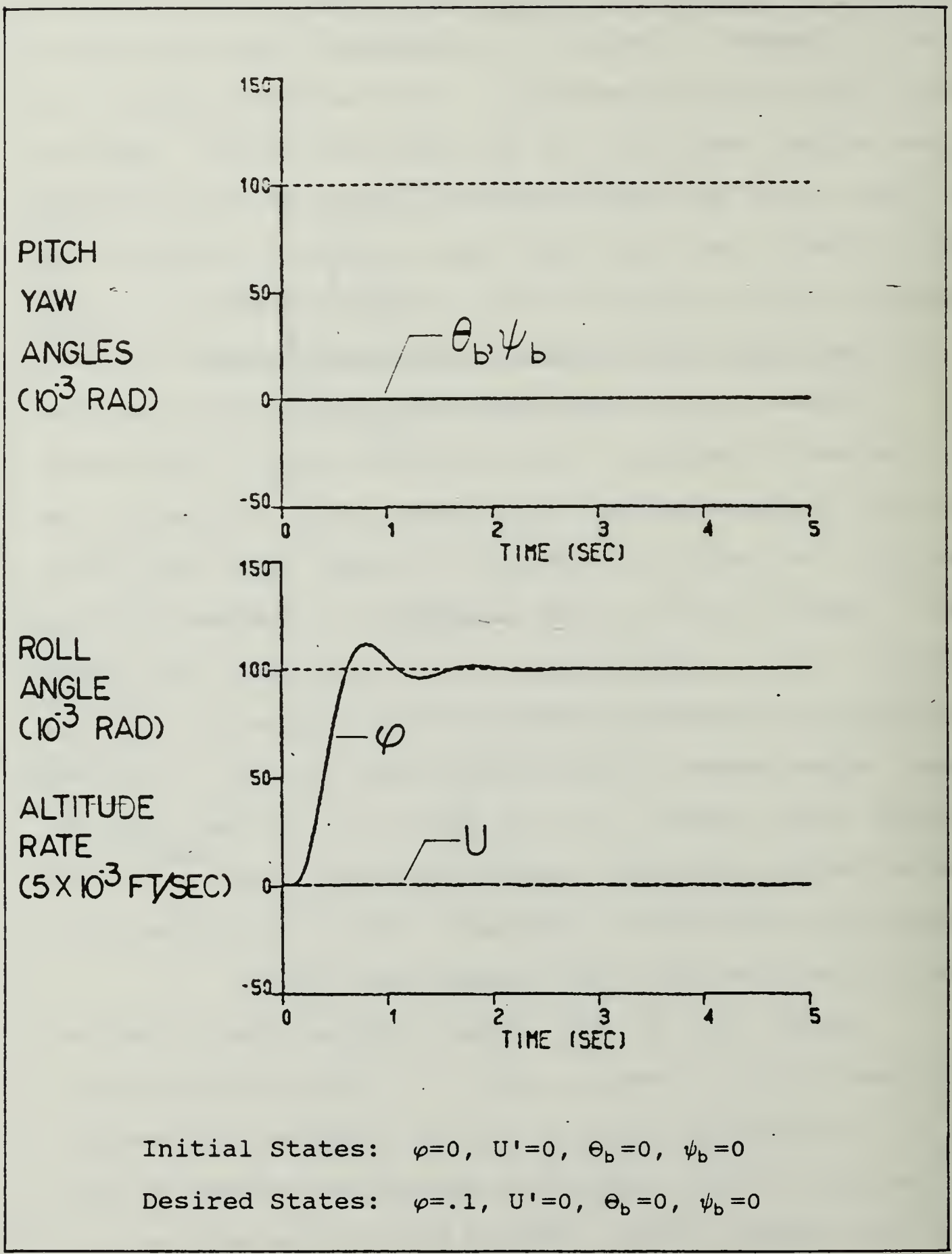

Initial States: $\varphi=0$, $U'=0$, $\Theta_b=0$, $\psi_b=0$

Desired States: $\varphi=.1$, $U'=0$, $\Theta_b=0$, $\psi_b=0$

Figure 3.11 (a) Nonlinear System Tracker Response
Heading Angle Command, φ

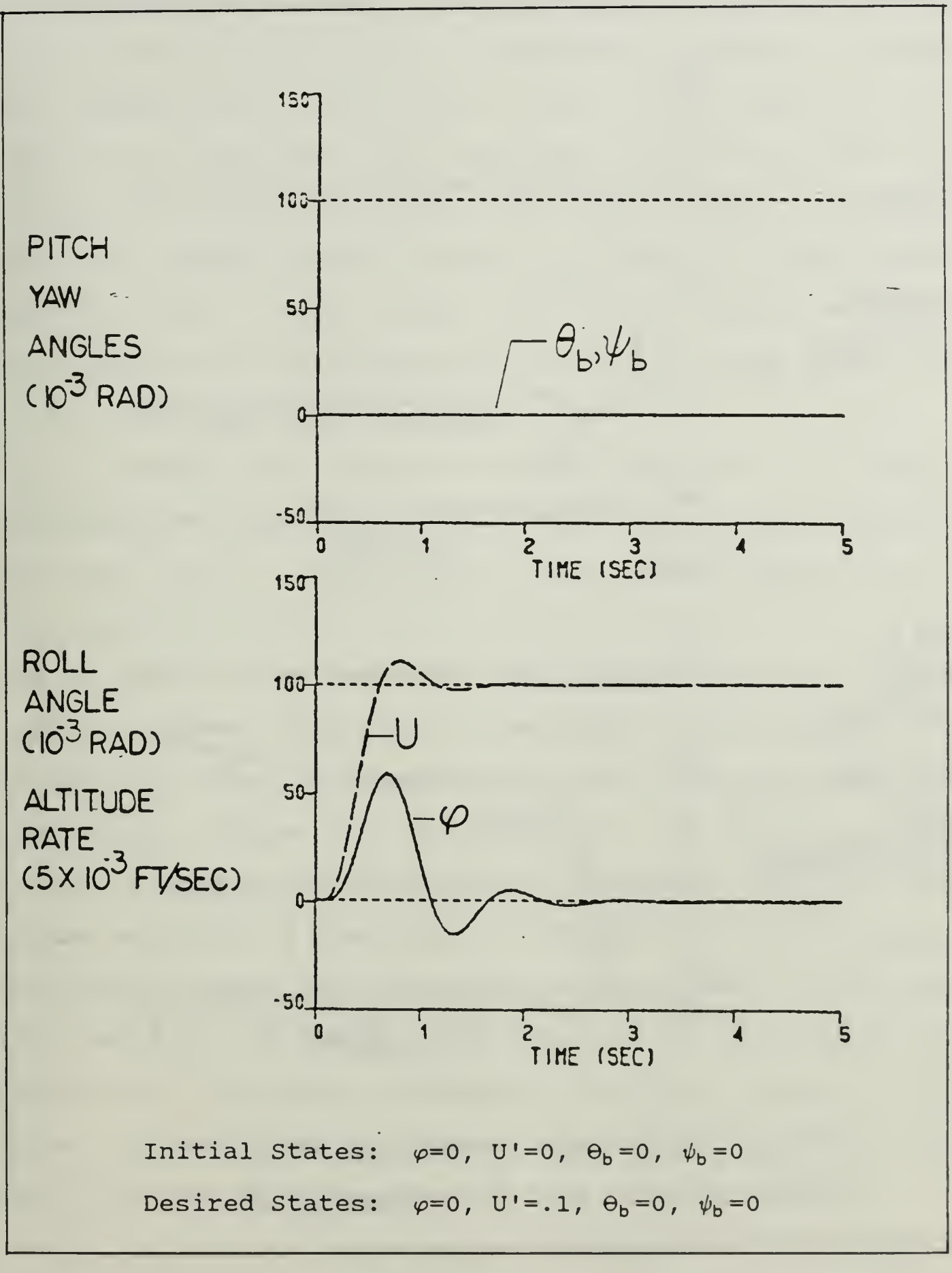

Figure 3.11 (b) Nonlinear System Tracker Response
Altitude Rate Command, U'

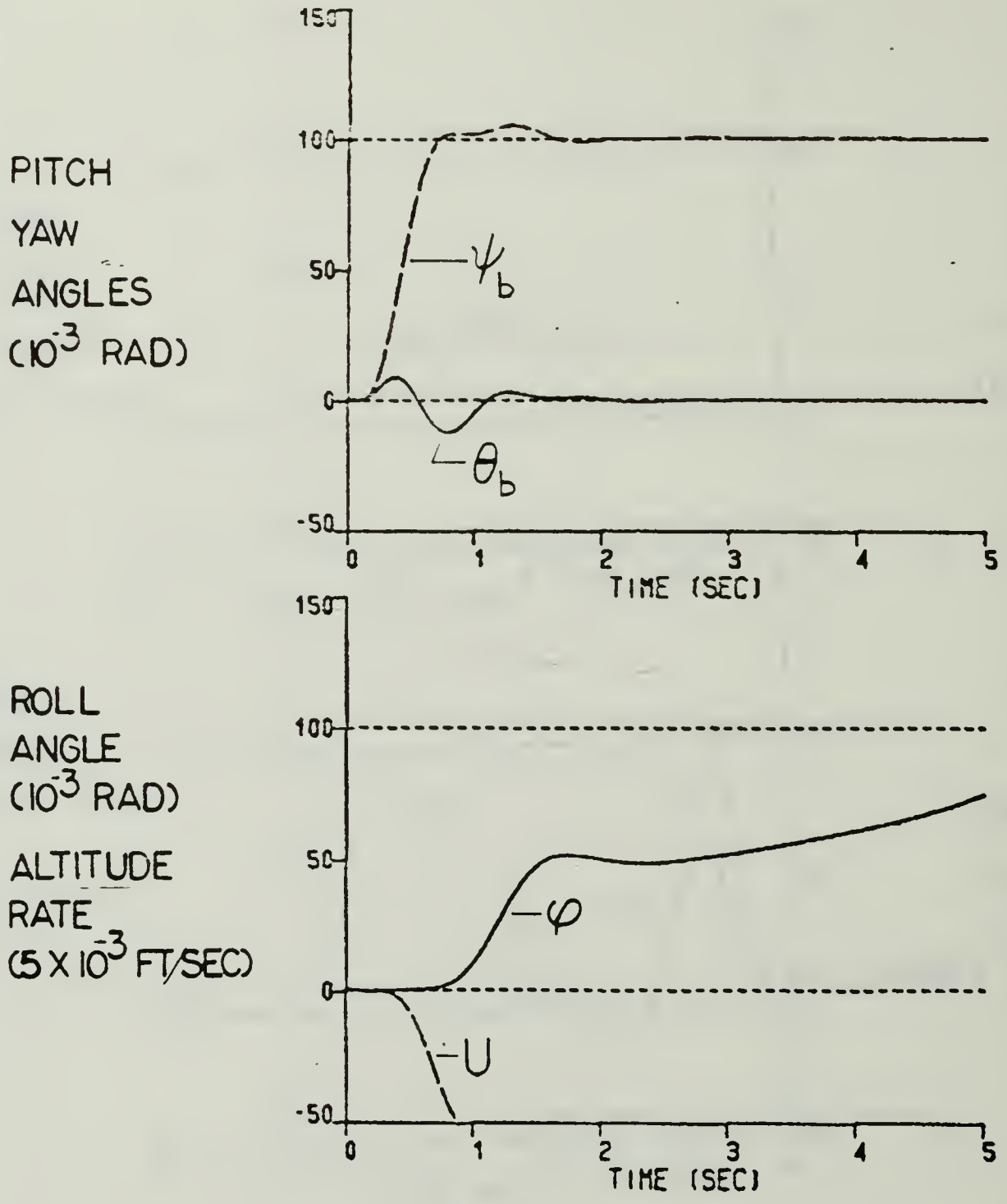

Initial States: $\varphi=0$, $U'=0$, $\theta_b=0$, $\psi_b=0$

Desired States: $\varphi=0$, $U'=0$, $\theta_b=0$, $\psi_b=.1$

Figure 3.12 Nonlinear System Tracker Response
Yaw Command

pitched (or yawed), some of the altitude holding thrust will be lost and redirected to a horizontal velocity. Figure 3.13 shows that if the pitch or yaw is kept small enough (here ψ_b=.03 radians), then the altitude rate can also be controlled. Figure 3.14 goes a step further and illustrates that if a bounded input (pitching the body for 1 second) is applied, then a speed across the ground can be realized while maintaining the desired heading and altitude rate.

2. Nonlinear Model Complete

Results for the controller applied to the full model including the troublesome pitch and yaw aerodynamic moments are shown here. Figure 3.15 is the system response to a step input on roll (φ=.1) A steady-state error of -.04 is and is due to the downwash swirl moment previously discussed. However, coupling to the other states causing the instability noted in Chapter II has been eliminated by the controller. Figure 3.16 is the result of a step input for U'=.5. Coupling of the velocity to the pitch and yaw axes causes enough of a disturbance in angle of attack to upset the system beyond the constraints of the control vanes and the controller is unable to correct it. To illustrate the behavior of the data to pitching and yawing, Figure 3.17 shows the resulting aerodynamic moments, L_a, M_a, N_a, for step input for altitude rate.

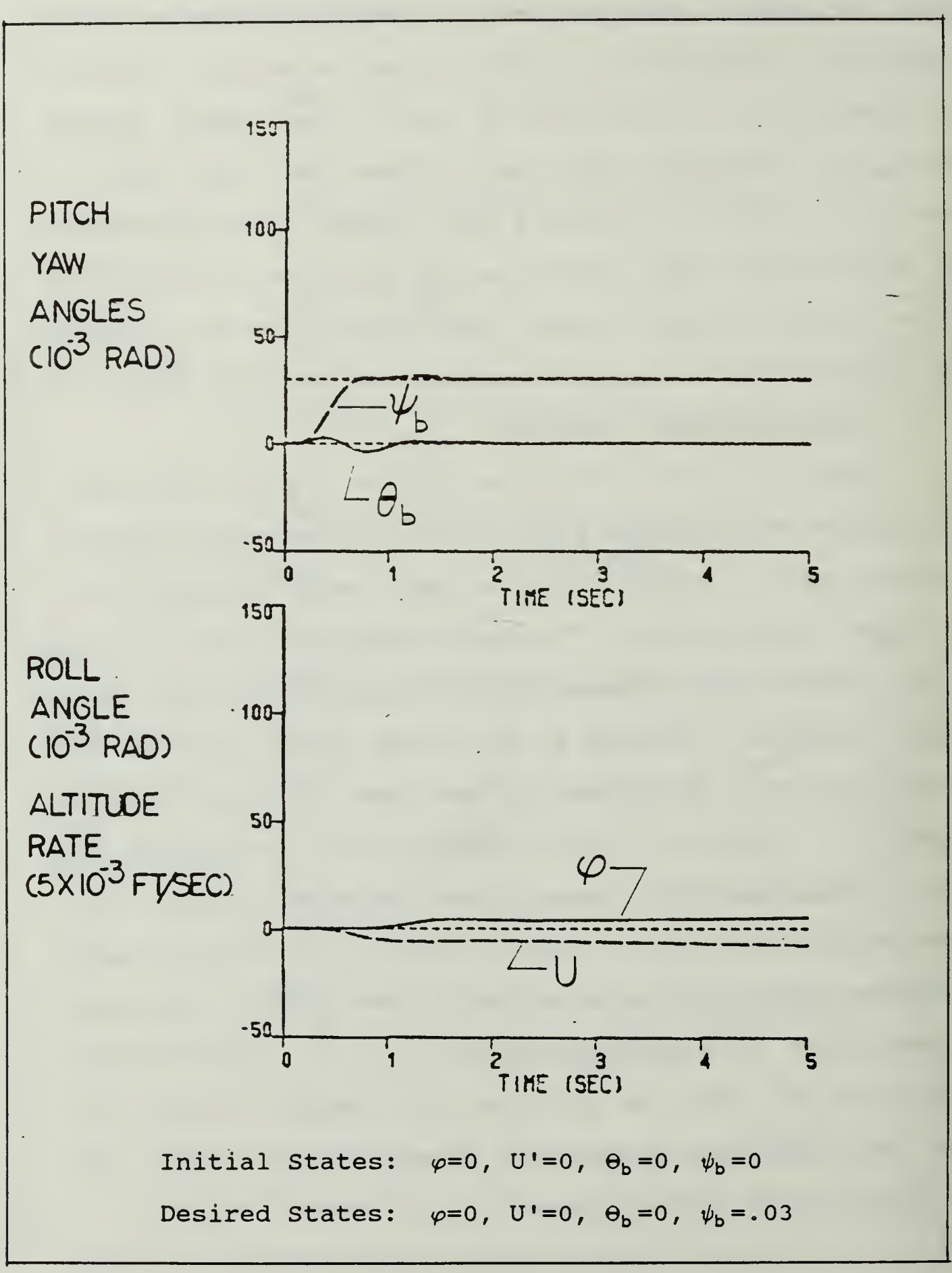

Initial States: $\varphi=0$, $U'=0$, $\theta_b=0$, $\psi_b=0$

Desired States: $\varphi=0$, $U'=0$, $\theta_b=0$, $\psi_b=.03$

Figure 3.13 Nonlinear System Tracker Response
Yaw Command for Minimum U', φ Deviation

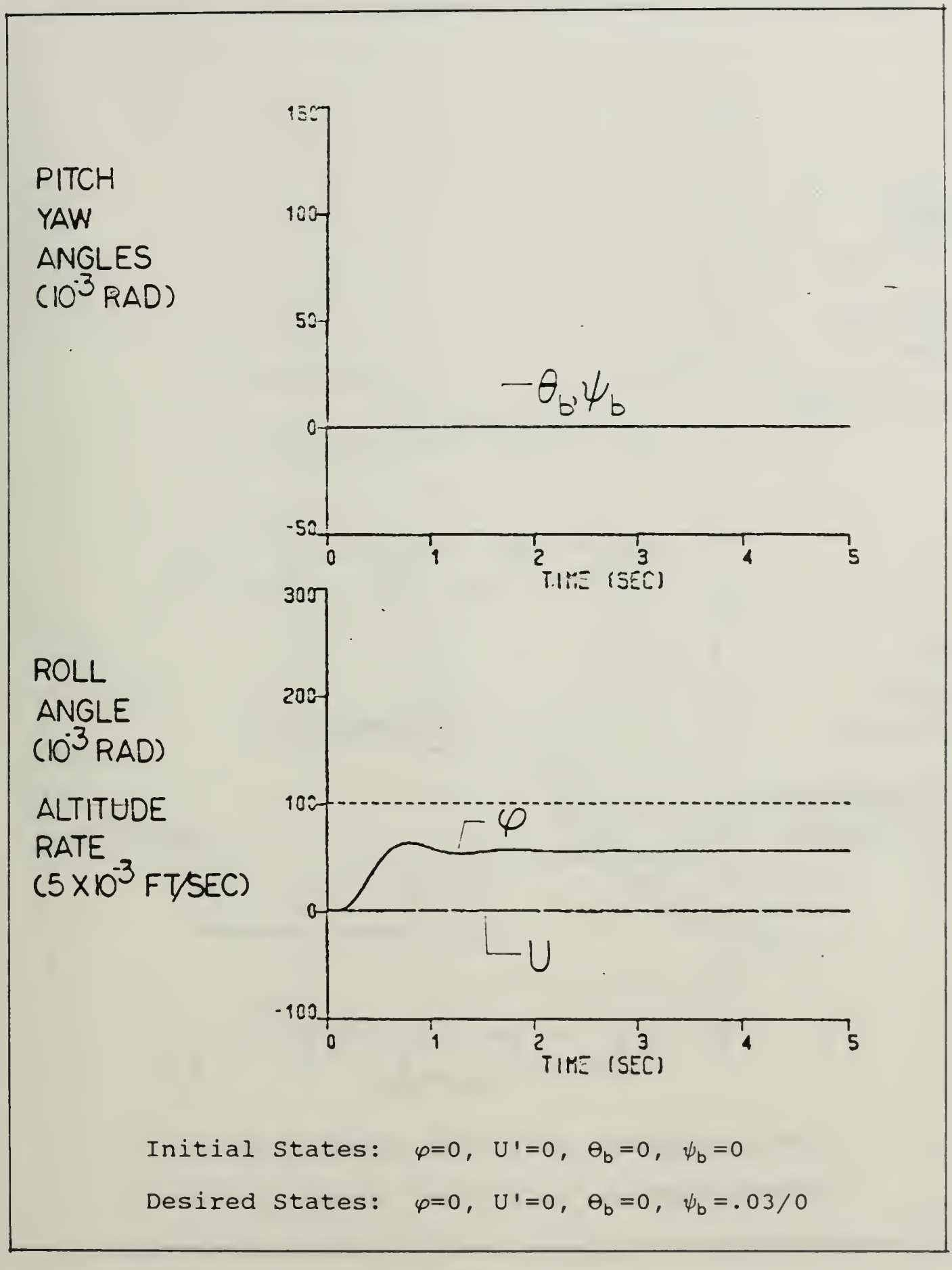

Initial States: $\varphi=0$, $U'=0$, $\theta_b=0$, $\psi_b=0$

Desired States: $\varphi=0$, $U'=0$, $\theta_b=0$, $\psi_b=.03/0$

Figure 3.14 Nonlinear System Tracker Response
Yaw Command is a 2 second step

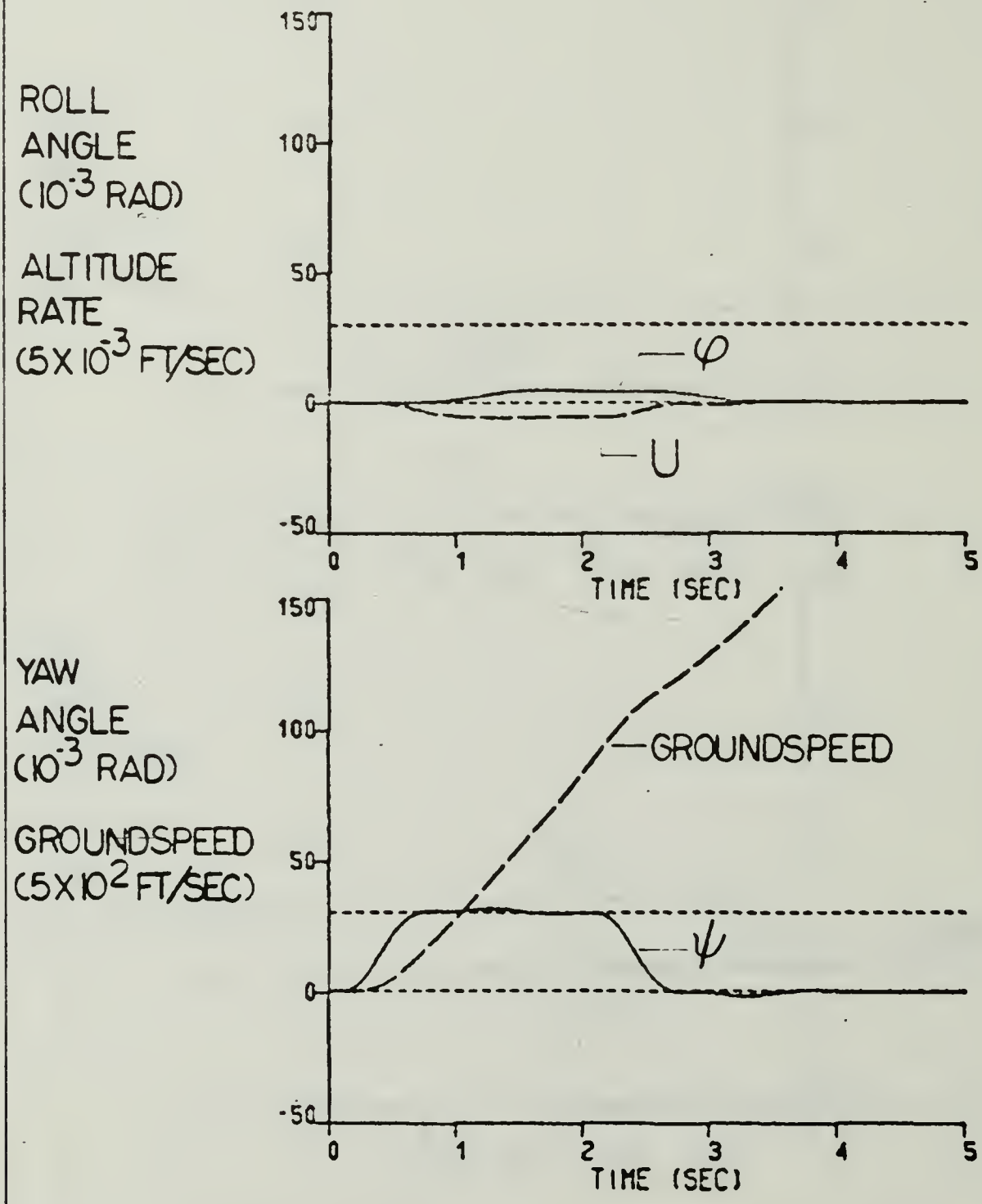

Initial States: $\varphi=0$, $U'=0$, $\theta_b=0$, $\psi_b=0$

Desired States: $\varphi=.1$, $U'=0$, $\theta_b=0$, $\psi_b=0$

Figure 3.15 Full Nonlinear Model Tracker Response
Heading Angle Command

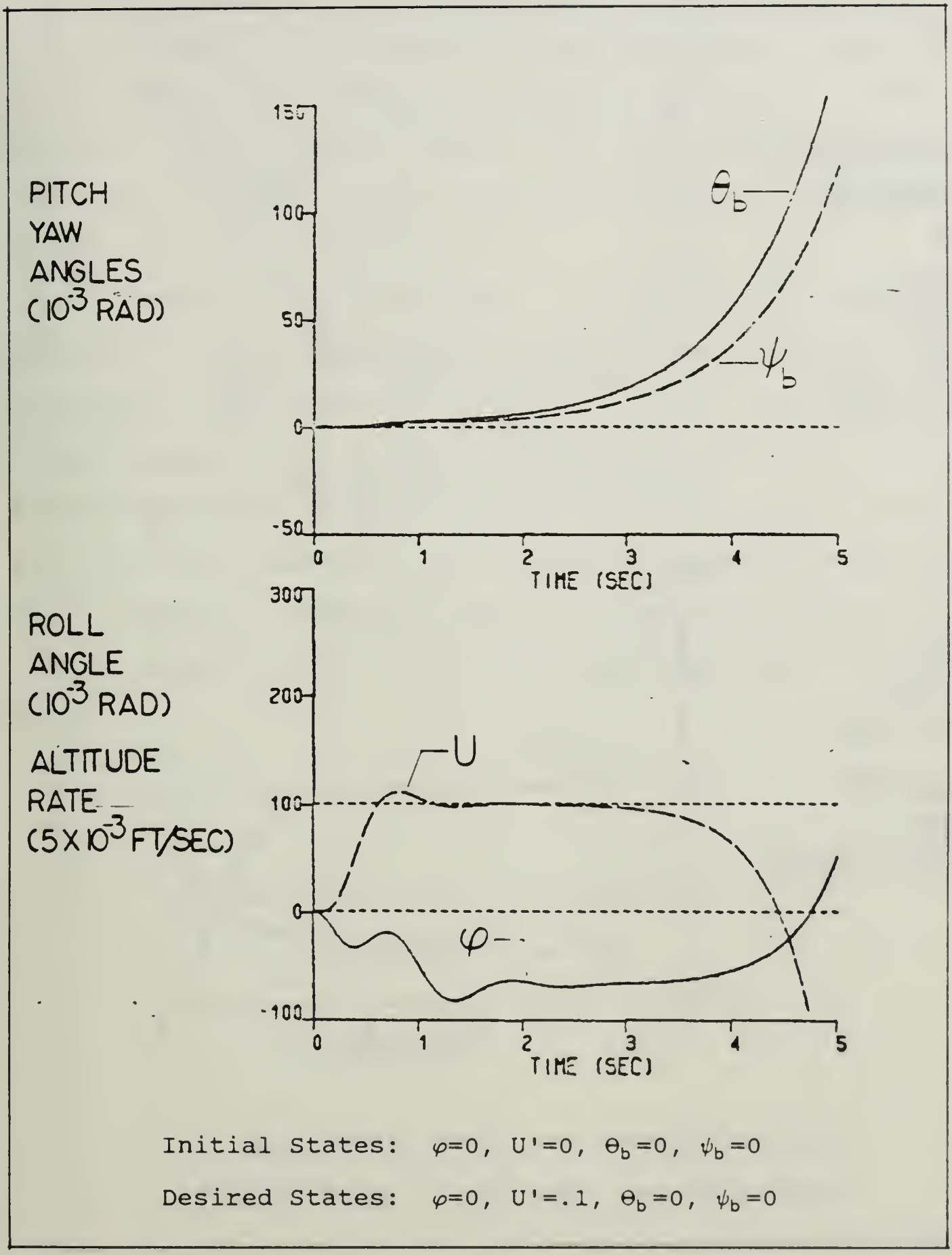

Initial States: $\varphi=0$, $U'=0$, $\theta_b=0$, $\psi_b=0$

Desired States: $\varphi=0$, $U'=.1$, $\theta_b=0$, $\psi_b=0$

Figure 3.16 Full Nonlinear Model Tracker Response
Altitude Rate Command

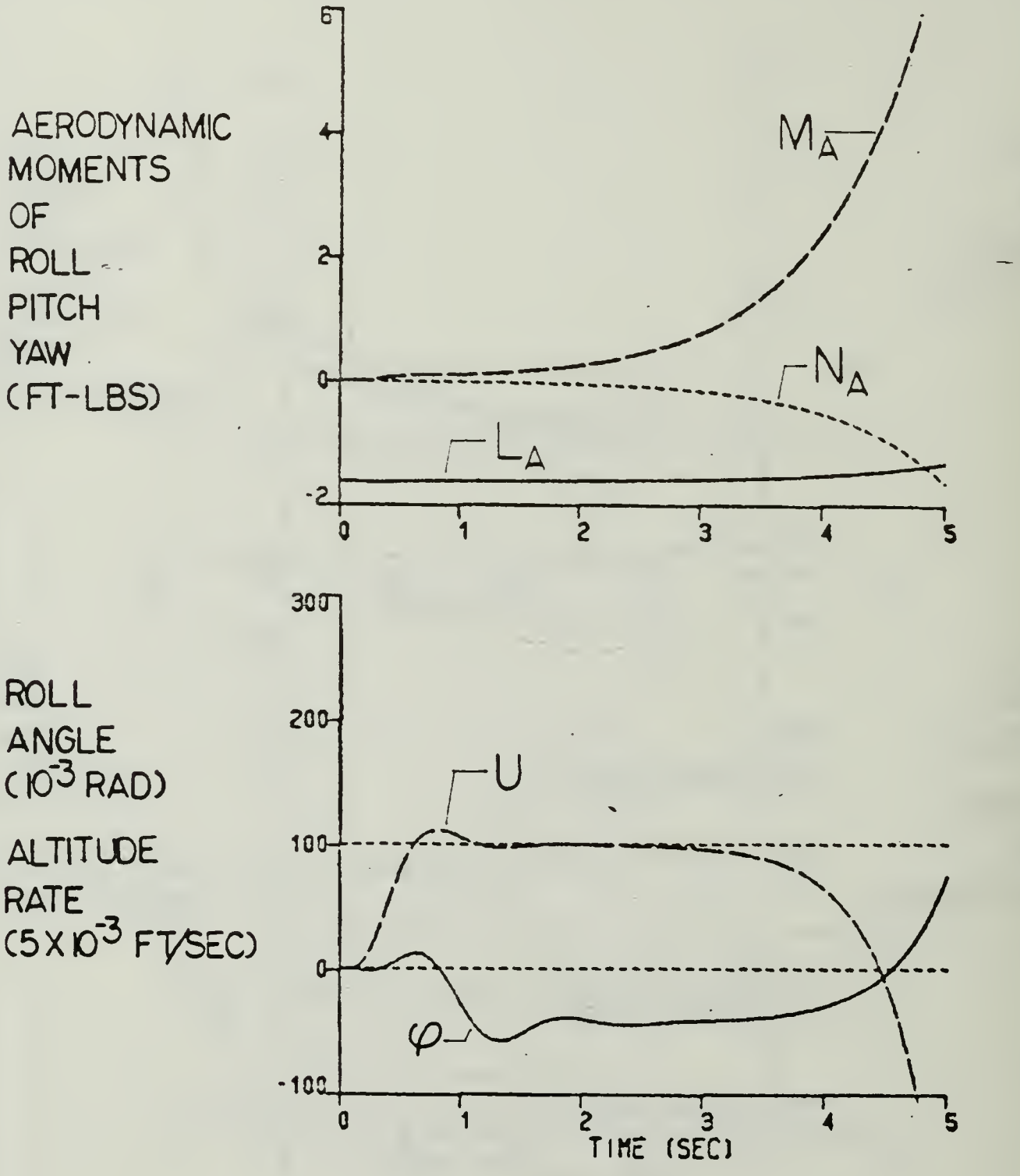

Initial States: $\varphi=0$, $U'=0$, $\theta_b=0$, $\psi_b=0$

Desired States: $\varphi=0$, $U'=.1$, $\theta_b=0$, $\psi_b=0$

Figure 3.17 Aerodynamic Moments Response to Altitude Rate Command

3. Conclusion

Clearly, the controller is not adequate to deal with such large discontinuities as the aerodynamic moments present. The control vanes are the limiting factor. Therefore, the data or the way it is related to the states in the model is not correct.

However, we concluded in Chapter II that the behavior of AROD without these moments closely resembles the gyroscopic model that we expected. If the controller is judged based on its performance with the nonlinear model without the pitch and yaw moments, then the control design is valid. The fact that the controller maintains stability while directing commanded inputs to steer and maneuver the vehicle supports the linear model approach taken in this work.

IV. RADIO FREQUENCY ANTENNA DESIGN

A. REQUIREMENTS FOR A RF ANTENNA

Detailed technical requirements for the AROD video downlink have not been specified by the GATERS project office as of this writing. Neither have the tactical or operational requirements been addressed in detail. However, GATERS project quarterly review conferences have undertaken discussion of this aspect of AROD and some consensus has emerged [2]. It is from these discussions and from the stated operational mission of AROD (see Chapter I) that assumptions are made on which to base the antenna design.

Several facts are known about AROD which pertain to RF wave propagation.

(1) Cost and weight are key factors and a simple design utilizing inexpensive, readily available materials is most appropriate.

(2) The AROD is intended to be man carried and easily readied for launch. Rugged, lightweight construction is required.

(3) A frequency range in the UHF band of 800 to 900 megahertz (MHz) has been tentatively identified for video signal transmission.

(4) A range of at least five kilometers is required if AROD is to be operated at the maximum planned distance from the operator.

(5) An omnidirectional pattern is desired for training purposes to ensure that the video signal can be received regardless of AROD's orientation.

(6) Angular speed of the propeller during hover is about 7200 rpm (120 Hz) and a three blade, carbon fiber composite propeller is to be used.

(7) The body is made of a carbon fiber composite and the frame is composed of aluminum. The forebody is fiberglass.

(8) The AROD contains an on board computer, sensors, and a radio receiver for the command uplink.

This list by no means includes all of the factors which contribute to the electromagnetic character of AROD nor does it address every possible requirement for a RF antenna on AROD. However, these requirements allow a design goal to be determined based on the following assumptions:

(1) The 120 Hz disturbance from the rotating propeller and the command uplink RF signal will not interfere with the 800 to 900 MHz transmission signal. An order of magnitude between signals is a common rule for non-interfering signals. The propeller (7200 rpm) and the command uplink (72 MHz) meet this constraint.

(2) For the purpose of electromagnetic analysis, the AROD can be modelled as the cylinder pictured in Figure 4.1. The cylinder has the outside dimensions of the AROD main body surface shown in Figure 1.1.

(3) The carbon fiber body is highly conductive. AROD project engineers have stated that the composite used has high conductivity characteristics.

(4) The carbon fiber body will essentially shield out electromagnetic interference from the on board computer and sensors.

(5) The antenna will conform to the body of AROD as much as possible to prevent breakage while being carried and snagging during operation in closed-in areas.

(6) The antenna will be fixed to facilitate simple launch preparation.

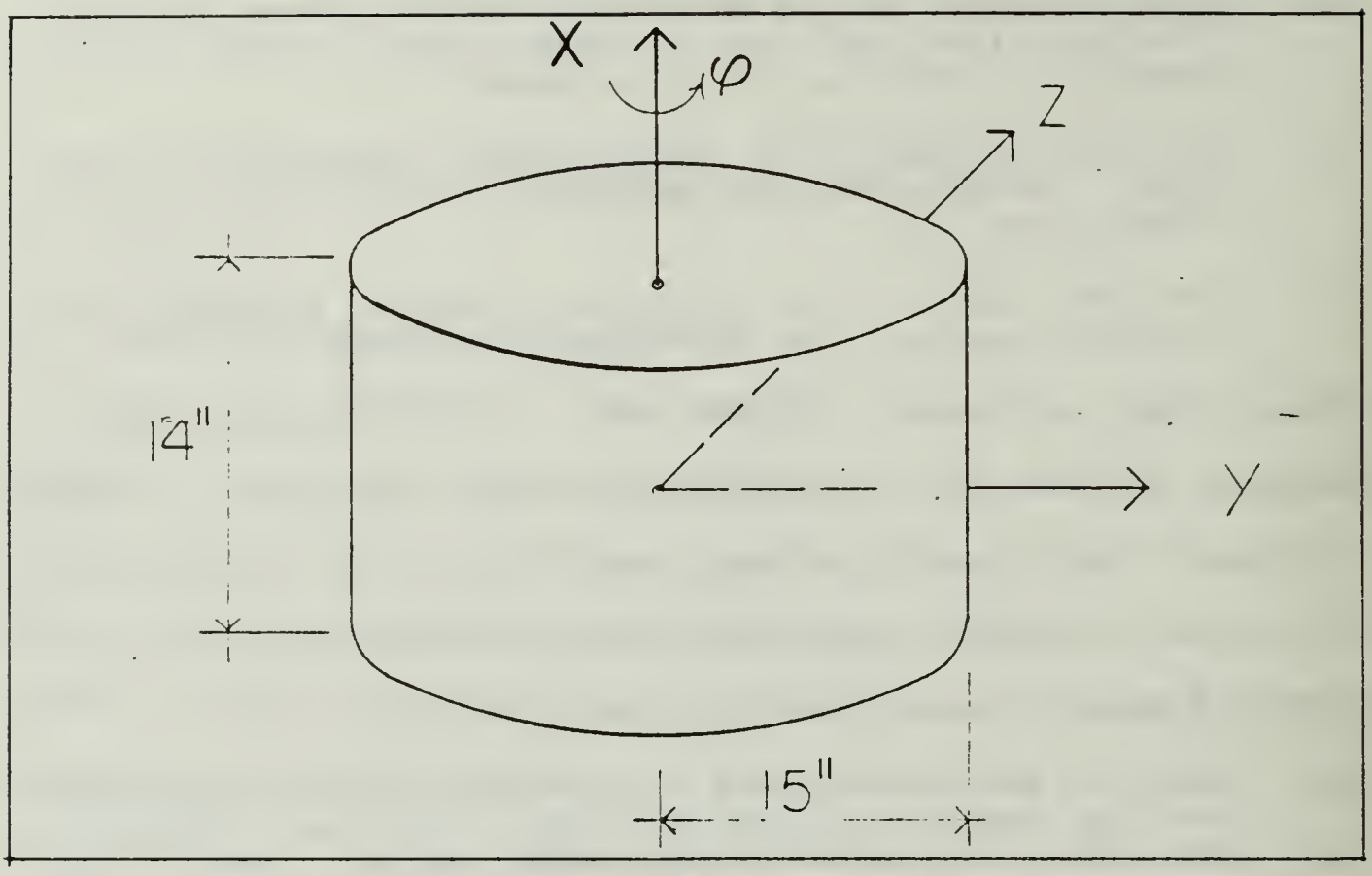

Figure 4.1 AROD Model for Antenna Simulation

B. DESIGN SELECTION

A logical point to start the choice of antenna is with devices already in use on similar vehicles. AROD is most similar to a satellite in that it is free flying yet not fast moving and aerodynamic influences are negligible. One UHF satellite antenna in common use is the mesh array commonly referred to as the umbrella [14]. However, the umbrella antenna is neither rugged nor omnidirectional and would be a poor choice for AROD.

Stripline antennas are arrays of slotted strips which are surface mounted to a vehicle. The slotted strips are cut for specific frequencies and are generally not tuneable.

These antennas are lightweight, able to be flush mounted and could be made rugged and durable for AROD. Research for this report has found only L-band and S-band variations of the stripline satellite antenna in use. However, the concept of a flush mounted stripline can potentially be exploited in the development of the UHF antenna for AROD. [15] A simple antenna to employ is a dipole extending from the top of AROD or out the bottom. At a transmission frequency of 800 MHz, the wavelength is

$$\lambda = \frac{c}{f} = 14.76 \text{ inches} \qquad (4.1)$$

where $c = 1.18 \times 10^{10}$ inches/second.

A half-wave dipole, for example would extend 7.38 inches above or below AROD. This design is not considered here. Instead, an antenna which conforms to the AROD body is developed to satisfy two of the needs listed above: the need for a rugged, fixed antenna and the presence of a conducting surface (the body).

The need for a rugged, fixed antenna is obvious and will not be discussed further. The conductivity of the AROD body, however, can possibly enhance the conformal antenna's radiation pattern characteristics if the body behaves like a reflecting ground plane. This potential and basic antenna's which can take advantage of the reflecting body are discussed in the next section.

C. THEORETICAL DEVELOPMENT

Two basic designs for the UHF antenna are considered here. Referring to Figure 4.1, the first is a vertically polarized dipole or dipole array and the second is a horizontally polarized loop antenna. The dipole array and the loop antenna are both very well developed in References 16 and 17. This work does not endeavor to recreate or expand on either books' theoretical development and the reader is encouraged to consult these sources if such information is desired. Instead, a brief explanation of the important characteristics of the dipole and the loop antenna is offered as a preface to the practical considerations which drive the design process.

1. Dipole Array

a. The Half-Wave Dipole

An omnidirectional far field pattern is the goal. For this reason, a dipole which radiates an omnidirectional pattern is desired. An obvious choice is the half-wave dipole. Fed at the center, the current on a half-wave dipole will decrease sinusoidally as it nears the end points.

A single half-wave dipole yields the far field pattern of Figure 4.2. The horizontal (azimuth) pattern is omnidirectional. If the X direction of the dipole corresponds to the X direction of AROD then it is the horizontal pattern of the dipole which is of greatest interest in

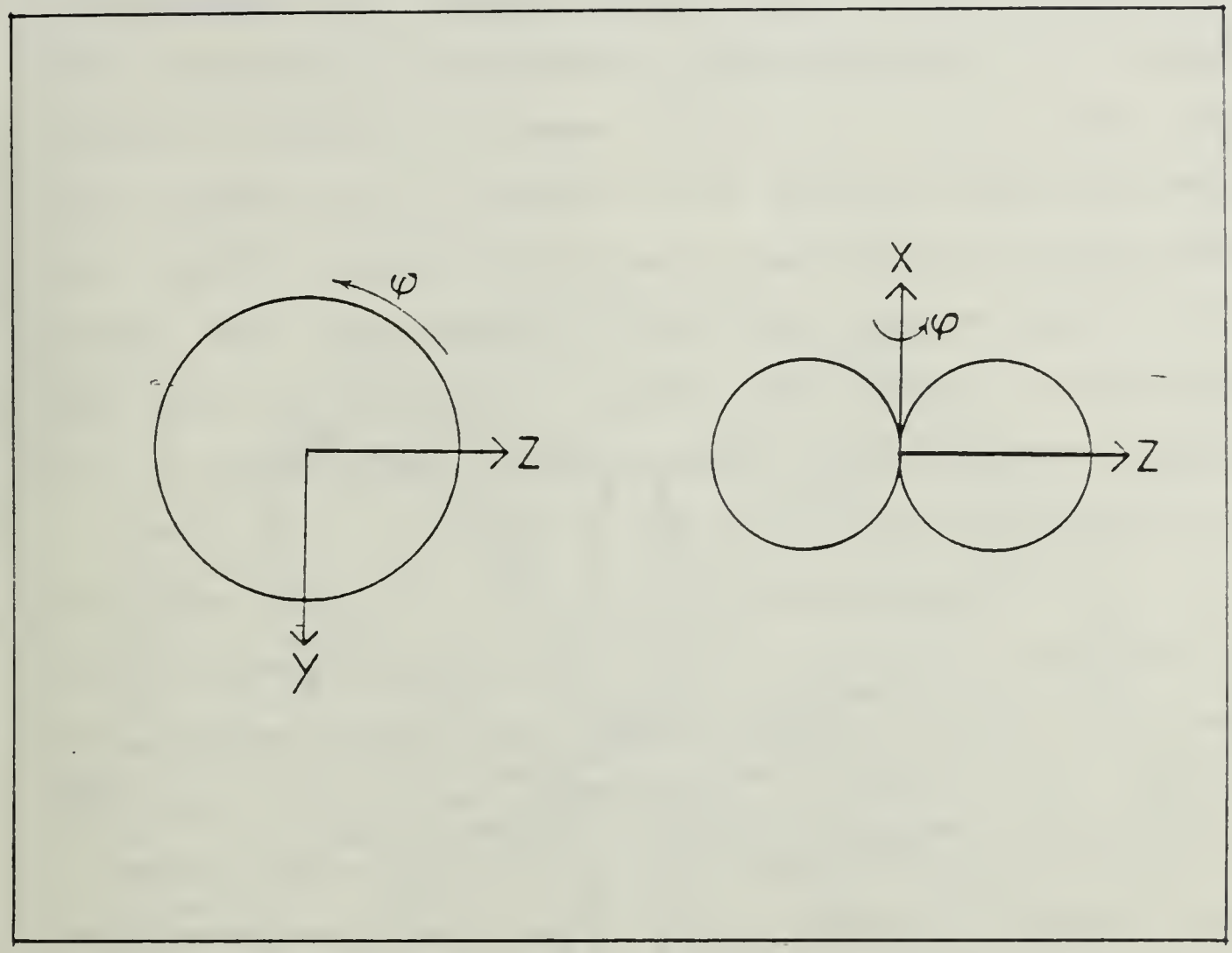

Figure 4.2 Far Field Patterns of a Half-Wave Dipole

obtaining an acceptable solution for AROD. Therefore, the emphasis is placed on obtaining an acceptable horizontal far field pattern from subsequent antenna designs.

b. Circular Array of Half-Wave Dipoles

A dipole which is close to the AROD body will have radiation characteristics far different from the free space or free standing half-wave dipole. The conducting body will, at the very least, block the dipole pattern in a direction "behind" or toward the body from the dipole. An array of dipoles which conforms to and encircles the body

will allow a signal to radiate through 360 degrees in azimuth (φ). Such an array is called a circular or ring array [16:p. 352]. A circular array of identical, equally spaced half-wave dipoles each excited at its center will result in a non-directional far field pattern. Figure 4.3 is the resulting far field gain pattern of a four dipole ring array. Although the pattern is plagued by peaks and valleys creating a wide dynamic range in directive gain, it is a good starting point for the design.

The theory and analysis for circular arrays is well developed and an array yielding an acceptable omni-directional pattern can be derived using the procedure given in [16:p. 354]. However, no procedure is found for an array with an obstructing body in its center. For this reason, a model of the AROD body which approximates its electromagnetic characteristics is useful. To such a model, various arrays can be added and the resulting far field patterns can be analyzed for adequacy.

2. Loop Antennas

The loop antenna is an attractive alternative for the AROD application. A loop would naturally conform to the body circumference and could be constructed easily. Loop antennas are thoroughly discussed in Reference 17. However, analytical results are readily derived only for "small" or "moderate" sized loops. A moderate size loop is defined as

$$\frac{2Pi}{\lambda} b \leq 2.5 \qquad (4.2)$$

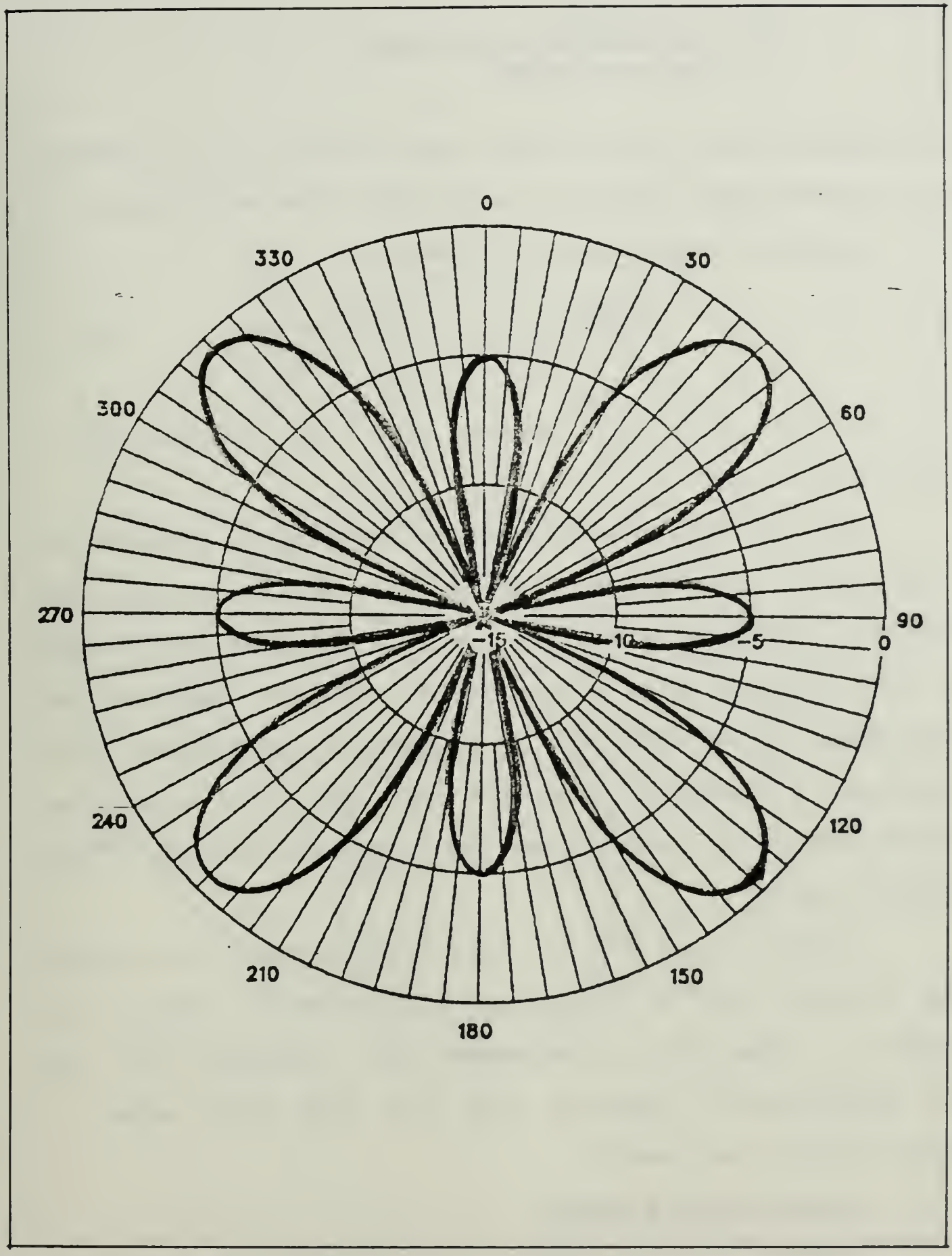

Figure 4.3 Horizontal Far Field Pattern - 4 Dipole Ring

where

Pi = 3.1415962,
b is the radius of the loop,
λ is the wavelength.

A circumferential loop on AROD has a radius b $\geq$ 15 inches. At a transmission frequency of 800 MHz, the wavelength λ = 14.76 inches and equation 4.2 becomes:

$$\frac{2Pi}{\lambda} b \geq 6.39 \quad (f = 800 \text{ MHz}) \qquad (4.3)$$

Clearly, AROD does not satisfy the requirements for a moderate size loop.

The difficulty with deriving analytical results for larger than moderate size loops lies in evaluating the Maxwell's Equations. Larger loops such as an antenna around the AROD body require a much more extensive mathematical development to evaluate the equations than is desired here. Therefore, a numerical technique with the aid of a computer is best suited for evaluating the radiation pattern of the proposed design.

Figure 4.4 is the far field gain pattern of a single loop antenna with a radius b = 15 inches. While this pattern is apparently directional and inadequate for the AROD application, combined with the AROD body model, a better pattern may result.

3. Ground Plane Effects

Perfect ground planes are defined as infinite, plane, and perfect conductors. Practical approximations to

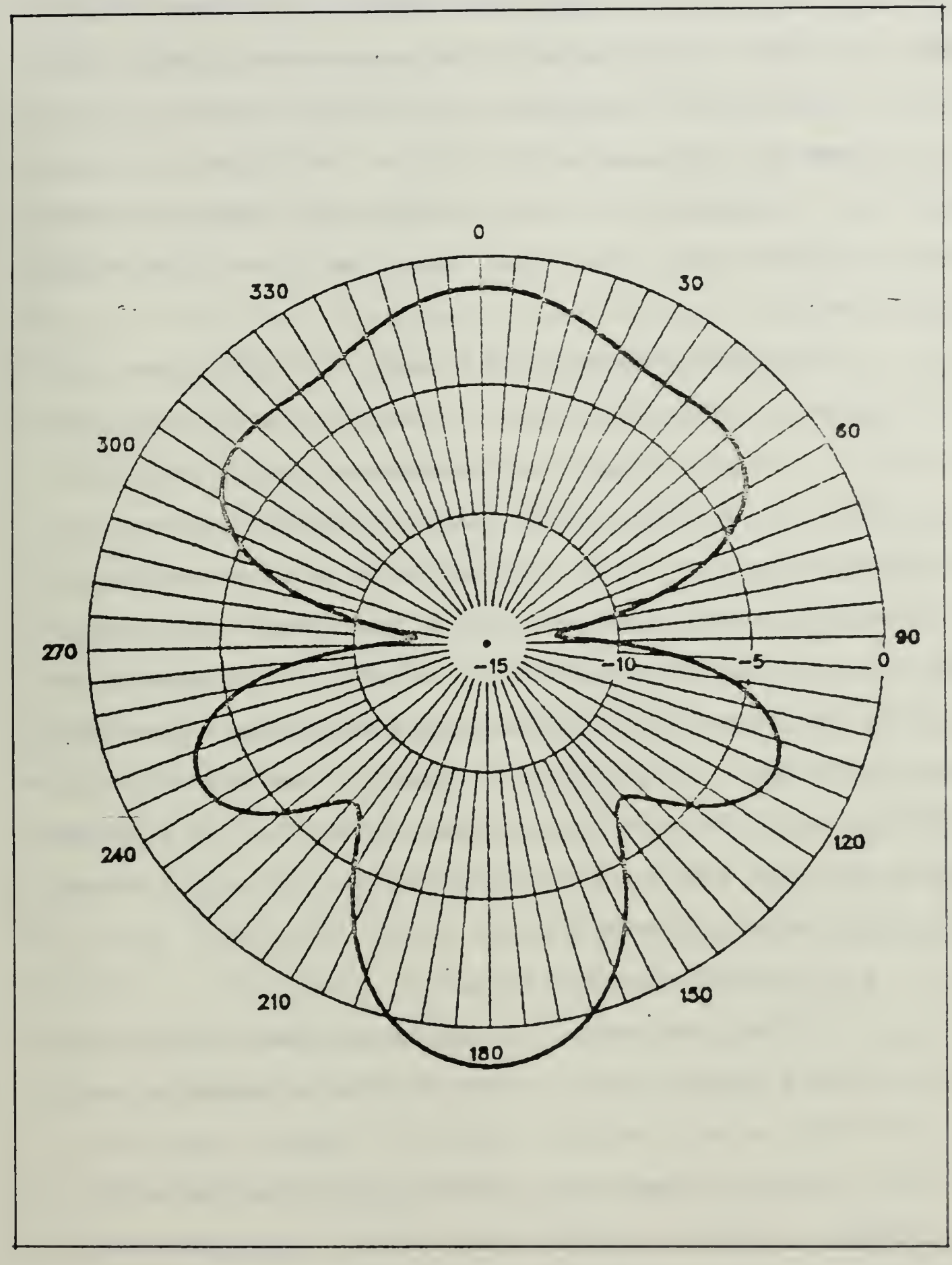

Figure 4.4 Horizontal Far Field Pattern- Single Loop

a perfect ground plane are planes much larger than λ^2 and good conductors on the order of 10^7 mhos/meter.[16:p. 239] Clearly, a cylindrical surface only slightly larger than 2λ at its greatest dimension can hardly be considered infinite and plane. Nevertheless, the fact that the AROD body does conduct suggests that some link to ground plane theory can be achieved.

Ground plane theory is the study of reflections. An ideal dipole oriented parallel to a perfect ground plane has an image in the plane which is directed out from the plane. The effect is to double the image radiated outward and perpendicular to the plane. In the case of AROD, the image is increased outward from the body in the horizontal plane. Further, since the body surface is curved, the image will be reflected at increasingly obtuse angles as distance from the dipole increases. The object of modeling the AROD body is to determine if this pattern of reflection can be used to enhance the far field patterns of Figure 4.3 and 4.4 and obtain an adequate antenna design.

a. Ground Planes and Phase

Before proceeding, an important consideration is phasing of the signal. The 800 to 900 MHz waveform planned for the video signal carries with it a period and phase. The phase of this waveform will vary as the distance from the antenna increases. Reflection theory stipulates that the distance a waveform travels to and from a reflecting

surface can be viewed as a straight line distance from the original source, in this case the antenna. Thus, a phase change is associated with any reflection. This phase change can act to complicate or, at 180 degrees, it can cancel the original signal. To minimize any such complications, the antenna should be positioned flush to the reflecting surface or at a distance resulting in zero phase change in the reflected signal. Further work, not considered here, might utilize phasing as a means to steer the pattern as desired.

b. Ground Planes and the Loop Antenna

One very important result of modelling the body as a conductor and approximating it as a ground plane is that it will significantly alter the characteristics of the loop antenna. In fact, a circumferential loop around the cylindrical body might alternatively be considered a line source over a ground plane. The "line" is the loop which carries a current from its source. Unlike a line source, however, this current would be seen on the loop from two different directions since the "line" ends are connected together. With these important differences in mind, line source effects will play a major part in shaping the numerically generated far field patterns in the next section.

D. BODY MODELLING AND COMPUTER AIDED DESIGN RESULTS

The complexity of the body conforming antenna makes use of a computer algorithm to model it very practical.

Although a simple array of dipoles lends itself to analytical solution, a large loop the size of the one proposed does not. A computer program written at the Naval Ocean Systems Center entitled Numerical Electromagnetics Code (NEC) is available on the Naval Postgraduate School's mainframe computer [18]. This code is used to obtain the far field patterns pictured in this work and is very suitable for this study.

The AROD body, although it can be pictured as a simple, conducting cylinder (Figure 4.1), is a very complex electromagnetic structure. One approach to simulate such a cylinder is to construct a wire grid outline. Another method is to utilize a continuous surface model. Both techniques are discussed in [16] and both can be modelled with NEC. In fact, because of the symmetry of the AROD body and the use of symmetry possible in NEC, the continuous surface model is somewhat less cumbersome to create. The modelling process and the resulting computer code are the subject of Appendix D.

1. Results with Dipole Arrays

The dipole arrays previously discussed are simulated here with the AROD body model. While array effects are expected to influence the resulting far field pattern, the conducting surface of the AROD will contribute significantly as well. All runs utilize a single center feed on a .1 inch diameter wire which is divided into 11 equal segments to

make a half-wave dipole. The first antenna simulated with the body model is the four dipole ring array pictured in Figure 4.5. Note that the array radius b = 15.5 inches.

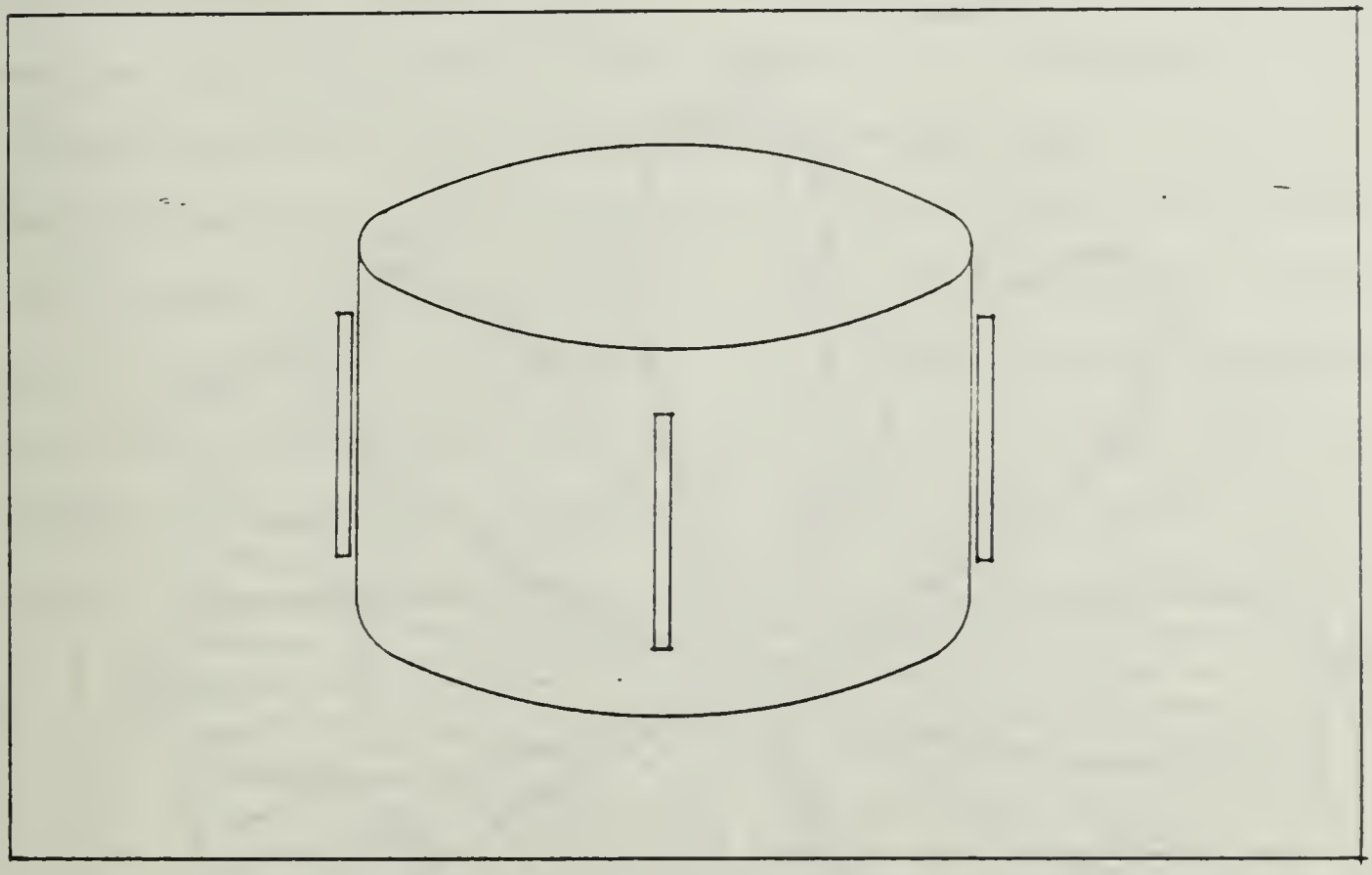

Figure 4.5 Body Model with 4 Dipole Ring Array

The half inch beyond the body radius of 15 inches is to account for practical considerations of mounting the dipoles and to prevent "electrical contact" with the body in the computer model. Results of the four dipole simulation are shown in Figure 4.6 and should be compared with the free standing ring array of Figure 4.3. While the resulting pattern is hardly adequate, it does demonstrate the beneficial effects of the reflecting AROD body. Directivity has been reduced.

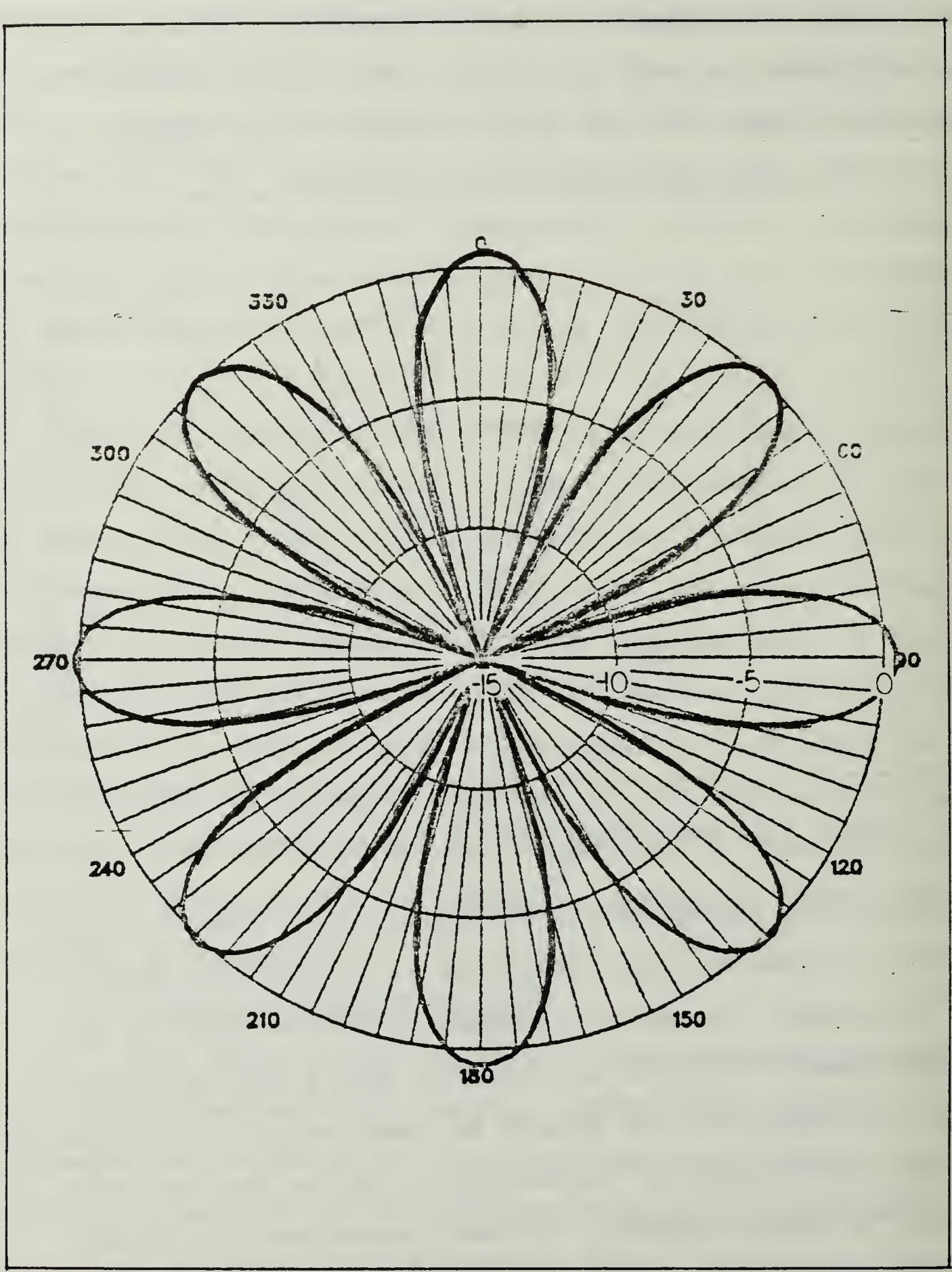

Figure 4.6 Horizontal Far Field - 4 Diple Ring and Body

Figure 4.6 indicates that the body has effectively duplicated the pattern of each dipole and doubled the radiating horizontal pattern. Since the pattern multiplication depends largely on the distance between radiating sources, an analysis of the spacing is revealing. The circumference of the 30 inch diameter AROD is 94.2 inches. The antenna radius b = 15.5 inches yields an array radius of 97.38 inches. The four dipoles, then, are each 24.3 inches apart along the circumference. In wavelengths this distance is 1.65λ. This is not the optimal spacing. The spacing sought is pictured in Figure 4.7. If the cylindrical

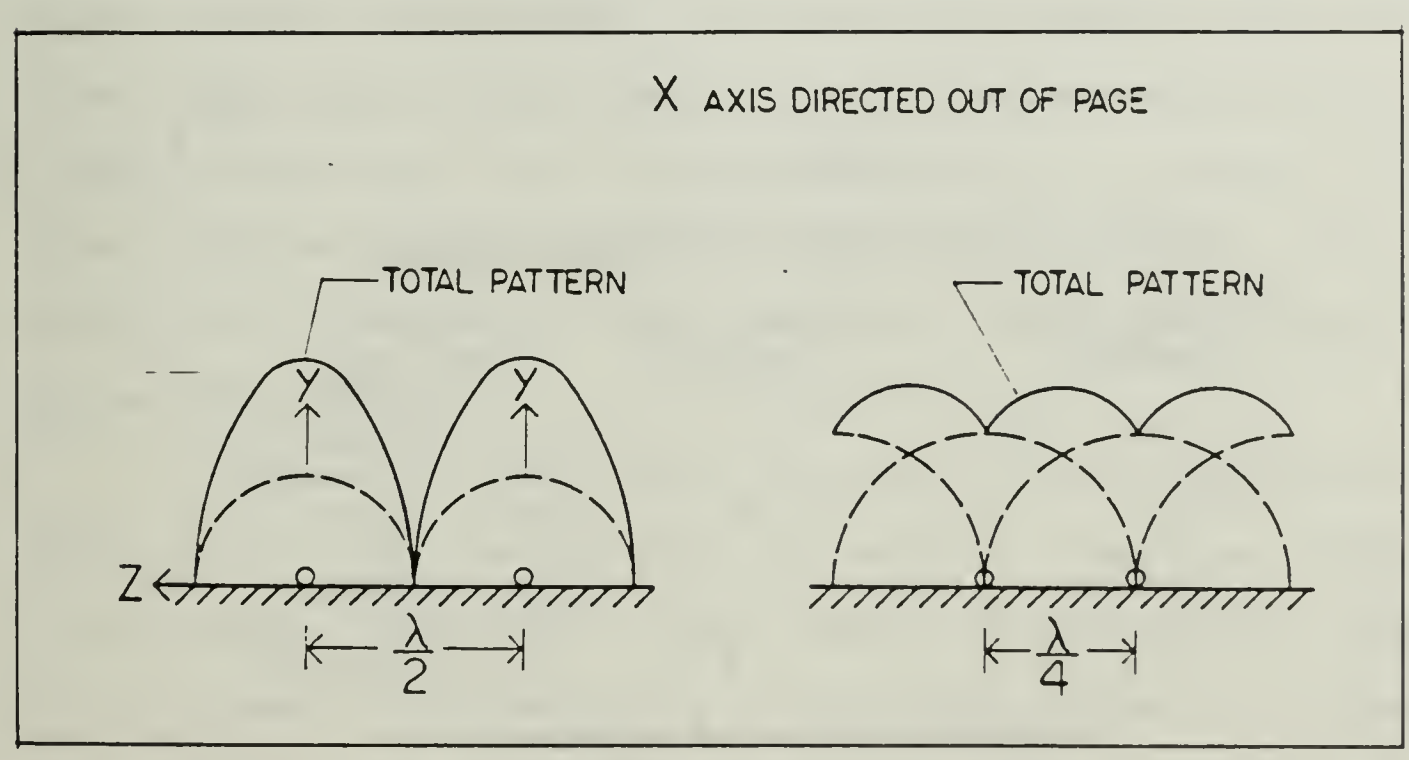

Figure 4.7 Pattern Multiplication of Dipoles Above a Ground Plane

surface can be ignored and instead thought of as a plane, then the interaction of the dipole patterns can be supposed. Figure 4.2 showed the horizontal pattern resulting from a

single half wave dipole. If the surface reflects, then the patterns from two adjacent dipoles will combine. Dipoles a half wavelength apart will result in patterns adding exactly in phase producing sharp peaks and valleys as seen in Figure 4.7. Patterns from dipoles a quarter wavelength apart will tend to smooth each other. Therefore, spacing close to .25λ is sought to reduce the dynamic range. Equal spacing is needed to maintain a non-directional array as previously discussed.

A circumference of 97.38 inches and wavelength λ = 14.76 inches yields no whole multiple of .25. Table 4.1 lists the multiples of quarter wavelength spacing

TABLE 4.1

QUARTER WAVELENGTH SPACING OF DIPOLES

Approximate Spacing	Number of Dipoles	Actual Spacing
$\lambda/4$	26	3.7 inches
$3\lambda/4$	9	10.8 inches
$5\lambda/4$	5	19.3 inches
$7\lambda/4$	4	24.3 inches

circumference= 97.8 inches
$\lambda/4$= 3.69 inches (800 Mhz)

possible on the body. Four dipoles did not yield an acceptable pattern. Figure 4.8 is the result of five equally spaced half-wave dipoles. The pattern is clearly

more smoothed although more complex than the four dipole case. The horizontal, vertical and total patterns are shown in Figure 4.8, but the total pattern (solid line) is of most interest here. In this case the smoothing effects of the reflecting body has reduced significantly the sharp drop off in directive gain characterized by the four dipole example.

The case of a nine dipole array deserves some practical discussion about feed points. The problem of feeding multiple points in phase from one transmitter, as in the case of AROD, is easy to overcome on the computer but more difficult with actual components. Finite distances exist between transmitter and feed point and phasing is simplified with fewer feed points. Additionally, power losses associated with resistive antennas may become too great with multiple loads. Therefore, for the nine dipole array, the simulation will consider only three equally spaced feed points.

Figure 4.9 shows the results of this arrangement. While not a very omnidirectional pattern, the nine dipole case reveals that reducing the number of feed points does not increase the directivity and,to the contrary, reduces the severity of the peak to valley gain difference of dynamic range. With this observation in mind, the five dipole antenna which produced a smoother pattern may be enhanced with fewer feed points. Figure 4.10(a) is the result with only one feed point at $\varphi = 0$ on the five dipole

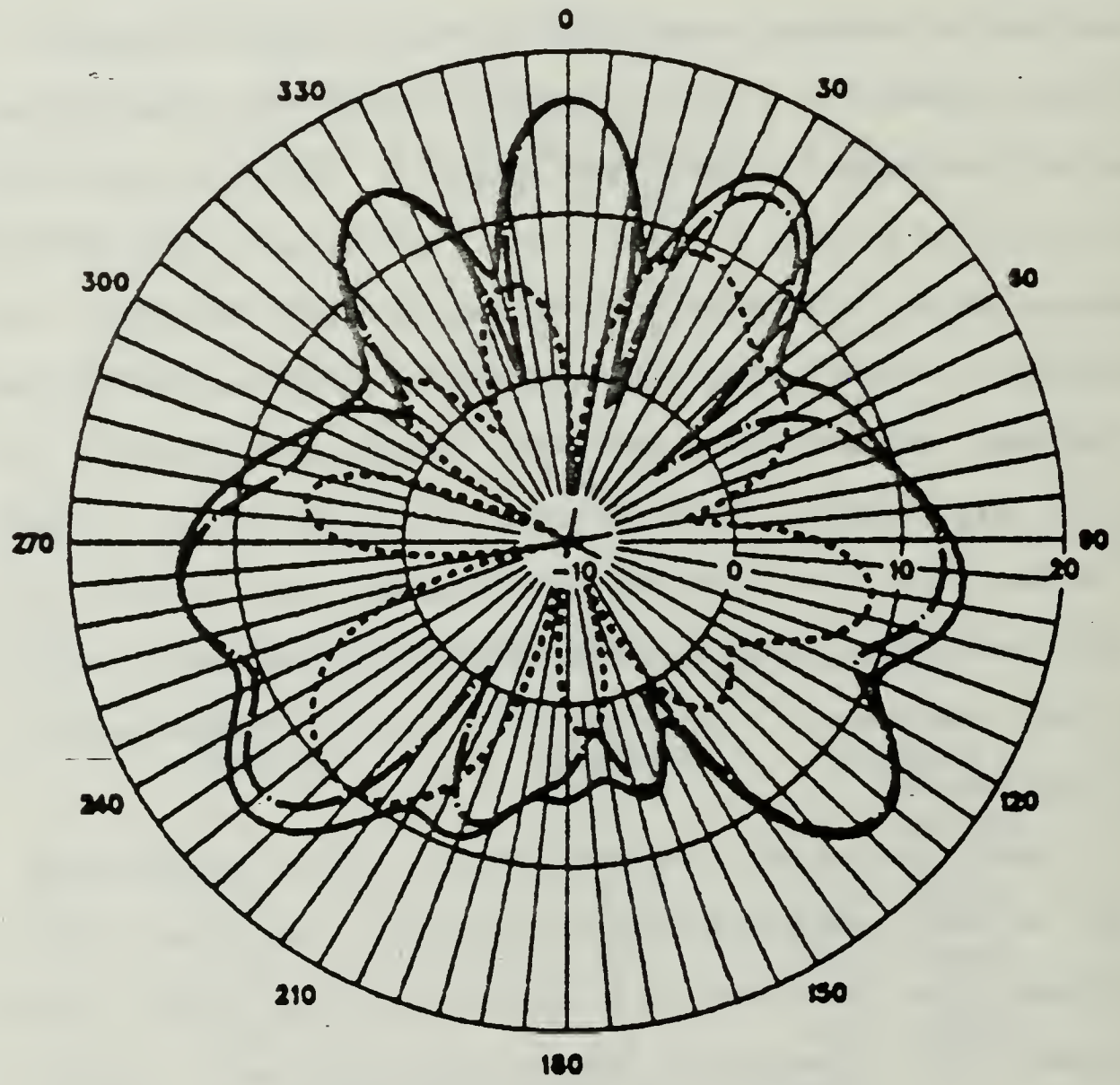

Figure 4.8 Horizontal Far Field - 5 Dipoles with Body

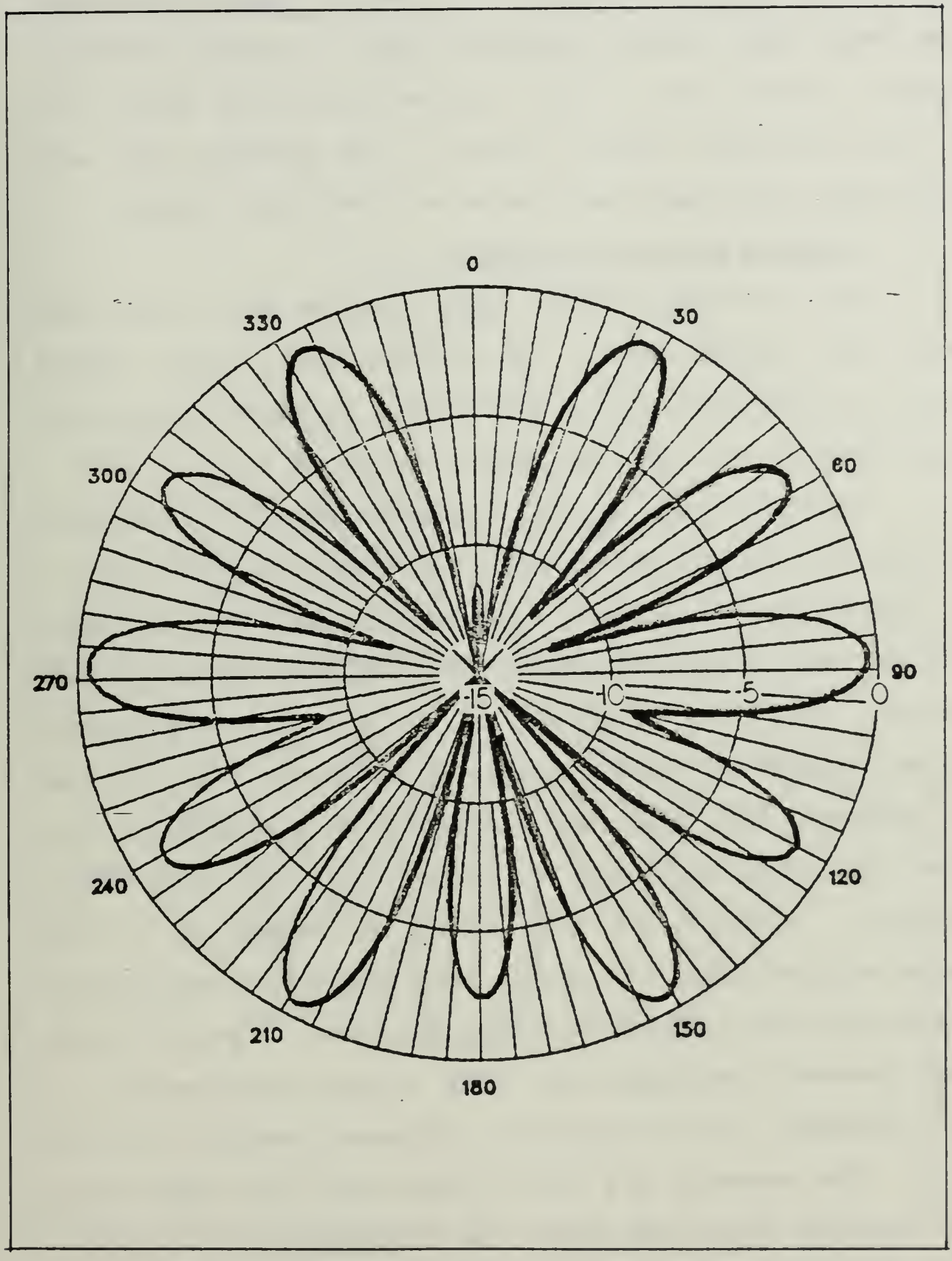

Figure 4.9 Horizontal Far Field - 9 Dipoles with Body

array. The far field pattern is greatly improved over the five feed case and the dynamic range is greatly reduced. Figures 4.10(b) and (c) are vertical cuts over zenith (θ) for two different azimuth angles. The patterns are non-directional and show some promise as a suitable antenna.

2. Results with Loop Antennas

Two variants of the loop antenna with AROD body model are studied here. As in the case of the dipole arrays, reflections play a major role in improving the far field pattern over the free space results of Figure 4.4.

The loop is a single, circumferential wire pictured in Figure 4.11. The first variant has one feed point at φ = 0. The horizontal pattern which results is shown in Figure 4.12(a) and differs markedly from the free standing loop pattern. While the gain peaks of the free standing pattern can be detected in Figure 4.12(a) at φ = 0, 60, 120, 240 and 300 degrees, the other peaks which give a desirable non-directional far field are not a result of the loop theory analysis. However, if the antenna is viewed as a line source as previously discussed, this pattern is essentially an 800 MHz wave propagating along the wire. A peak is seen every quarter wavelength with only slight variation at φ = 180^{o} probably due to opposing currents meeting at this point. The currents are not in phase when they meet since the distance travelled (half the circumference) is not a whole multiple of .5λ. The 97.38 inch circumference fits

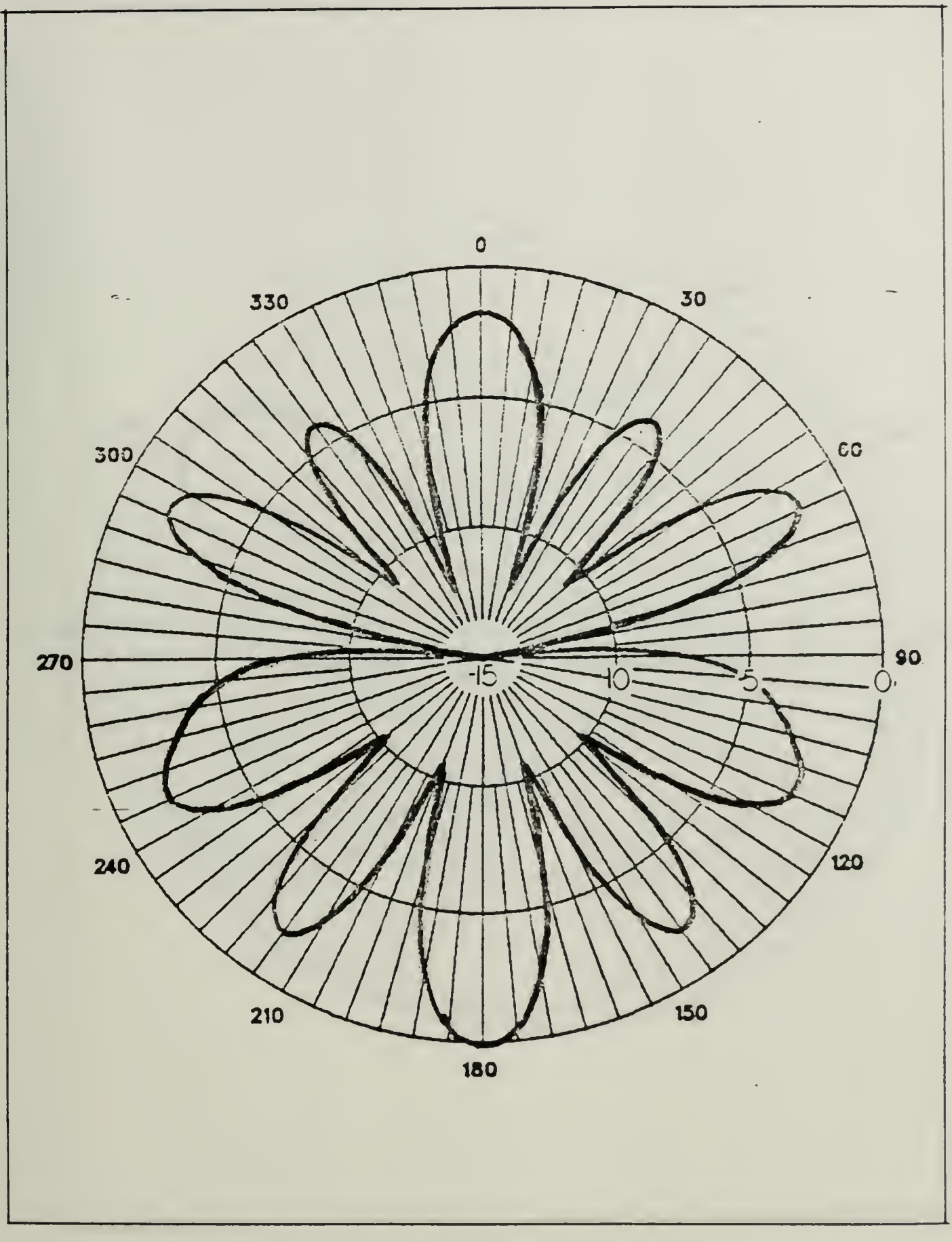

Figure 4.10 (a) Horizontal Far Field
5 Dipoles with Body

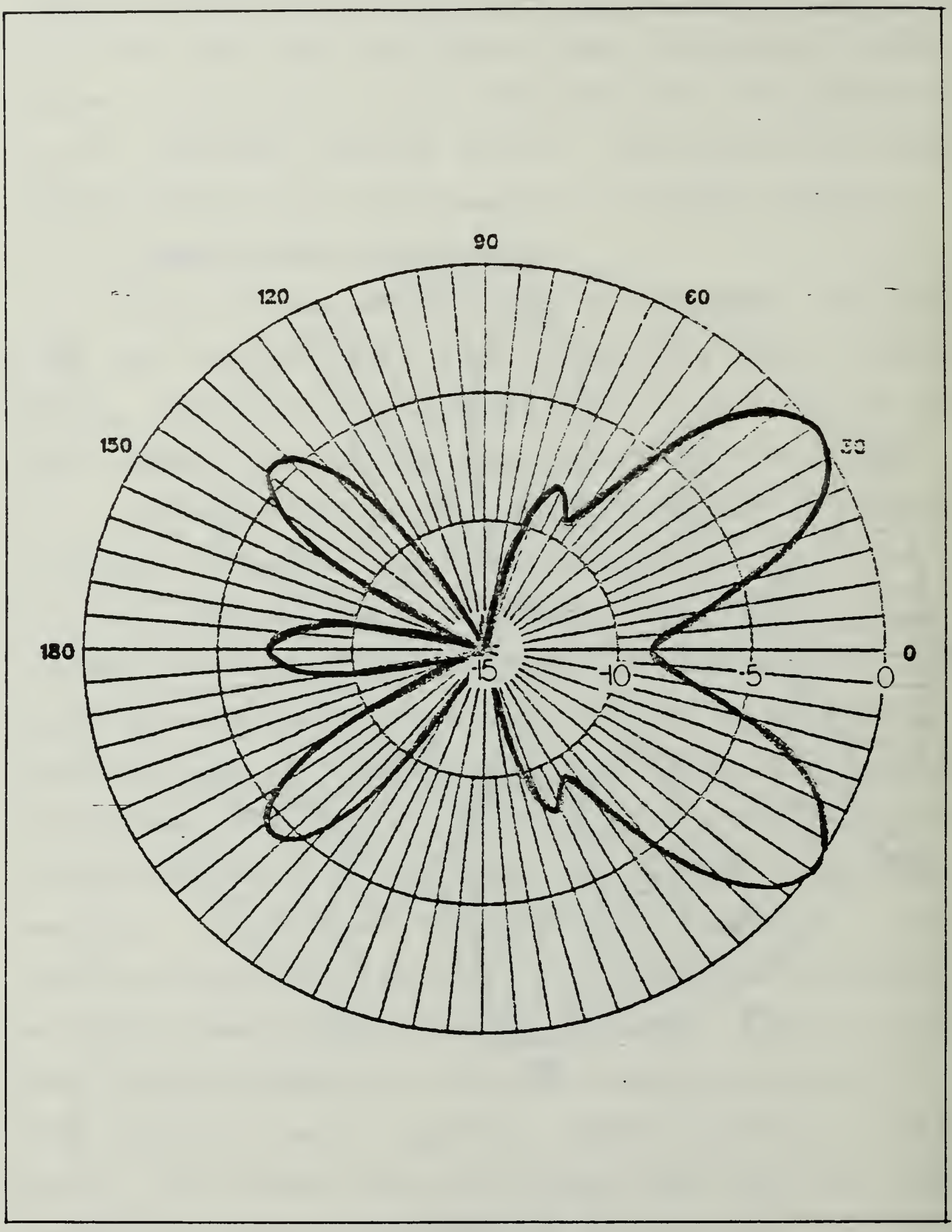

Figure 4.10 (b) Vertical Far Field (φ=0)
5 Dipoles with Body

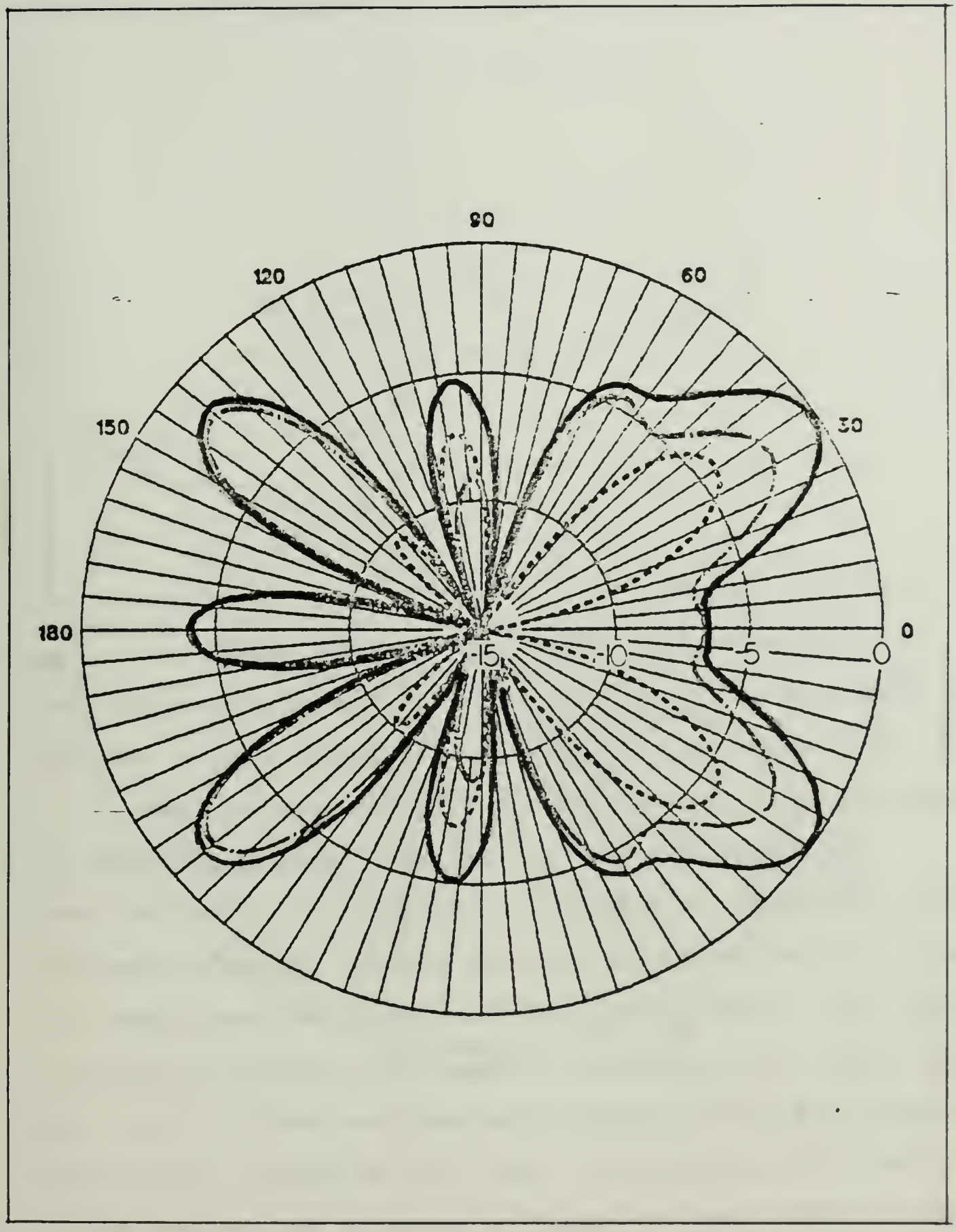

Figure 4.10 (c) Vertical Far Field (φ=45°)
5 Dipoles with Body

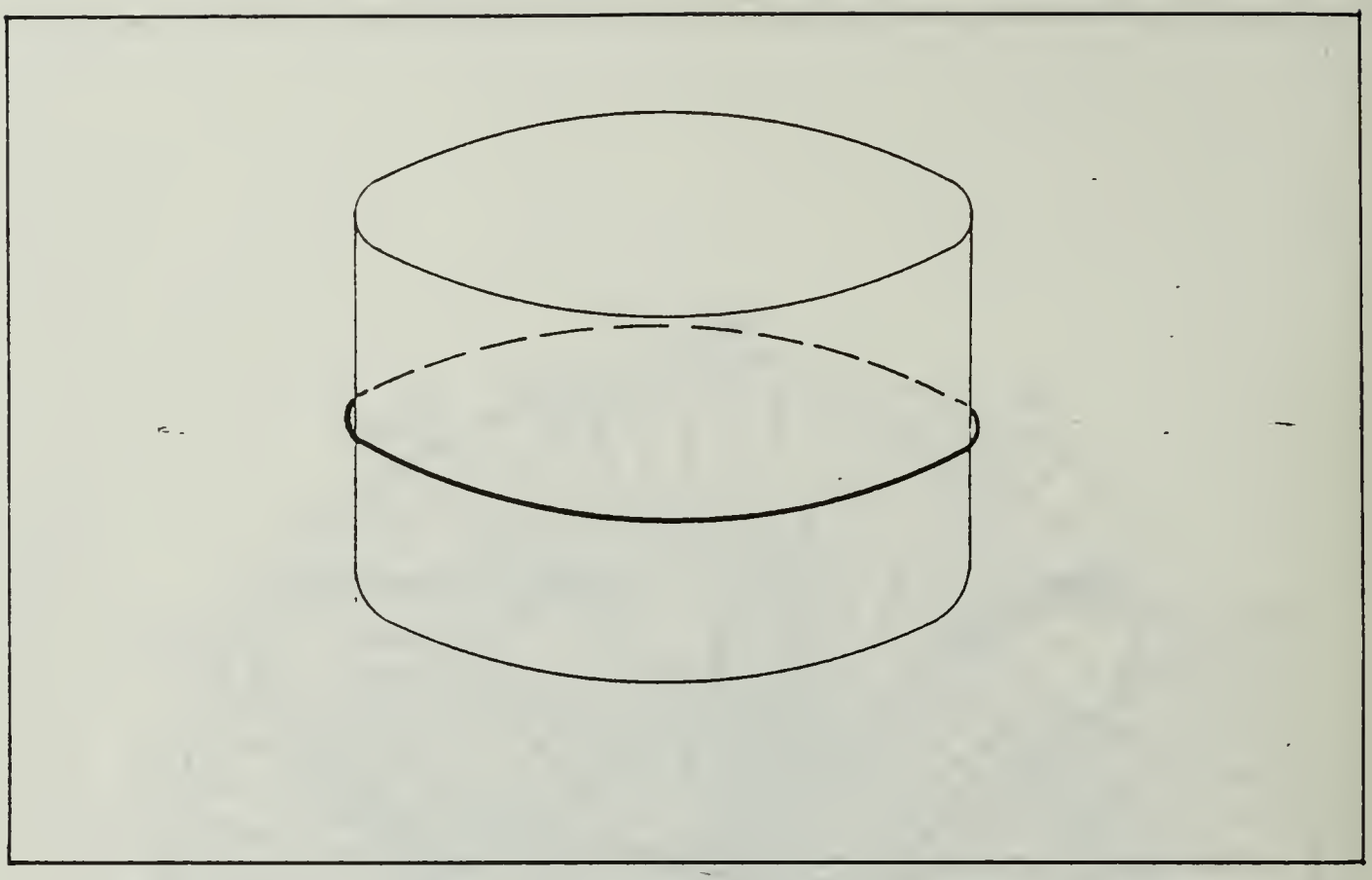

Figure 4.11 Single Loop and Body Model

a 6λ line source with a feed at $\varphi = 0$. The peaks which are seen on the far field pattern of Figure 4.12(a) can be viewed as the peaks which result from the line source.

The far field pattern of the single feed loop is further described in Figures 4.12(b) and (c). For the case when $\varphi = 0$, the zenith or vertical pattern resembles that of a long (6λ) lines source endfire array as described in [16:p. 180]. Discrepancies between the theoretical endfire far field and that pictured here are the result of (1) the fact that this antenna is a loop, (2) an actual line source lenght of 6.5λ, and (3) opposing currents due to the shape of the wire as a loop.

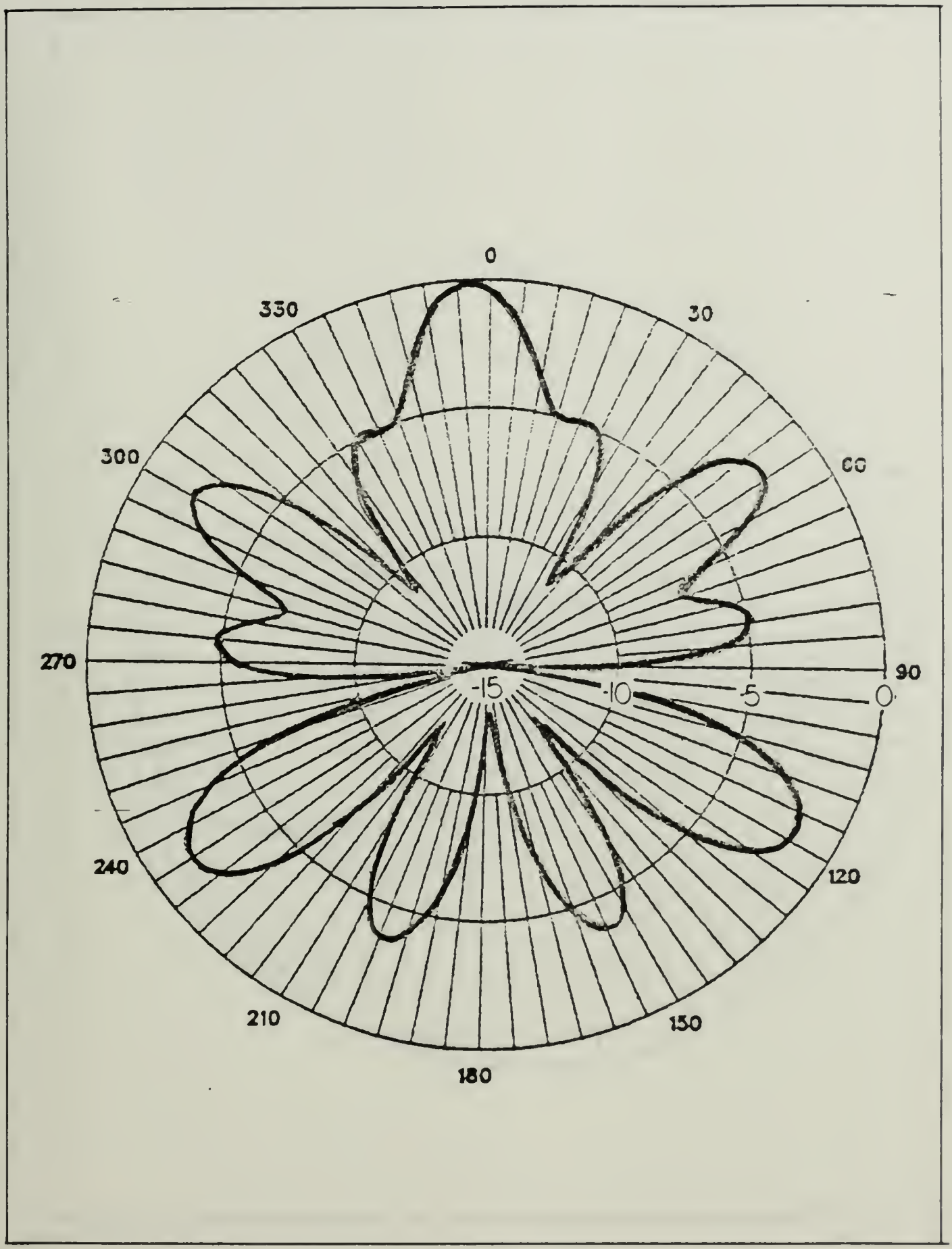

Figure 4.12 (a) Horizontal Far Field - 1 Loop 1 Feed

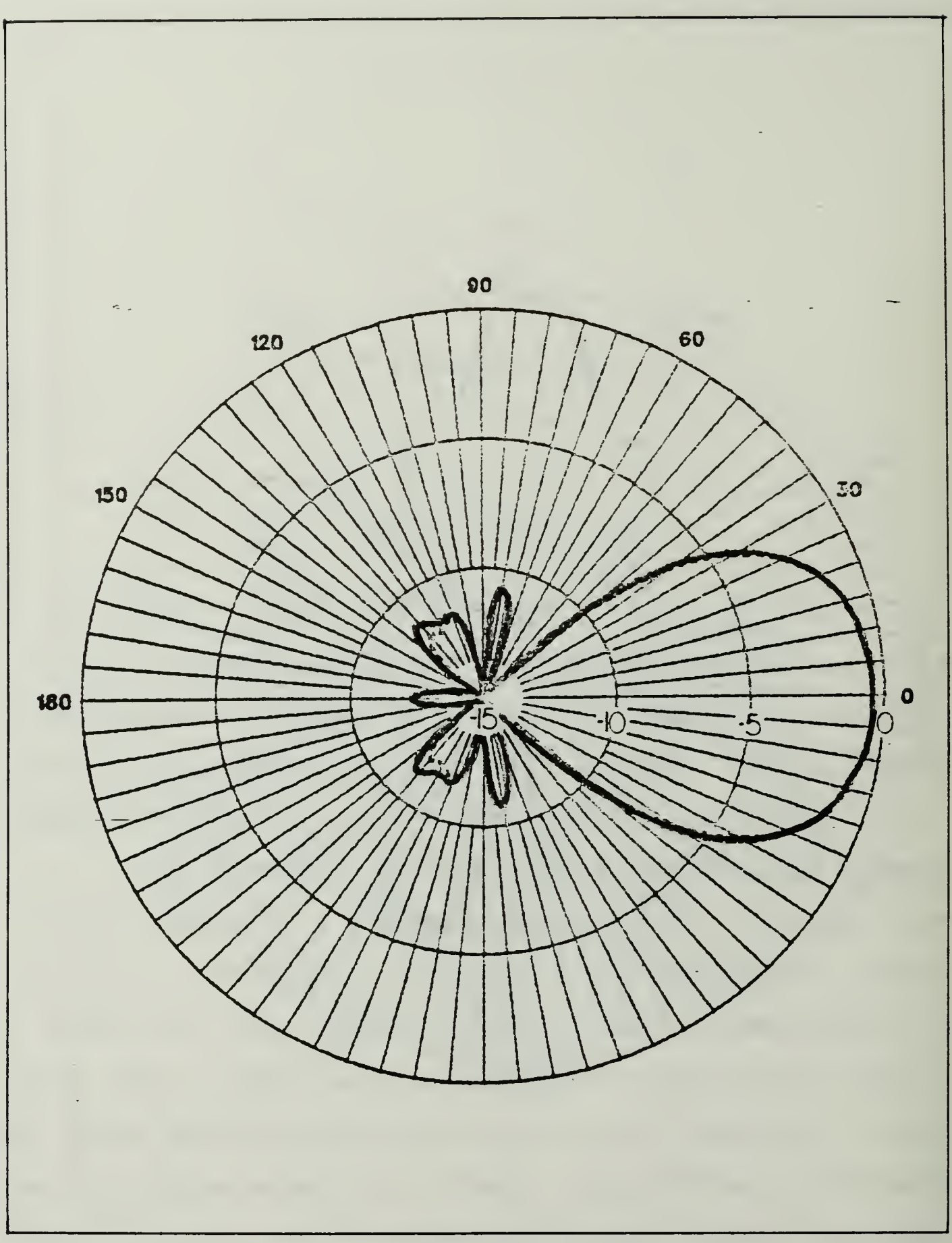

Figure 4.12 (b) Vertical Far Field (φ=0)
One Loop - One Feed

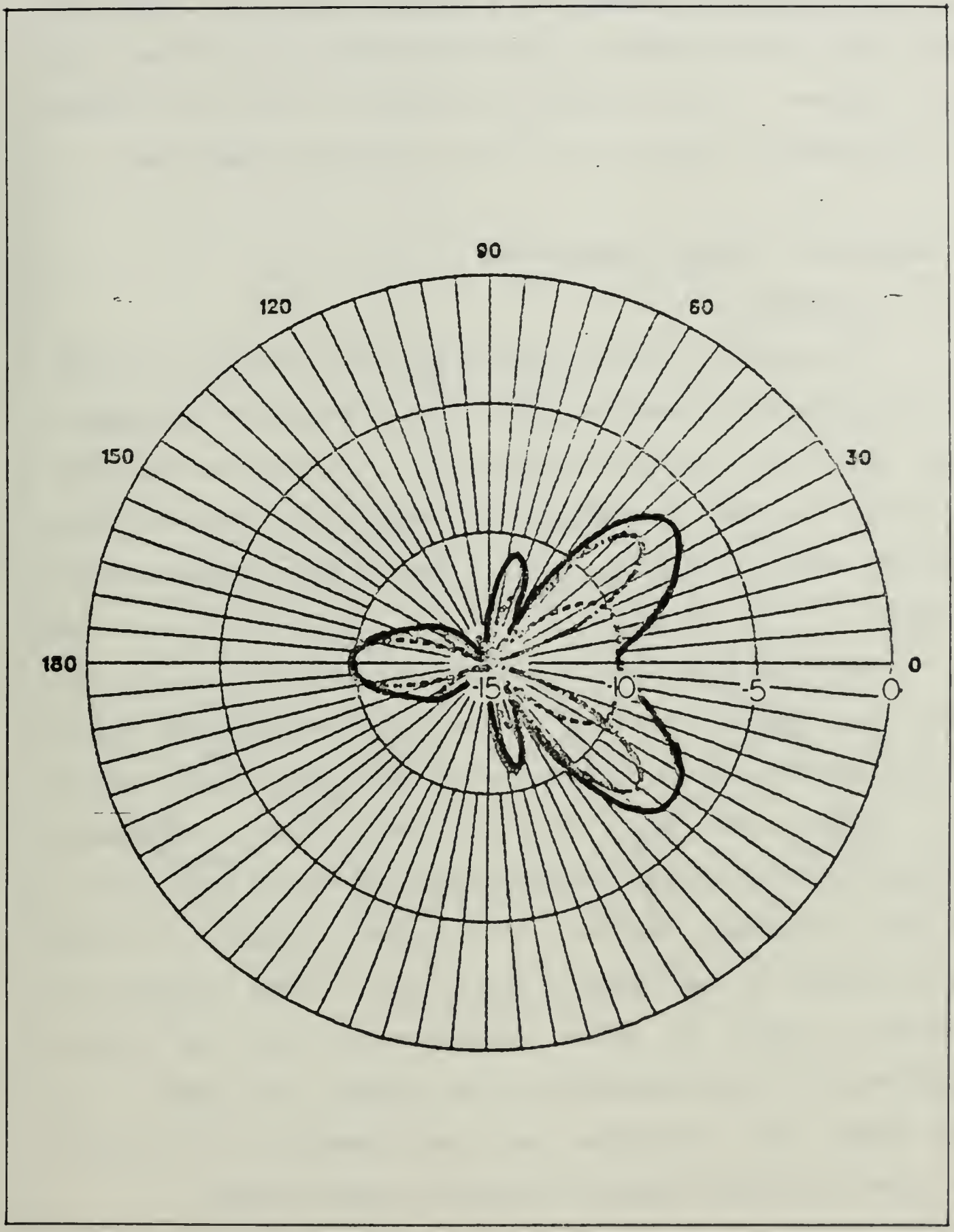

Figure 4.12 (c) Vertical Far Field (φ=45)
One Loop - One Feed

The second variant is a single loop with two feed points fed out of phase. The feed points are at φ=0 and φ=180 degrees. The horizontal pattern is shown in Figure 4.13 and has more directivity than the single feed case.

E. ANALYSIS & DESIGN CONCLUSIONS

1. Analysis

The goal of the design process was to model the AROD body and determine some basic antennas that yield omnidirectional horizontal far field patterns. An iterative approach utilizing numerical techniques in the form of NEC was used to screen various designs. Only a few of these designs were discussed.

The physical requirement most restrictive to the design was that it conform to the cylindrical AROD body. This constraint led to the choice of half-wave dipole arrays and a loop. The study did not result in a perfectly omnidirectional antenna, but two designs which show potential for refinement may have been found. Adequacy in this case is judged by the dynamic range that a radio receiver is required to have in order to sense an 800 MHz signal regardless of the orientation, in azimuth, of AROD. In other words, the horizontal far field pattern of the AROD must have a minimum dynamic excursion between peaks.

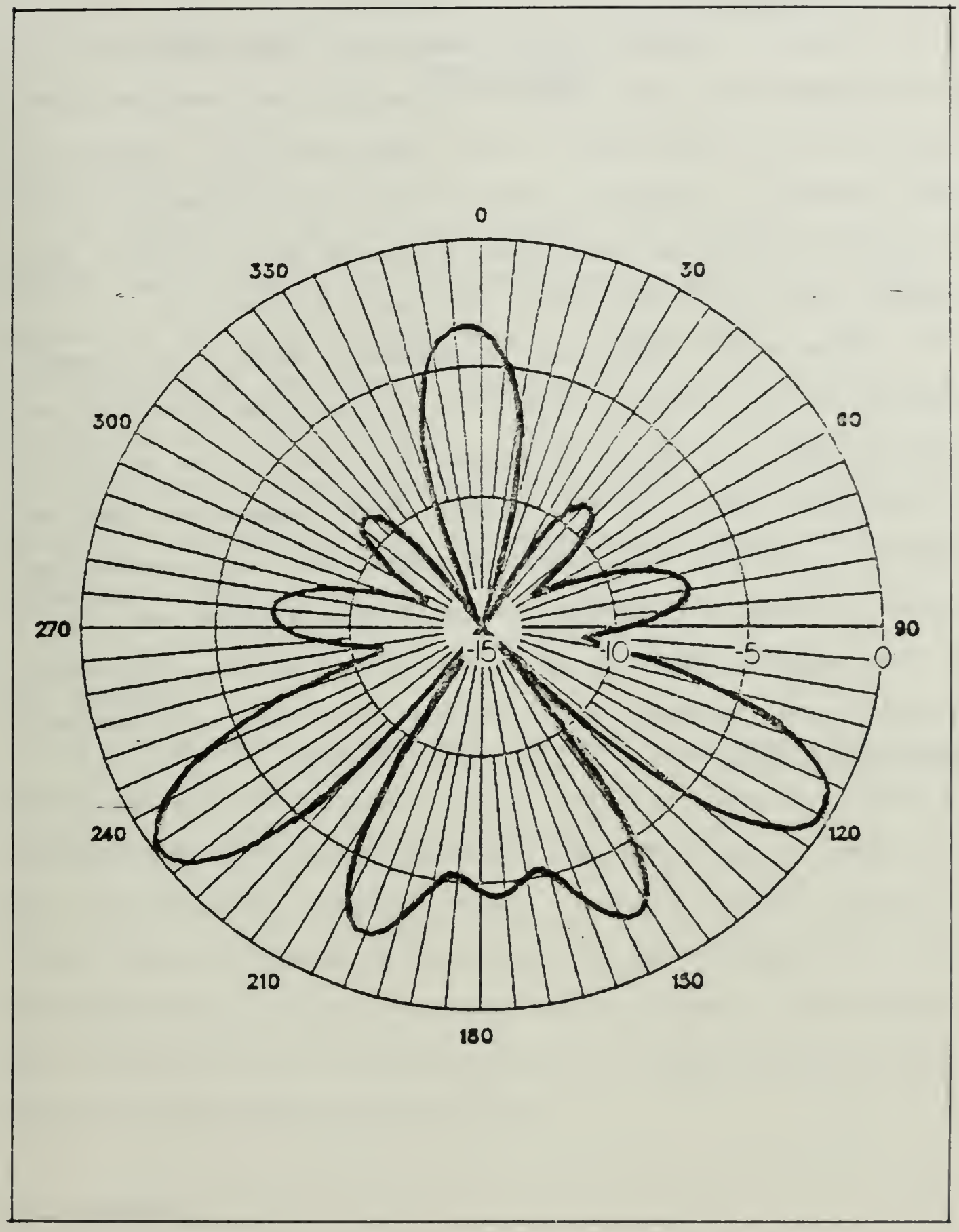

Figure 4.13 Horizontal Far Field (θ=0)
One Loop - Two Feed

2. Conclusions

The two designs which present the best potential in for refinement are the single loop, single feed and the five dipole, single feed array. This conclusion is a result of their overall, relatively smooth horizontal pattern. Both of these antennas are described in terms of horizontal and vertical far field patterns in Figures 4.12 and 4.10.

The most important assumption which was made, relative to the resulting patterns, is that the AROD body is a good conductor. This assumption is based on the electrical characteristics of the carbon fiber composite used to construct the body. It should be noted that this conducting shield is needed to provide the reflecting surface exploited by the antenna designs as well as to shield frequency interference between the antenna and the electronics internal to AROD.

V. CONCLUSIONS

A. DYNAMIC MODEL

A computer model of the ducted fan hovering vehicle, AROD, was developed by considering the vehicle as both a gyroscope and as a flying vehicle. Experimental data was integrated with the model to simulate the forces and moments which act on AROD in flight. Problems with the application of some of the data to the computer model were experienced. However, the model without the problematic data behaved as expected of such a device.

B. CONTROL

A linearized approximation of the nonlinear model was developed so that optimal control could be used to obtain a steady-state gain matrix with the ultimate goal of controlling the nonlinear computer model. Optimal control proved a viable means of determining a constant gain schedule for the multiple-input, multiple-output linear system. The resulting controller also found application to the nonlinear model with the problematic data removed.

C. ANTENNA

Two basic antenna designs were analyzed for use as an omnidirectional antenna for a UHF video downlink on the

AROD. A five dipole array and a single loop antenna were found to have the best potential of the designs which were tested using a computer simulation. The body of the AROD was found to significantly alter the directivity characteristics of the antennas.

D. FURTHER WORK

In the areas of dynamic modelling and control of AROD:

(1) The aerodynamic data and its application should be verified.

(2) A training simulator based on the linear model can be implemented utilizing the gain schedule derived here on small, readily available computers.

In the area of a UHF antenna:

(1) Modelling the entire AROD including the forebody and testing the designs for variation from these results.

(2) Modelling multiple loop antennas with differing phasing in an effort to steer the vertical pattern.

(3) Analyze the antennas for power requirements as weight of batteries and power supplies is critical to the AROD.

(4) Test the designs on the AROD prototype for suitability.

List of References

1. Jennings Jr, J.F., "Why the Corps Needs Robots", Marine Corps Gazette, pp. 36-39, August 1986.

2. RGATERS Discussions, GATERS Program Quarterly Review Conference, 10-12 February 1987, Naval Ocean Systems Center (NOSC) San Diego, CA and 23-25 June 1987, NOSC, Kaneohe Bay, HI.

3. Kirk, D.E., Optimal Control Theory, Prentice-Hall, Inc., 1970.

4. Roskam, J., Airplane Flight Dynamics and Automatic Flight Controls, Roskam Aviation & Engineering Inc., 1979.

5. Etkin, B., Dynamics of Flight, 2nd ed., John Wiley & Sons., 1982.

6. Discussions with John E. White, Engineer at Sandia National Laboratories, January through March, 1987, by telephone and by mail.

7. International Business Machines, Incorporated, Program #5798-PXJ, Dynamic Simulation Language (DSL), First Edition, 1984

8. Thaler, G. J., Automatic Control, class notes for EC2300, Naval Postgraduate School, Monterey, CA, 1987

9. Lewis, F. L., Optimal Control, John Wiley & Sons, NY, 1986.

10. RFALB Athans, M., and Falb, P. L., Optimal Control, McGraw Hill Book Company, 1966.

11. Astrom, K. J., and Wittenmark, B., Computer Controlled Systems, Prentice-Hall, Inc., 1984.

12. Class notes, EC4310, Digital Control Systems, Prof. R. Cristi, Naval Postgraduate School, Monterey, CA, Summer Quarter, 1986.

13. Brenny, M. K., An Interactive Discrete Controls Analysis Option (ORACLS) For the Controls Analysis Package on the IBM 3033, Masters Thesis, Naval Postgraduate School, Monterey, CA, June 1985.

14. Defense Documentation Center report ESD-TR-74-111 MTR-2672, Deployable UHF Spacecraft Antennas, by B.M. Hadfield, February 1974.

15. Air Force Cambridge Research Laboratories report AFCRL-TR-75-0181, Research and Development of Antennas for Rocket and Satellite Transmissions, by A. Waterman and D.G. Henry, March 1975.

16. Stutzman, W.L. and Thiele, G.A., Antenna Theory Design, John Wiley & Sons, Inc., 1981.

17. King, R.W., and Harrison, C.W., Antennas and Waves: A Modern Approach, MIT Press, 1969.

18. Naval Ocean Systems Center technical document NOSC TD 116 vol 2, part III, Numerical Electromagnetics Code (NEC) - Method of Moments, by G.J. Burke and A.J. Pogio, January 1981.

APPENDIX A

EXPERIMENTAL DATA

Empirical data received from Sandia National Laboratories is listed here. This data was obtained experimentally through measurements and wind tunnel testing.

1. Weights and Moments of Inertia

Description	Name	Value(units)
Weight of Prototype	WtPro	85 (lbs)
Weight of Model	WtMod	76.5 (lbs)
Moments of Inertia:		
about X-axis	I_x	1.5246 (ft^2 lbs)
about Y-axis	I_y	1.6767 (ft^2 lbs)
about Z-axis	I_z	1.6684 (ft^2 lbs)
Products of Inertia:(assumed)	$I_{xy}= I_{xz}= I_{yz}$	0
Moment of Inertia of Propeller		
about X-axis	I_r	.015012 (ft^2 lbs)
about Y-axis(assumed)	--	0
about Z-axis(assumed)	--	0
Propeller Weight(derived)	PropWt	4.50017 (lbs)

2. Hardware Characteristics

Propeller Efficiency	Pref	10.472	(rad/lb-sec)
Minimum Thrust of Engine	Thr_{min}	35	(lbs)
Maximum Thrust of Engine	Thr_{max}	115	(lbs)
Maximum Throttle Setting	TA_{max}	100	(lbs/sec)
Maximum Change in Throttle	RT_{max}	100	(lbs/sec^2)
Propeller Speed at Hover	HovRat	7200	(rpm)
Propeller Compensation	RHo	.0019	($ft\text{-}lb_m$)
Max Deflection of Vanes	MaxDef	.5236	(rad)
Max Def Rate of Vanes	MaxRatDef	.87266	(rad/sec)

Description	Name	Value(units)
Control Surface Effectiveness		
Aileron	L_{aeff}	-21.29 (sec^{-2})
Rudder	M_{eeff}	-14.51 (sec^{-2})
Elevator	N_{reff}	-16.68 (sec^{-2})

3. Aerodynamic Data

The data listed in the table below is obtained from wind tunnel tests. The manner in which it is applied in the simulation (relationship to forces and moments on the AROD body) is given in the next section.

Angle of Attack, AOATOT = $\sqrt{(\alpha^2 + \beta^2)}$

Name	50	55	60	65	70	75	80	90
CRdel	--	--	--	.0807	.0743	.0712	.881	.085
Rslope	.1514	.1533	.1673	.1977	.1834	.1764	.2041	.20
Req	9.293	8.82	8.115	7.848	7.347	7.134	5.011	0.0
CPdel	--	--	--	.3106	.3081	.3305	.3515	0.0
Pslope	.5633	.5123	.6974	.7612	.7603	.8189	.8853	.90
Peq	43.14	31.00	29.58	26.74	24.55	20.43	15.17	0.0
CYdel	--	--	--	.0024	-.002	.0090	.0120	0.0
Yslope	.0609	.0663	.0215	.0060	-.004	.0223	.0302	.04
Yeq	.555	.576	.006	-.09	-1.63	-1.77	-1.74	-1.8
VanEff	--	--	--	1.5	1.5	1.5	1.9	1.0
Veq	51.62	44.96	38.56	32.94	27.76	21.83	13.31	0.0
CLdel	--	--	--	.2428	.2391	.1907	.1734	.1046
Lslope	.7954	.7183	.6598	.5949	.5901	.4726	.4366	0.0
Leq	85.	85.	85.	85.	85.	85.	85.	85.
CDdel	--	--	--	.5754	.6052	.5922	.4966.	3890
Dslope	1.302	1.313	1.371	1.410	1.493	1.467	1.251	1.2
Deq	0.0	0.0	0.0	0.0	0.0	0.0	0.0	0.0
CSdel	--	--	--	.0091	.0258	.0331	.0318	0.0
CSslope	.0801	.0801	.0801	.0801	.0801	.0801	.0801	.0801
Seq	0.0	0.0	0.0	0.0	0.0	0.0	0.0	0.0

NOTE: (--) indicates that no data under this heading was received for this angle.

4. Aerodynamic Forces and Moments

The aerodynamic data listed in paragraph 3, above, results in forces moments about the velocity axes, V_{tot}. The relationships developed by the engineers who obtained the data are reproduced here. Some convenient groupings of constants and parameters of the system are given here.

$$WtRat = \frac{WtMod}{WtPro}$$

$$Vdelta = V_{tot} - \sqrt{(WtRat)} * V_{eq}(AOATOT)$$

$$RHovA = RHo*Pi* \sqrt{(WtRat)} * V_{eq}(AOATOT)$$

ω_r = angular speed of propeller (rad/sec)

$$UseDel = -\dot{\omega}_r * RHovA * WtRat$$

$$UseEq = \left(1 + \frac{2}{\omega r} * \dot{\omega}_r\right) * WtRat$$

$$UseSlp = WtRat * (V_{tot} - \sqrt{(WtRat)} * V_{eq}(AOATOT)$$

The Forces and Moments which result from the aerodynamic data are given here.

FORCES (with respect to V_{tot})

Due to Body Aerodynamics

$$F_{al} = UseDel*CLdel(AOATOT) + UseSlp*Lslope(AOATOT)$$

$$F_{ad} = UseDel*CDdel(AOATOT) + UseSlp*Dslope(AOATOT)$$

$$F_{as} = UseDel*CSdel(AOATOA) + UseSlp*Sslope$$

Due to Thrust Force Aerodynamics

$$F_{tl} = UseEq*Leq$$

Total Aerodynamic Forces

$$F_l = F_{al} + F_{tl}$$

$$F_d = F_{ad}$$

$$F_s = F_{as}$$

MOMENTS (with respect to V_{tot})

Due to Body Aerodynamics

R_{ar}= UseDel*CRdel(AOATOT) + UseSlp*Rslope(AOATOT)

P_{ap}= UseDel*CPdel(AOATOT) + UseSlp*Pslope(AOATOT)

Y_{ay}= UseDel*CYdel(AOATOA) + UseSlp*Yslope(AOATOT)

Due to Thrust Force Aerodynamics

R_{tr}= UseEq*Req(AOATOT)

P_{tp}= UseEq*Peq(AOATOT)

Y_{ty}= UseEq*Yeq(AOATOT)

Total Aerodynamic Moments

$R_r = R_{ar} + R_{tr}$

$P_p = P_{ap} + P_{tp}$

$Y_y = Y_{ay} + Y_{ty}$

APPENDIX B

SIMULATIONS SOURCE CODE

1. Simple Gyroscope Simulation

The following source code is a Dynamic Simulation Language (DSL) program to simulate the AROD as a gyroscope. This simulation is discussed in Chapter II.

```
TITLE BASIC AROD GYRO SIMULATION
*
CONST IRX=69.52,IXX=7063.39,IYY=7768.22,IZZ=7729.58,WRX=784.
*
INIT
      P0= 0.
      Q0=0.
      R0= 0.
      MX = 0.
      MZ = 0.
*
DYNAMIC
      IF (TIME .LT. T0) THEN
         MY = 0
      ELSE
***   STEP INPUT  ***
            T1 = T0 + DUR
            MY = AMP*(STEP(T0) - STEP(T1))
      END IF
*
DERIV
      HX = IRX*WRX + IXX*P
      HY = IYY*Q
      HZ = IZZ*R
      PD =(-1.*HZ/IXX)*Q + (HY/IXX)*R + MX/IXX
      QD =(HZ/IYY)*P - (HX/IYY)*R + MY/IYY
      RD =(-1.*HY/IZZ)*P + (HX/IZZ)*Q + MZ/IZZ
      P = INTGRL(P0,PD)
      Q = INTGRL(Q0,QD)
      R = INTGRL(R0,RD)
*
PARAM T0=1, DUR=1, AMP=10000
CONTROL FINTIM=5, DELT=.05
SAVE .05, P,Q,R,MY
PRINT .1,MY,P,Q,R
```

```
GRAPH (G0,DE=TEK618) TIME(NI=5,UN=SEC) MY(UN='LB-IN(SQ)')
LABEL (G0) INPUT TORQUE
GRAPH (G1,DE=TEK618) TIME(NI=5,UN=SEC) P(UN='RADIANS/SEC',NI=3,...
      SC=2.,LO=-2.) Q(LI=3,NI=3,SC=2.,LO=-2.) R(LI=4,NI=3, ...
      SC=2.,LO=-2.)
LABEL G2 ROLL, PITCH, YAW RESULTING FROM STEP PITCH INPUT
END
STOP
```

2. Complete Equations of Motion Simulation

The following source code is the DSL program used to generate the results discussed in Chapter II for the complete AROD model. Notation follows that of Appendix ADATA wherever possible. Data listed in Appendix ADATA is also reproduced here in the form used by DSL.

```
TITLE AROD EQUATIONS OF MOTION - FULL MODEL, NO CONTROL - 7 MAY 87
CONST GRAV= 32.174, PI= 3.1415962
ARRAY TRANS(9), ABTRAN(9)
*
*************************************************************************
*                          MNEMONICS                                    *
*    CR/P/YDEL == ROLL/PITCH/YAW COEFFICIENTS                           *
*    R/P/YSLOPE== ROLL/PITCH/YAW SLOPES OF COEFFICIENT CURVES           *
*    THRMIN/MAX== THRUST FORCE LIMITS (LBS)                             *
*    R/P/YEQ    == EQUIVALENT ROLL/PITCH/YAW FORCE FACTOR               *
*    VEQ        == EQUIVALENT VELOCITY FACTOR                          *
*    VANEFF     == CONTROL SURFACE EFFECTIVENESS                       *
*    CL/S/DDEL  == LIFT/SIDEFORCE/DRAG COEFFICIENTS                    *
*    L/S/DSLOPE== LIFT/SIDEFORCE/DRAG SLOPES OF COEFFICIENT CURVES     *
*    FRCSLG     == CONVERSION FOR IN**2-LB(FORCE) TO FT**2-SLUGS       *
*    WTRAT      == RATIO OF AROD WEIGHT TO WIND TUNNEL MODEL WEIGHT    *
*    P/Q/R      == ROLL/PITCH/YAW ANGLE RATES FOR EOM (RAD/SEC)        *
*    UU/VV/WW   == BODY-FIXED VELOCITY COMPONENTS (X/Y/Z)(FT/SEC)      *
*    PHI/THT/PSI== EARTH-FIXED EULER ANGLES (RADIANS)                  *
*    ALPHA/BETA/AOATOT== ANGLES OF ATTACK (RADIANS)                    *
*    DELE/R/A   == ELEVATOR/RUDDER/AILERON/THROTTLE POSITIONS BASED ON *
*                  IDENTICAL SERVO EQUATIONS (RADIANS)                 *
*    THROT      == CHANGE IN THRUST FORCE BASED ON THROTTLE SERVO (LBS)*
*    ALT        == ALTITUDE BASED ON INTEGRATION OF VERTICAL SPEED (FT)*
*    U/V/WERTH  == EARTH FIXED VELOCITIES (X/Y/Z) (FT/SEC)             *
*    GRNSPD/DIST== SPEED AND DISTANCE (NO DIRECTION) OVER GROUND(FT/S)*
*    THRHOV     == THRUST FORCE REQUIRED IN HOVER (LBS)                *
*    HOVRAT     == ANGULAR RATE OF PROPELLER IN HOVER (RAD/SEC) BASED  *
*                  ON EXPERIMENTAL DATA                                *
*    THR        == TOTAL THRUST FORCE (LBS)                            *
```

```
*    NEWVEQ     == IMPIRICAL DATA FOR VELOCITY CALCULATIONS              *
*    VDELTA     == EQUIVALENT VELOCITY FOR FORCE CALCULATIONS (FT/SEC)   *
*    RHOVA      == WEIGHTING FACTOR  FOR AERO COEFFICIENTS BASED ON      *
*                  VEQ AND AOATOT                                        *
*    DELTIP     == CHANGE IN ROTOR ANGULAR VELOCITY (RAD/SEC)            *
*    VTIP       == ROTOR ANGULAR VELOCITY (DISCRETE) (RAD/SEC)           *
*    USEDEL/SLP/EQ== COMBINATIONS OF VARIABLES WITH WHICH AERODYNAMIC    *
*        DATA CAN BE USED FOR MOMENTS AND FORCES (UNITS BASED ON DATA    *
*    L/S/DAF   == LIFT/SIDE FORCE/DRAG AERO FORCE COMPONENT (LBS)        *
*    L/S/DTF   == LIFT/SIDE FORCE/DRAG THRUST FORCE COMPONENT (LBS)      *
*    FAX/Y/Z    == AERODYNAMIC FORCES (LBS)                              *
*    FTX/Y/Z    == THRUST INDUCED FORCES (LBS)                           *
*    R/P/YAM    == ROLL/PITCH/YAW AERODYNAMIC MOMENT COMPONENT (FT-LBS)  *
*    R/P/YTM    == ROLL/PITCH/YAW THRUST MOMENT COMPONENT (FT-LBS)       *
*    LA/MA/NA   == ROLL/PITCH/YAW AERODYNAMIC MOMENT (FT-LBS)            *
*    LT/MT/NT   == ROLL/PITCH/YAW MOMENT DUE TO THRUST/ROTOR (FT-LBS)    *
*    GX/Y/Z     == BODY-FIXED GRAVITY COMPONENT (FT/SEC**2)              *
*                                                                        *
**************************************************************************
**********       EXPERIMENTALLY OBTAINED DATA          ******************
*                                                                        *
**************************************************************************
*    UNITS                                                               *
*                                                                        *
*    MOMENTS OF INERTIA      IXX,IYY,IZZ,IRX          LB-FT-SEC**2       *
*    FORCES                  FATX,FATY,FATZ,ETC       LB                 *
*    MOMENTS                 LAT,MAT,NAT,ETC          LB-FT              *
*    ANGLES                  PSI,THT,PHI              RADIANS            *
*                            PSIDEG,THTDEG,PHIDEG     DEGREES            *
*    ANGLE RATES             P,Q,R                    RADIAN / SEC       *
*    VELOCITIES              UU,VV,WW,UERTH,ETC       FT / SEC           *
*                            WR                       RADIAN / SEC       *
*                                                                        *
**************************************************************************
*
CONST IXXM=7063.39,IYYM=7768.22,IZZM=7729.58,IRXM=69.552, WEIGHT= 76.5
* MEASURED IN**2-LB      IN**2-LB      IN**2-LB      IN**2-LB         LB
*
CONST PROPWT= 4.50017, PROPEF= 10.472, RHO= .00192
*              LB              UNITLESS      PROPELLER WEIGHT/EFFICIENCY
CONST  THRMIN= 35., THRMAX= 115.
*               LB             LB    MIN/MAX THROTTLE POSITION
CONST  TAMAX= 100., RMAXT= 100.
*          LBS/SEC     LB/SEC*SEC  MAX CHANGE/RATE OF CHANGE OF THRUST
CONST  MAXDFL= .5236, RMAX= .87266
*             RADIANS         RAD/SEC   CONTROL VANE MAX DEFLECTION & RATE
CONST LAEFF= -21.29, MEEFF= -14.51, NREFF= -16.68
*  ROLL, PITCH, YAW VANE EFFECTIVENESS
CONST H1= 17.77, H2= 157.91, HG1= 219.912, HG2= 24674.126
*ELEV, RUD, AIL, THROTTLE GAINS/ GYRO GAINS
*
CONST WE= 1., K= .5
```

```
* THROTTLE INTEGRATION LOOP GAINS
CONST ALPMIN= .8727, ALPMAX= 1.570796, AOAMIN= 50., AOAMAX= 90.
* ANGLE OF ATTACK LIMITS FOR TABLE DATA REFERENCE
*
***********  AERODYNAMIC PARAMETERS FROM WIND TUNNEL TESTS  **********
*
* NOTE:  ALL TABLE DATA IS A FUNCTION OF ANGLE OF ATTACK (TOTAL),
*        AOATOT RANGES FROM 50 TO 90 DEGREES.
*
*************************  ROLL DATA  ***********************************
AFGEN  CRDEL = 50,.0807,  55,.0807,  60,.0807,  65,.0807, ...
               70,.0743,  75,.0712,  80,.0810,  90,.0850
AFGEN RSLOPE = 50,.1514,  55,.1533,  60,.1673,  65,.1977, ...
               70,.1834,  75,.1764,  80,.2041,  90,.2000
FGEN2    REQ = 8,2,16,  50,55,60,65,70,75,80,90,  0,10, ...
               9.293,8.5,  8.82,7.1,  8.115,7.2,  7.848,6.4, ...
               7.347,5.9,  7.134,5.4, 5.011,4.67, 0.0,0.0
*************************  PITCH DATA  **********************************
AFGEN  CPDEL = 50,.3106,  55,.3106,  60,.3106,  65,.3106, ...
               70,.3081,  75,.3305,  80,.3515, 90,.0000
AFGEN PSLOPE = 50,.5633,  55,.5123,  60,.6974,  65,.7612, ...
               70,.7603,  75,.8189,  80,.8853,  90,.9000
FGEN2    PEQ = 8,2,16,  50,55,60,65,70,75,80,90,  0,10, ...
               34.138,11.69, 31.002,10.45, 29.576,9.72, 26.738,9.44,...
               24.545,6.78,  20.427,4.66,  15.168,-0.53, 0.0,-5.92
*************************  YAW DATA  ************************************
AFGEN  CYDEL = 50,.0024,  55,.0024,  60,.0024,  65,.0024, ...
               70,-.0015,  75,.0090,  80,.0120,  90,.0000
AFGEN YSLOPE = 50,.0609,  55,.0663,  60,.0215,  65,.0060, ...
               70,-.0038, 75,.0223,  80,.0302,  90,.0400
FGEN2    YEQ = 8,2,16,  50,55,60,65,70,75,80,90,  0,10, ...
               0.555,0.04,   0.576,-.51,  0.006,-.46, -.09,-.49,...
               -1.634,-1.3, -1.771,-.55, -1.736,-1.1, -1.8,-1.2
****************  CONTROL SURFACE EFFECTIVENESS  ***********************
AFGEN VANEFF = 50,1.5,  55,1.5,  60,1.5,  65,1.5, ...
               70,1.5,  75,1.5,  80,1.9,  90,1.0
******************  VELOCITY COMPENSATING FACTOR  ************************
FGEN2   VEQ = 8,2,16,  50,55,60,65,70,75,80,90,  0,10, ...
              51.616,44.93, 44.955,39.11, 38.564,33.00, 32.935,27.45,...
              27.757,21.31, 21.829,15.06, 13.314,11.65, 0.0,0.0
*************************  LIFT DATA  ***********************************
AFGEN  CLDEL = 50,.2428,  55,.2428,  60,.2428,  65,.2428, ...
               70,.2391,  75,.1907,  80,.1734,  90,.1046
AFGEN LSLOPE = 50,.7954,  55,.7183,  60,.6598,  65,.5949, ...
               70,.5901,  75,.4726,  80,.4366,  90,.0000
CONST    LEQ = 85.
*************************  DRAG DATA  ***********************************
AFGEN  CDDEL = 50,.5754,  55,.5754,  60,.5754,  65,.5754, ...
               70,.6052,  75,.5922,  80,.4966,  90,.3890
AFGEN DSLOPE = 50,1.3017,  55,1.3131,  60,1.3711,  65,1.4103, ...
               70,1.4933,  75,1.4674,  80,1.2507,  90,1.2000
CONST    DEQ = 0.0
```

```
*************************  SIDE FORCE DATA  *************************
AFGEN  CSDEL = 50,.0091,  55,.0091,  60,.0091,  65,.0091, ...
               70,.0258,  75,.0331,  80,.0318,  90,.0000
CONST SSLOPE = 0.0801
CONST    SEQ = 0.0
*********************************************************************
INITIAL
*
***  CONVERSIONS
*****  FORCE TO SLUGS AND IN**2 TO FT**2
      FRCSLG= 1./(GRAV*144.)
      IXX= IXXM*FRCSLG
      IYY= IYYM*FRCSLG
      IZZ= IZZM*FRCSLG
      IRX= IRXM*FRCSLG
***  MOMENTS OF INERTIA
      IYMIZ= IYY - IZZ
      IZMIX= IZZ - IXX
      IXMIY= IXX - IYY
*
      MASS= WEIGHT/GRAV
      WTRAT= WEIGHT/85.
***********************  INITIAL CONDITIONS  ***************************
      P0   = 0.
      Q0   = 0.
      R0   = 0.
      U0   = 0.
      V0   = 0.
      W0   = 0.
      PHI0= 0.
      THT0= 0.
      PSI0= 0.
      DELED0= 0.
      DELE0 = 0.
      DELRD0= 0.
      DELR0 = 0.
      DELAD0= 0.
*     DELA0 = 0.
      DLTRD0= 0.
      DLTR0 = 0.
      THROT0= 0.
      ALT0  = 0.
      GRNSP0= 0.
      THRHOV= WEIGHT
      HOVRAT= (THRHOV - PROPWT)*PROPEF
*************  DEFINE MACRO TO LIMIT ANGLE  ****************************
MACRO  ANGOUT= ANLIM(ANGIN,ANGMIN,ANGMAX)
      ANSIGN= SIGN(1.,ANGIN)
      ANGOUT= LIMIT(ANGMIN,ANGMAX,ANSIGN*ANGIN)
      ANGOUT= ANSIGN*ANGOUT
ENDMAC
**********  DEFINE MACRO FOR USE IN SERVO EQUATION LIMITING  **********
```

```
MACRO  OUT= SERVO(OUT0,OUTD,LIM)
       OUT= INTGRL(OUT0,OUTD)
       OUT= LIMIT(-LIM,LIM,OUT)
ENDMAC
*******************************************************************************
DYNAMIC
*
**************  COORDINATE TRANSLATION COMPONENTS  ********************
*****  BODY-FIXED TO EARTH FIXED (EULER ANGLES)
*   ROW 1
       TRANS(1)= COS(PSI)*COS(THT)
       TRANS(2)= COS(PSI)*SIN(THT)*SIN(PHI) - SIN(PSI)*COS(PHI)
       TRANS(3)= COS(PSI)*SIN(THT)*COS(PHI) + SIN(PSI)*SIN(PHI)
*   ROW 2
       TRANS(4)= SIN(PSI)*COS(THT)
       TRANS(5)= SIN(PSI)*SIN(THT)*SIN(PHI) + COS(PSI)*COS(PHI)
       TRANS(6)= SIN(PSI)*SIN(THT)*COS(PHI) - SIN(PHI)*COS(PSI)
*   ROW 3
       TRANS(7)= -SIN(THT)
       TRANS(8)= COS(THT)*SIN(PHI)
       TRANS(9)= COS(THT)*COS(PHI)
*
************************  VELOCITIES  ***********************************
       VTOT = SQRT(UU*UU + VV*VV + WW*WW)
       UERTH= UU*TRANS(1) + VV*TRANS(2) + WW*TRANS(3)
       VERTH= UU*TRANS(4) + VV*TRANS(5) + WW*TRANS(6)
       WERTH= UU*TRANS(7) + VV*TRANS(8) + WW*TRANS(9)
       GRNSPD= SQRT(VERTH*VERTH + WERTH*WERTH)
*
****************************  ANGLE OF ATTACK  ****************************
*      IF(VTOT.LE..5) THEN
            ALPHA= 1.570796
            BETA = 0.
*      ELSE
*           ALPHA= ASIN(WW/VTOT)
*           BETA = ASIN(VV/VTOT)
*      ENDIF
       ALPHA = ANLIM(ALPHA,ALPMIN,ALPMAX)
       BETA  = ANLIM(BETA,0.,1.570796)
       AOATOT= RADEG*SQRT(ALPHA*ALPHA + BETA*BETA)
       AOATOT= LIMIT(AOAMIN,AOAMAX,AOATOT)
*
**************  ANGLE OF ATTACK COORDINATE TRANSFORMATION  ************
***  BODY-FIXED TO VELOCITY
*   ROW 1
       ABTRAN(1)= -COS(ALPHA)*COS(BETA)
       ABTRAN(2)= SIN(BETA)
       ABTRAN(3)= SIN(ALPHA)*COS(BETA)
*   ROW 2
       ABTRAN(4)= COS(ALPHA)*SIN(BETA)
       ABTRAN(5)= COS(BETA)
       ABTRAN(6)= -SIN(ALPHA)*SIN(BETA)
```

```
*  ROW 3
      ABTRAN(7)= -SIN(ALPHA)
      ABTRAN(8)= 0.
      ABTRAN(9)= -COS(ALPHA)
*
********************  FORCE COMPONENTS   ********************************
      THR = LIMIT(THRMIN, THRMAX, THRHOV+THROT)
      NEWVEQ= FGEN2(VEQ,AOATOT,0.)
      VDELTA= VTOT- SQRT(WTRAT)*NEWVEQ
      RHOVA = RHO*PI*SQRT(WTRAT)*NEWVEQ
*
      DELTIP= (THR - WEIGHT)*PROPEF
      VTIP  = HOVRAT + DELTIP
*
      USEDEL= -DELTIP*RHOVA*WTRAT
      USESLP= VDELTA*WTRAT
      USEEQ = (1. + (2./VTIP)*DELTIP.) * WTRAT
***   FORCES
      LAF   = USEDEL*AFGEN(CLDEL,AOATOT) + USESLP*AFGEN(LSLOPE,AOATOT)
      SAF   = USEDEL*AFGEN(CSDEL,AOATOT) + USESLP*SSLOPE
      DAF   = USEDEL*AFGEN(CDDEL,AOATOT) + USESLP*AFGEN(DSLOPE,AOATOT)
      LTF   = USEEQ*LEQ
*
      FAX    = ABTRAN(1)*DAF + ABTRAN(2)*SAF + ABTRAN(3)*LAF
      FAY    = ABTRAN(4)*DAF + ABTRAN(5)*SAF + ABTRAN(6)*LAF
      FAZ    = ABTRAN(7)*DAF + ABTRAN(8)*SAF + ABTRAN(9)*LAF
      FTX    = ABTRAN(3)*LTF
      FTY    = ABTRAN(6)*LTF
      FTZ    = ABTRAN(9)*LTF
      FATX   = FAX + FTX
      FATY   = FAY + FTY
      FATZ   = FAZ + FTZ
***   MOMENTS
      RAM = USEDEL*AFGEN(CRDEL,AOATOT) + USESLP*AFGEN(RSLOPE,AOATOT) ...

            + USEEQ*FGEN2(REQ,AOATOT,0.)
      PAM = USEDEL*AFGEN(CPDEL,AOATOT) + USESLP*AFGEN(PSLOPE,AOATOT) ...

            + USEEQ*FGEN2(PEQ,AOATOT,0.)
      YAM = USEDEL*AFGEN(CYDEL,AOATOT) + USESLP*AFGEN(YSLOPE,AOATOT) ...

            + USEEQ*FGEN2(YEQ,AOATOT,0.)
*
      LA = ABTRAN(1)*RAM +ABTRAN(2)*PAM +ABTRAN(3)*YAM
      MA = ABTRAN(4)*RAM +ABTRAN(5)*PAM +ABTRAN(6)*YAM
      NA = ABTRAN(7)*RAM +ABTRAN(8)*PAM +ABTRAN(9)*YAM
      LT   = -DELTIP*DELTIP*FRCSLG*.0729 + IXX*LAEFF*DELA
      MT   =  MEEFF*IYY*DELE
      NT   =  NREFF*IZZ*DELR
      LAT = LA + LT
      MAT = MA + MT
      NAT = NA + NT
```

```
************************  GRAVITY COMPONENTS  ************************
      GX   = -GRAV*TRANS(1)
      GY   = -GRAV*(-TRANS(4))
      GZ   = -GRAV*(-TRANS(7))
*********************************************************************
*+++++++++++++++++++++++++++++++++++++++++++++++++++++++++++++++++++++
SAMPLE
****    INSERT CONTROLLER HERE
*
*
*+++++++++++++++++++++++++++++++++++++++++++++++++++++++++++++++++++++
DERIVATIVE
*
*********************  MOMENT DERIVATIVES  ******************************
      PD   = (IYMIZ*R*Q - IRX*DELTIP + LAT)/IXX
      QD   = (IZMIX*P*R - IRX*VTIP*R + MAT)/IYY
      RD   = (IXMIY*P*Q + IRX*VTIP*Q + NAT)/IZZ
*********************  FORCE DERIVATIVES  ******************************
      UD   = (VV*R - WW*Q) + FATX/MASS + GX
      VD   = (WW*P - UU*R) + FATY/MASS + GY
      WD   = (UU*Q - VV*P) + FATZ/MASS + GZ
*********************  ANGLE DERIVATIVES  ******************************
      PHID= P + (Q*SIN(PHI) + R*COS(PHI))*TAN(THT)
      THTD= Q*COS(PHI) - R*SIN(PHI)
      PSID= (Q*SIN(PHI) + R*COS(PHI))/COS(THT)
*********************  SERVO DERIVATIVES  ******************************
***  ELEVATOR, RUDDER, AILERON, THROTTLE
      DELEDD= -H1*DELED - H2*DELE + H2*UE
      DELRDD= -H1*DELRD - H2*DELR + H2*UR
      DELADD= -H1*DELAD - H2*DELA + H2*UA
      DLTRDD= -H1*DLTRD - H2*DLTR + H2*UT
      THROTD= -WE*THROT + K*WE*DLTR
*
***INTEGRATIONS
************************  MOMENT EQUATIONS  ****************************
      P = INTGRL(P0,PD)
      Q = INTGRL(Q0,QD)
      R = INTGRL(R0,RD)
************************  FORCE EQUATIONS  *****************************
      UU= INTGRL(U0,UD)
      VV= INTGRL(V0,VD)
      WW= INTGRL(W0,WD)
************************  EULER ANGLES  ********************************
      PHI = INTGRL(PHI0,PHID)
      THT = INTGRL(THT0,THTD)
      PSI = INTGRL(PSI0,PSID)
      PHIDEG= RADEG*PHI
      THTDEG= RADEG*THT
      PSIDEG= RADEG*PSI
************************  SERVO EQUATIONS  *****************************
      DELED = SERVO(DELED0,DELEDD,RMAX)
      DELRD = SERVO(DELRD0,DELRDD,RMAX)
```

```
      DELAD  = SERVO(DELAD0,DELADD,RMAX)
      DLTRD  = SERVO(DLTRD0,DLTRDD,RMAXT)
      DELE   = INTGRL(DELE0,DELED)
      DELR   = SERVO(DELR0,DELRD,MAXDFL)
      DELA   = INTGRL(DELA0,DELAD)
      DLTR   = SERVO(DLTR0,DLTRD,TAMAX)
      THROT  = INTGRL(THROT0,THROTD)
***   ALTITUDE
      ALT  = INTGRL(ALT0,UERTH)
      DIST= INTGRL(GRNSP0,GRNSPD)
*
CONTRL FINTIM= 5
PRINT .5, PHIDEG,THTDEG,PSIDEG,P,Q,R,UU,VV,WW,DELA
SAVE .05, PHIDEG, THTDEG,PSIDEG,P,Q,R,UU,VV,WW
PARAM UE =0.,UR =0.,UA=-.052,UT= 0.,DELA0=0
LABEL (G1) TIME RESPONSE TO UA =-.052(NO CONTROL)
GRAPH (G1,DE=TEK618) TIME(NI=5,UN=SEC) PHIDEG(NI=4,SC=45,LI=1, ...
 UN='THTDEG AND PSIDEG (DEGREES)',LO=-90) THTDEG(AX=OMIT,NI=4, ...
  SC=45,LI=3,LO=-90) PSIDEG(AX=OMIT,NI=4,SC=45,LI=4,LO=-90)
GRAPH (G2,DE=TEK618,OV,PO=0,5) TIME(NI=5,UN=SEC) P(NI=4, ...
      UN='Q AND R (RAD/SEC)',LO=-2,SC=1,LI=1) Q(AX=OMIT, ...
      NI=4,LO=-2,SC=1,LI=3) R(AX=OMIT,NI=4,LO=-2,SC=1,LI=4)
GRAPH (G2,DE=TEK618,OV,PO=6,0) TIME(NI=5,UN=SEC) VV(NI=4, ...
      UN='UU AND WW (FT/SEC)',LO=-2,SC=5,LI=3) UU(AX=OMIT, ...
      NI=4,LO=-2,SC=5,LI=1) WW(AX=OMIT,NI=4,LO=-2,SC=5,LI=4)
END
STOP
```

APPENDIX C

CONTROLLER AND LINEAR MODEL SIMULATION

The DSL/VS source code used to simulate the linearized model is listed here. The steady-state controller is implemented under the "SAMPLE" segment. This same controller is used in the nonlinear model.

```
TITLE  SIMPLE MODEL WITH OPTIMAL GAINS FROM CONTROLS - 9 AUG 87
*** FEED BACK GAINS USING THE ERROR STATE CONTROL LAW U= -F(X-R)    ***
ARRAY RKPT(8),RKQR(8),XPT(8),XQR(8),UPT(2),UQR(2),EPT(8),EQR(8)
FGEN2 FBKPT= 2,8,16,  1,2,1,2,3,4,5,6,7,8, ...
      -1.99484,-.60299,-.71717,.27437,1.74559,.00994,.14049,.00016, ...
      -.58535,111.16428,-.20533,28.90878,.58170,1.66845,.00962,.13667
*
FGEN2 FBKQR= 2,8,16,  1,2,1,2,3,4,5,6,7,8, ...
     -1.61288,-1.61027,-.55320,.31985,1.05412,-.20752,.12656,-.00264,...
     1.56829,-1.59987,-.30479,-.56615,.10693,1.23477,.00096,.12962
*
CONST RMAXT= 100., TAMAX= 100., MAXDFL= .5236, RMAX= .87266
CONST A1=.0236133,A2=-3.7381,A3=-6.750686,A4=.4830933
CONST A5=6.784433,A6=.107891,A7=.893727
CONST LAE=-21.29,MEE=-14.51,NRE=-16.68
CONST H1= 17.77, H2= 157.91
CONST PHDES=.0,ALRDES=.00,THDES=.0,PSDES=.0
CONST RKPT(3)=0,RKPT(4)=0,RKPT(5)=0,RKPT(6)=0,RKPT(7)=0,RKPT(8)=0
CONST RKQR(3)=0,RKQR(4)=0,RKQR(5)=0,RKQR(6)=0,RKQR(7)=0,RKQR(8)=0
INIT
      DELEDO= 0
      DELRDO= 0
      DELADO= 0
      DLTRDO= 0
      DELEO= 0
      DELRO= 0
      DELAO= 0
      DLTRO= 0
      PO= 0
      QO= 0
      RO= 0
      THRO= 0
      I= 1
      J= 1
```

```
********* DEFINE MACRO FOR USE IN SERVO EQUATION LIMITING **********
MACRO  OUT= SERVO(OUT0,OUTD,LIM)
       OUT= INTGRL(OUT0,OUTD)
       OUT= LIMIT(-LIM,LIM,OUT)
ENDMAC
DYNAMIC
**** INPUT CALCULATIONS
       RKPT(1) = PHDES*STEP(0.)
       RKPT(2) = ALRDES*STEP(0.)
       RKQR(1) = THDES*STEP(0.)
       RKQR(2) = PSDES*STEP(0.)
*
       XPT(1)= PHIB
       XPT(2)= U
       XPT(3)= P
       XPT(4)= THROT
       XPT(5)= DELA
       XPT(6)= DLTR
       XPT(7)= DELAD
       XPT(8)= DLTRD
       XQR(1)= THTB
       XQR(2)= PSIB
       XQR(3)= Q
       XQR(4)= R
       XQR(5)= DELE
       XQR(6)= DELR
       XQR(7)= DELED
       XQR(8)= DELRD
*
SAMPLE
*
       DO 30 I=1,2
            BUPT =0
            BUQR =0
            DO 20 J=1,8
                 EPT(J)= XPT(J) - RKPT(J)
                 EQR(J)= XQR(J) - RKQR(J)
                 FBPT= FGEN2(FBKPT,I,J)
                 FBQR= FGEN2(FBKQR,I,J)
                 BUPT= BUPT + EPT(J)*FBPT
                 BUQR= BUQR + EQR(J)*FBQR
20          CONTINUE
            UPT(I)= -(BUPT)
            UQR(I)= -(BUQR)
30     CONTINUE
*
       UA= UPT(1)
       UT= UPT(2)
       UE= UQR(1)
       UR= UQR(2)
```

```
DERIV
      PHIBD= P
      UD  = A7*THROT
      THTBD= Q
      PSIBD= R
      PD= A1*U + A2*THROT + LAE*DELA
      THROTD= -THROT + .5*DLTR
      QD= A3*R + MEE*DELE
      RD= A5*Q + NRE*DELR
***   ELEVATOR, RUDDER, AILERON, THROTTLE
      DELADD= -H1*DELAD - H2*DELA + H2*UA
      DLTRDD= -H1*DLTRD - H2*DLTR + H2*UT
      DELEDD= -H1*DELED - H2*DELE + H2*UE
      DELRDD= -H1*DELRD - H2*DELR + H2*UR
*
      PHIB= INTGRL(PHIBO,PHIBD)
      U     =INTGRL(UO,UD)
      THTB= INTGRL(THTBO,THTBD)
      PSIB= INTGRL(PSIBO,PSIBD)
      P= INTGRL(PO,PD)
      THROT= INTGRL(THRO,THROTD)
      Q= INTGRL(QO,QD)
      R= INTGRL(RO,RD)
*
      DELED = SERVO(DELEDO,DELEDD,RMAX)
      DELRD = SERVO(DELRDO,DELRDD,RMAX)
      DELAD = SERVO(DELADO,DELADD,RMAX)
      DLTRD = SERVO(DLTRDO,DLTRDD,RMAXT)
      DELE  = INTGRL(DELEO,DELED)
      DELR  = SERVO(DELRO,DELRD,MAXDFL)
      DELA  = INTGRL(DELAO,DELAD)
      DLTR  = SERVO(DLTRO,DLTRD,TAMAX)
      DES=.1
      ZER= 0.
CONTROL FINTIM=5,DELS=.04,DELT=.005
PARAM PHIBO=.00,UO=0,THTBO=0,PSIBO=0
SAVE .04,PHIB,U,THTB,PSIB,ZER,DES
PRINT .2,PHIB,U,THTB,PSIB
LABEL (G1) REGULATOR GAINS - ERROR STATE - PHI (0)= .1
GRAPH (G1,DE=TEK618) TIME(NI=5,UN=SEC) PHIB(NI=4,SC=.05,LI=1, ...
 UN='R/SEC AND ALT RATE F/SEC',LO=-.05) U(AX=OMIT,NI=4, ...
  SC=.5,LI=3,LO=-.5) DES(AX=OMIT,NI=10,SC=.05,LI=4,LO=-.05) ...
   ZER(AX=OMIT,NI=4,SC=.05,LI=4,LO=-.05)
GRAPH (G2,DE=TEK618,OV,PO=6,4.5) TIME(NI=5,UN=SEC) THTB(NI=4,...
      UN='AND PSIB R/SEC',LO=-.05,SC=.05,LI=1) PSIB(AX=OMIT, ...
    NI=4,LO=-.05,SC=.05,LI=3) DES(AX=OMIT,NI=4,LO=-.05,SC=.05,LI=4) ...
   ZER(AX=OMIT,NI=4,SC=.05,LI=4,LO=-.05)
END
STOP
```

APPENDIX D

NUMERICAL ELECTROMAGNETICS CODE

1. Modelling the AROD Body

The Numerical Electromagnetics Code (NEC) enables the user to simulate a solid surface using either the wire grid or the surface patch technique. Extensive use of symmetry in the program and the circular symmetry of the AROD model allow that the surface patch approach be easily implemented. Figure D.1 illustrates the procedure schematically.

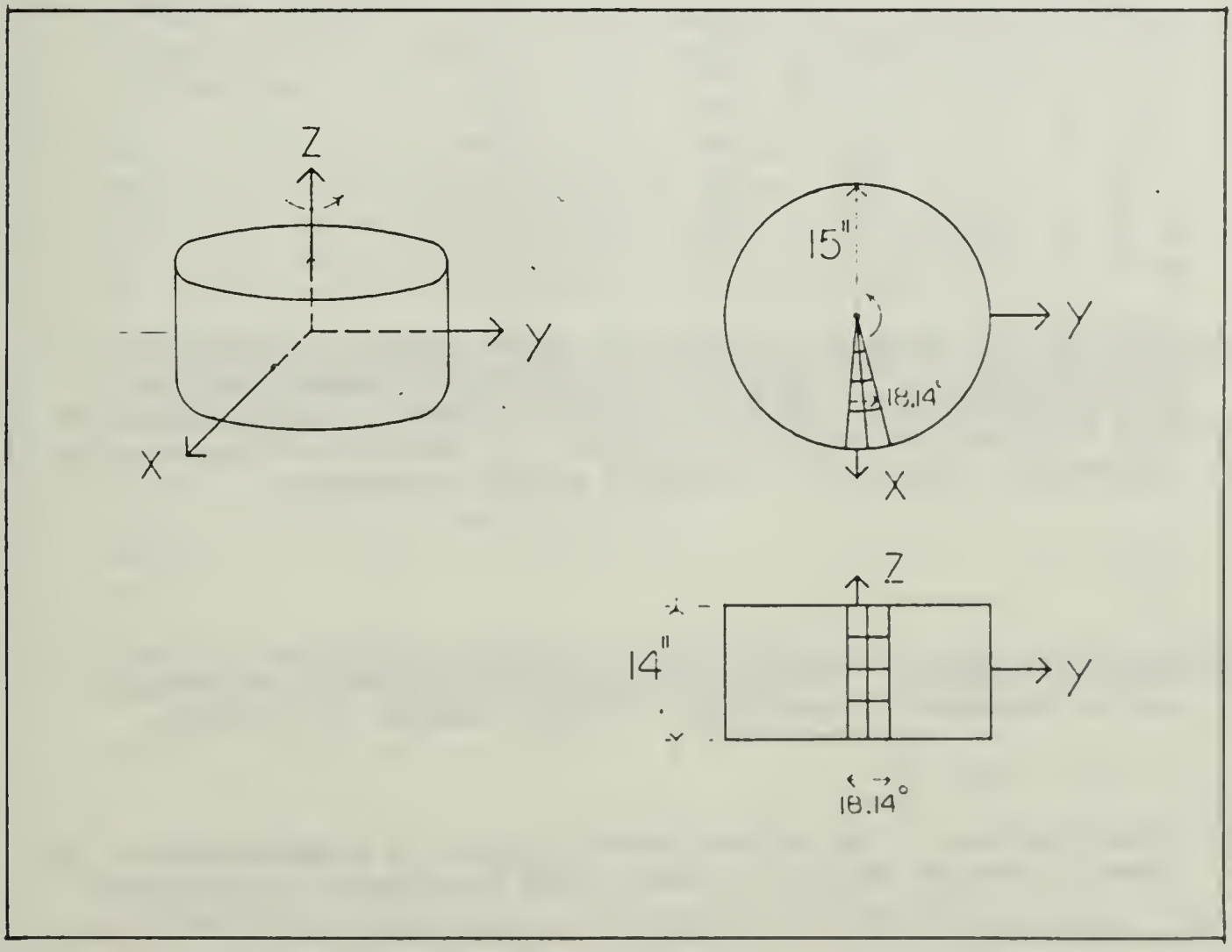

Figure D.1 Schematic for AROD Body Modelling

The following computer code is the NEC model of the body which was utilized.

(1) Build the 1st column of patches. The column is 9.92° in angular width (arc) and 14 inches high. The arc of the column is in the XY plane and the height of the column is in the Z direction at a radius of 15 inches from the Z axis.

```
SP 0, 0, 15., 0., 5., 18.435, 0., 9.92
SP 0, 0, 15., 0., 1.5, 5.711, 0., 7.44
SP 0, 0, 15., 0.,-1.5,-5.711, 0., 7.44
SP 0, 0, 15., 0.,-5.,-18.435, 0., 9.92
```

(2) Rotate and duplicate the column. The 1st column is rotated in the XY plane and duplicated to form a column that is now 18.84° wide and 14 inches high.

```
GM 0, 1, 0., 0., 9.4735, 0., 0., 0.
```

(3) Add patches to top and bottom to form wedge. These patches together with the column form a 18.84° section of the cylinder.

```
SP 0, 0, 13.95, 1.16, 7., 90., 4.737, 9.26
SP 0, 0, 13.95, 1.16,-7.,-90., 4.737, 9.26
SP 0, 0, 11.96, .990, 7., 90., 4.737, 7.94
SP 0, 0, 11.96, .990,-7.,-90., 4.737, 7.94
SP 0, 0, 9.470, .785, 7., 90., 4.737, 9.425
SP 0, 0, 9.470, .785,-7.,-90., 4.737, 9.425
SP 0, 0, 4.980, .413, 7., 90., 4.737, 9.92
SP 0, 0, 4.980, .413,-7.,-90., 4.737, 9.92
```

(4) Complete the cylinder. The entire 18.84° wedge is rotated 19 times to form a 360° cylinder which is missing only a top and bottom center piece. These two center pieces are added along with each antenna that is to be simulated. GS scales the dimensions to meters from inches and GE declares an end to geometry.

```
GR 0, 19
GS 2
GE
```

(5) Specify frequency. The frequency at which the model and antenna are to simulated is specified. In this example, f = 800 MHz.

```
FR 0,0,0,0,800.,0.
```

(6) Store the model. The entire symmetric model is stored in a Green's function matrix for recall when the antenna is simulated.

```
WG
```

2. Antenna Simulation

A dipole array and a loop antenna are simulated in the NEC code which follows.

a. 5 Dipole Ring Array

A five dipole ring array consists of five half-wave dipoles that are arranged in a circle.

(1) Read the Green's function. The AROD body model which is stored in a Green's function matrix is recalled to start the simulation. This matrix also includes the frequency at which the antenna will transmit.

```
GF
```

(2) Specify the dipoles. Wire .1 inch in radius and 7.38 inches long is used to model a half-wave dipole at f = 800 MHz. 11 segments in each dipole is used so that NEC automatically calculates current losses. 5 dipoles are spaced equally around the circle at a radius of 15.5 inches. The dipoles longitudinal axis is in the Z direction.

```
GW 1, 11, 15.5, 0., 3.69, 15.5, 0.,-3.69, .1
GW 2, 11, 4.79, 14.74, 3.69, 4.79, 14.74,-3.69, .1
GW 3, 11, -12.54, 9.11, 3.69, -12.54, 9.11,-3.69, .1
GW 4, 11, -12.54, -9.11, 3.69, -12.54, -9.11,-3.69, .1
GW 5, 11, 4.79,-14.74, 3.69, 4.79, -14.74,-3.69, .1
```

(3) Complete the cylinder. The two center patches which were excluded from the symmetric AROD body model are added, the dimensions are scaled to meters, and the geometry is ended with no ground plane.

```
SP 0, 0, 0., 0., 7., 90, 0., 12.57
SP 0, 0, 0., 0.,-7.,-90, 0., 12.57
GS 2
GE 0
```

(4) Specify the driving source. In this example, a feed point at the center of each dipole provides 1.0 volts.

```
EX 0, 1, 6, 01, 1., 0.
```

b. Loop Antenna

A single wire loop antenna is added to the AROD body model. The loop is flush to the surface of the AROD.

(1) Read the Green's function. The AROD body model which is stored in a Green's function matrix is recalled to start the simulation. This matrix also includes the frequency at which the antenna will transmit.

```
GF
```

(2) Specify 1st wire in the circle. The circle will consist of wire arc segments connected together. The 1st segment spans 10^{o} and is at a radius of 15.5 inches. The wire is in the XZ plane initially and is then moved to the XY plane.

```
GA 1, 3, 15.5, -5., 5., .1
GM 0, 0, 90., 0., 0., 0., 0., 0., 1
```

(3) Create the loop. The first wire is duplicated and rotated 36 times to form a complete circle.

```
GR 1, 36
```

(3) Complete the cylinder. The two center patches which were excluded from the symmetric AROD body model are added, the dimensions are scaled to meters, and the geometry is ended with no ground plane.

```
SP 0, 0, 0., 0., 7., 90, 0., 12.57
SP 0, 0, 0., 0.,-7.,-90, 0., 12.57
GS 2
GE 0
```

(4) Specify the driving source. In this example, a feed point at φ = 0^{o} provides 1.0 volts.

```
EX 0, 1, 6, 01, 1., 0.
```

INITIAL DISTRIBUTION LIST

		No. Copies
1.	Defense Technical Information Center Cameron Station Alexandria, Virginia 22304-6145	2
2.	Library, Code 0142 Naval Postgraduate School Monterey, California 93943-5002	2
3.	Chairman, Code 62 Department of Electrical and Computer Engineering Naval Postgraduate School Monterey, California 93943	1
4.	Ground/Air Tele Robotics Project Office Development Center Marine Corps Development and Education Command Quantico, Virginia 22340	1
5.	Professor H. A. Titus Code 62TS Naval Postgraduate School Monterey, California 93943	20
6.	Professor H. M. Lee Code 62LH Naval Postgraduate School Monterey, California 93943	1
7.	Captain W. G. Bassett Code LMC-3 Installations and Logistics Headquarters, U.S. Marine Corps Washington, D.C. 20380	4

18767

Thesis
B242555 Bassett
c.1 A dynamic simulation and feedback control scheme for the U.S. Marine Corps' Airborne Remotely Operated Device (AROD).

8 NOV 89 35216
26 FEB 91 38083
16 MAR 93 38357

Thesis
B242555 Bassett
c.1 A dynamic simulation and feedback control scheme for the U.S. Marine Corps' Airborne Remotely Operated Device (AROD).

thesB242555
A dynamic simulation and feedback contro
3 2768 000 74851 1
DUDLEY KNOX LIBRARY